

Dissertation zur Erlangung des Doktorgrades  
der Fakultät für Chemie und Pharmazie  
der Ludwig-Maximilians-Universität München

The Eukaryotic Chaperonin TRiC  
*Domain-Wise Folding of Multi-Domain Proteins*

Florian Rüßmann

aus

Wuppertal

2013

## Erklärung

Diese Dissertation wurde im Sinne von § 7 der Promotionsordnung vom 28. November 2011 von Herrn Prof. Dr. F. Ulrich Hartl betreut.

## Eidesstattliche Versicherung

Diese Dissertation wurde eigenständig und ohne unerlaubte Hilfe erarbeitet.

Florian Rübmann

Dissertation eingereicht am	8. Januar 2013
1. Gutacher	Prof. Dr. F. Ulrich Hartl
2. Gutachterin	PD Dr. Dr. Konstanze Winklhofer
Mündliche Prüfung am	8. April 2013

# Acknowledgements

I would like to thank Prof. Dr. F.-Ulrich Hartl for giving me the opportunity to work in his laboratory and for his optimism and his creative input during the entire course of my project.

I would like to thank my supervisors Dr. Stephanie Etchells and Dr. Andreas Bracher. Many obstacles have been overcome by their support. Their questions and ideas shaped the project significantly.

I would like to thank Dr. Markus Stemp who had started the project and who introduced me into many of the necessary skills and techniques.

I would like to thank my colleagues in the lab for creating a unique working atmosphere and for many shared moments that I will never forget.

I would like to thank Dr. Birgitta Beatrix and Prof. Dr. Don Lamb for the discussions during the TAC meetings that provided helpful external input.

I would like to thank the members of my PhD committee PD Dr. Dr. Konstanze Winklhofer, PD Dr. Dietmar E. Martin, Prof. Dr. Roland Beckmann, Prof. Dr. Jürgen Soll and Prof. Dr. Karl-Peter Hopfner.

I would like to thank IMPRS-LS for organizing lectures, seminars, workshops and retreats and for all further extracurricular support.

Last but not least I would like to thank my family for supporting me all along the way.

<b>1. Summary</b>	<b>- 4 -</b>
<b>2. Introduction</b>	<b>- 6 -</b>
<b>2.1 Protein Folding</b>	<b>- 6 -</b>
2.1.1 Proteins Consist of Amino Acids Connected by Peptide Bonds	- 6 -
2.1.2 The Thermodynamic Hypothesis	- 8 -
2.1.3 Thermodynamics and Kinetics of Protein Folding	- 9 -
<b>2.2 Molecular Chaperones Assist Protein Folding in the Cell</b>	<b>- 10 -</b>
2.2.1 Many Molecular Chaperones are Heat Shock Proteins	- 10 -
2.2.2 Pathways of <i>de novo</i> Protein Folding in the Cytosol	- 13 -
<b>2.3 Different Classes of Molecular Chaperones</b>	<b>- 14 -</b>
2.3.1 Small Heat Shock Proteins	- 14 -
2.3.2 Hsp70	- 14 -
2.3.3 Hsp70 Co-Chaperones	- 15 -
2.3.4 Hsp90	- 16 -
2.3.5 Hsp100	- 16 -
<b>2.4 The Chaperonins</b>	<b>- 17 -</b>
2.4.1 Differences between Group I and Group II Chaperonins	- 17 -
2.4.2 Structural Characterization of Chaperonins	- 20 -
2.4.3 The Intra- and Interring Arrangement of TRiC Subunits	- 21 -
2.4.4 TRiC Co-Chaperones	- 21 -
<b>2.5 Chaperonin-Substrate Interaction</b>	<b>- 22 -</b>
2.5.1 Binding of Substrates to Chaperonins	- 24 -
2.5.2 The Size of the Chaperonin Cavity	- 24 -
<b>2.6 Chaperonin Interactomes</b>	<b>- 25 -</b>
2.6.1 Comparison of Prokaryotic and Eukaryotic Proteomes	- 25 -
2.6.2 TRiC Interactors	- 25 -
2.6.3 GroEL Interactors	- 28 -
2.6.4 Comparison of Interactors of GroEL and TRiC	- 28 -
<b>2.7 Aim of the Study</b>	<b>- 29 -</b>
<b>3. Results</b>	<b>- 31 -</b>
<b>3.1 TRiC-dependent Folding of Actin Fusion Proteins</b>	<b>- 31 -</b>
3.1.1 Actin Fusion Proteins as Model for Multi-Domain TRiC Substrates	- 32 -
3.1.2 Actin Folding Estimated by DNase I Binding Experiments	- 33 -
3.1.3 Actin Folding Estimated by Protease-Resistant Actin Fragment	- 36 -

3.1.4	Depletion of TRiC from RRL	- 38 -
<b>3.2</b>	<b>Stalling of Actin Fusion Proteins on the Ribosome</b>	<b>- 39 -</b>
3.2.1	Stalling of Actin-GFP on the Ribosome	- 39 -
3.2.2	Stalling of Actin-Luciferase on the Ribosome	- 40 -
3.2.3	Stalling of Actin with a Flexible Linker on the Ribosome	- 42 -
<b>3.3</b>	<b>Proteinase K Protection Experiments</b>	<b>- 46 -</b>
3.3.1	PK Protection of Purified Bovine TRiC by ATP and AIFx	- 46 -
3.3.2	PK Protection of Actin Fusion Proteins in RRL by ATP and AIFx	- 48 -
<b>3.4</b>	<b>Analysis of TRiC-bound Proteins by Native PAGE</b>	<b>- 49 -</b>
3.4.1	Native PAGE of Purified Bovine TRiC	- 50 -
3.4.2	Native PAGE of RRL Reactions Translating Actin Fusion Proteins	- 50 -
3.4.3	Elution of TRiC-bound Proteins from Native PAGE Gels	- 52 -
<b>3.5</b>	<b>A Protease-Sensitive GFP-Mutant</b>	<b>- 54 -</b>
3.5.1	$\Delta$ N-GFP-Actin is Completely Encapsulated inside the TRiC Cavity	- 54 -
3.5.2	Native PAGE Mobility Shift Assay	- 55 -
3.5.3	DNase I Binding of $\Delta$ N-GFP-Actin Fusion Proteins	- 56 -
<b>3.6</b>	<b>Investigating Naturally Occurring Large TRiC Substrates</b>	<b>- 58 -</b>
3.6.1	Testing Human Homologs of Known TRiC Interactors	- 58 -
3.6.2	hSnu114 – A Strong TRiC Interactor	- 59 -
3.6.3	$\beta$ '-COP – A WD40 Domain Containing Interactor of TRiC	- 62 -
3.6.4	Expressing N- and C-terminal hSnu114 and $\beta$ '-COP Parts separately	- 62 -
3.6.5	Partial Encapsulation of hSnu114	- 63 -
3.6.6	The C-terminal Part of hSnu114 Binds Strongly to TRiC	- 65 -
3.6.7	Protected Fragments Originate from the C-terminus of hSnu114	- 67 -
<b>4.</b>	<b>Discussion</b>	<b>- 72 -</b>
<b>4.1</b>	<b>Partial Encapsulation of Multi-Domain Proteins</b>	<b>- 72 -</b>
<b>4.2</b>	<b>Factors Influencing Partial Encapsulation</b>	<b>- 74 -</b>
4.2.1	Initial Binding of Substrates to TRiC	- 74 -
4.2.2	Sequential Release of Substrates into the TRiC Cavity	- 75 -
4.2.3	Position of the TRiC-dependent Domain	- 75 -
<b>4.3</b>	<b>Structural and Evolutionary Aspects of Partial Encapsulation</b>	<b>- 77 -</b>
4.3.1	The Built-in Lid in Group II Chaperonins	- 77 -
4.3.2	Evolution of Different Lids in Group I and II Chaperonins	- 77 -

<b>5. Materials and Methods</b>	<b>- 79 -</b>
<b>5.1 Materials</b>	<b>- 79 -</b>
5.1.1 Chemicals	- 79 -
5.1.2 Media and Buffers	- 80 -
5.1.3 Plasmids	- 83 -
5.1.4 Oligonucleotides	- 88 -
<b>5.2 Molecular Biology Methods</b>	<b>- 89 -</b>
5.2.1 Preparation of Chemically Competent Cells	- 89 -
5.2.2 Transformation of Chemically Competent Cells	- 90 -
5.2.3 Preparation of Plasmid DNA	- 90 -
5.2.4 Gel Electrophoresis of DNA	- 91 -
5.2.5 Polymerase Chain Reaction	- 91 -
5.2.6 Restriction Digest	- 91 -
5.2.7 DNA Ligation	- 92 -
<b>5.3 Biochemical Methods</b>	<b>- 92 -</b>
5.3.1 Purification of TRiC from Bovine Testes	- 92 -
5.3.2 <i>In vitro</i> Translation in Rabbit Reticulocyte Lysate	- 94 -
5.3.3 Depletion of TRiC from Rabbit Reticulocyte Lysate	- 95 -
5.3.4 Preparation of DNase I - Sepharose	- 95 -
5.3.5 DNase I Binding Assay	- 96 -
5.3.6 Protease Protection Assay	- 97 -
5.3.7 Native PAGE Mobility Shift Assay	- 99 -
5.3.8 Electrophoresis of Proteins	- 99 -
5.3.9 Western Blotting	- 101 -
<b>6. References</b>	<b>- 103 -</b>
<b>7. Abbreviations</b>	<b>- 121 -</b>

# 1. Summary

The eukaryotic cytosolic chaperonin TRiC is a hexadecamer consisting of two eight-membered rings that are stacked back to back. Each ring forms a central cavity, which is large enough to accommodate proteins up to 70 kDa according to structural studies. TRiC supports folding of its substrates by ATP-dependent rounds of binding, encapsulation and release. Surprisingly, one third of the known TRiC interactors exceed the size of the TRiC cavity. In the present work, experimental evidence for partial encapsulation of large substrates inside the central TRiC cavity is presented.

The cytoskeletal protein actin is a well-described obligate TRiC substrate. Upon *in vitro* translation in rabbit reticulocyte lysate, fusion proteins containing actin and GFP or actin, GFP and BFP connected by flexible linkers were used as model multi-domain proteins containing a TRiC dependent domain. Folding of actin was monitored by specific binding to DNase I as well as by occurrence of a protease-resistant actin fragment that derived from native actin. Folding of actin was impaired but not prevented by fusion with GFP. Interestingly, folding of actin was more severely impaired by fusion of GFP to its C-terminus (AG) than by fusion of GFP to its N-terminus (GA), suggesting that flexibility of the actin C-terminus is important for actin folding. Folding of actin was prevented by simultaneous fusion of BFP to the N- and of GFP to the C-terminus of actin (BAG), apparently due to steric problems hindering partial encapsulation. Folding of actin was possible when both BFP and GFP were fused to the actin N-terminus (BGA), even though the resulting polypeptide had a molecular weight of almost 100 kDa, indicating that TRiC-dependent folding of large multi-domain proteins exceeding the size of the TRiC cavity is possible.

Proteinase K treatment in presence of ATP and AlFx, resulting in a stably closed state of TRiC, was used to probe which parts of the actin fusion proteins were encapsulated inside the TRiC cavity. Protection of the full-length proteins against proteolysis was observed in case of the smaller actin fusion proteins GA and AG upon closure of the TRiC cavity by ATP and AlFx. However, full-length BAG and BGA were not protected. Instead, the largest stable fragment of BGA had the same apparent molecular weight as GA, suggesting that cleavage occurred in the linker region between BFP and GFP and that the linker was probably located outside TRiC after

closure of the cavity. Interestingly, no protected fragment of BAG was detected, indicating that this particular fusion protein was not encapsulated, explaining its inability of being folded.

Furthermore, PK protection experiments indicated that the spliceosomal protein hSnu114 (109 kDa), a previously reported naturally occurring TRiC interactor, is also partially encapsulated inside the TRiC cavity. hSnu114 is likely a complex multi-domain protein with structural homology to eEF2, for which crystal structures are available. Several fragments of 15-45 kDa are protected by TRiC from PK digest in presence of ATP and AlFx. All these fragments include the C-terminus of the protein as inferred from protection of C-terminally HA-tagged fragments of comparable sizes derived from hSnu114-HA. Surprisingly, when the C-terminal part of hSnu114 (hSnu114-C, 45 kDa) was expressed separately, no smaller protected fragments were observed and instead the complete hSnu114-C was encapsulated inside the TRiC cavity.

The occurrence of several fragments of different sizes indicates heterogeneity of TRiC-hSnu114 complexes with regard to the encapsulated part of hSnu114. Furthermore, the observed protected segments were much smaller (15-45 kDa) than the size of the TRiC cavity (up to 70 kDa), suggesting that TRiC might preferentially encapsulate only the TRiC-dependent domain(s) and might exclude the rest of the protein. How TRiC recognizes domain boundaries is not clear. However, the absence of smaller protected fragments in absence of the N-terminal part of hSnu114 (hSnu114-N) suggests that hSnu114-N plays an important role in the selection of which parts of the C-terminal region of hSnu114 will be encapsulated, even though hSnu114-N itself appears to be TRiC-independent. Rather, it appears that interactions between the N- and C-terminal parts of the protein guide proper binding of hSnu114 to TRiC and subsequent domain-wise encapsulation.

Taken together, these experiments provide evidence for partial encapsulation and folding of large proteins by TRiC, allowing a mechanism of domain-wise folding. This mechanism, which is not accessible to the prokaryotic chaperonin, may have facilitated the evolution of multi-domain proteins, a class of proteins highly prevalent in eukarya.

## 2. Introduction

### 2.1 Protein Folding

#### 2.1.1 Proteins Consist of Amino Acids Connected by Peptide Bonds

The genetic information encoded in the DNA is eventually transformed into the linear amino acid sequence of a polypeptide after transcription into mRNA and translation thereof at the ribosome. The translation of an mRNA sequence into an amino acid sequence is determined by a universal genetic code. 64 different codons exist, 61 of which code for the 20 different canonical proteinogenic amino acids. The remaining three codons are stop codons that lead to stop of translation and release of the polypeptide from the ribosome. Additionally, two of the stop codons encode for two non-canonical proteinogenic amino acids, selenocysteine and pyrrolysine. Selenocysteine containing proteins are found in all kingdoms of life. However, only few proteins contain selenocysteine (e.g. 25 proteins in humans), mostly proteins involved in redox reactions (Mariotti et al., 2012). Pyrrolysine is not found in eukaryotes but only in a few archaeal and prokaryotic enzymes required for production of methane from methylamines (Krzycki, 2005).

Proteinogenic amino acids consist of an amino group and a carboxyl group, which are both connected to the same C $\alpha$  carbon atom (Figure 1). This carbon is furthermore bound to a hydrogen atom and to a side chain R, which differs between different amino acids and confers the individual chemical properties to the amino acid residues in a polypeptide chain. The side chains can be as small as a single hydrogen atom in case of glycine; there are positively or negatively charged side chains as well as aliphatic and aromatic side chains. More than half of the side chains of proteinogenic amino acids contain hetero-atoms beside carbon and hydrogen such as oxygen, nitrogen or sulfur.

The peptide bond between individual amino acids is formed by a condensation reaction between the amino group of one amino acid and the carboxyl group of another one (Figure 1). As the peptide bond has a partial double bond character (Pauling et al., 1951), the rotation around the peptide bond is strongly restricted and the adjacent groups practically exist only in two

conformations called trans and cis. The trans conformation is energetically favored and therefore less than 0.5% of the peptide bonds in native proteins are found in the cis conformation (Weiss et al., 1998). An exception is the peptide bond preceding proline residues, which occurs in the cis conformation in approximately 5% of the cases in native proteins (Weiss et al., 1998).

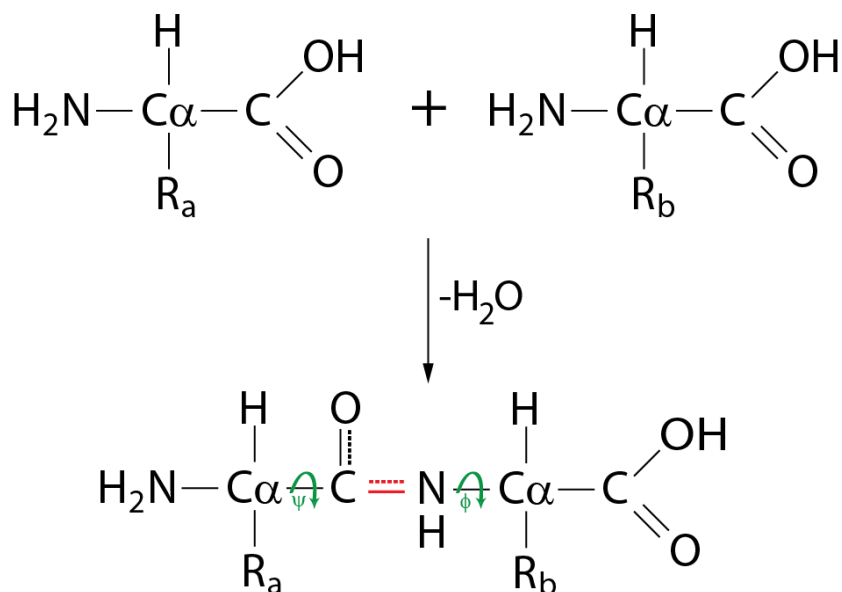


Figure 1: Simplified scheme of peptide bond formation. Top: Two amino acids with different side chains  $R_a$  and  $R_b$  are shown on top. Note that elongation of polypeptide chains at the ribosome occurs with amino acids activated by ester formation with the 3'-OH of tRNA. Bottom: The peptide bond is shown in red. Partial double bond character is indicated by dashed line. The angles  $\phi$  and  $\psi$  defined by rotation around the N- $C\alpha$  and the  $C\alpha$ -C bond, respectively are indicated in green.

The polypeptide backbone contains two other kinds of bonds in addition to the peptide bond that connects the different amino acids, namely the bonds connecting  $C\alpha$  with the amide nitrogen and the carbon atom of the carbonyl group, respectively. The angle between the groups of the N- $C\alpha$  bond is usually termed  $\phi$  and the angle between the groups of the  $C\alpha$ -C bond is called  $\psi$ . In principle, a free rotation around these two bonds is possible. However, steric constraints lead to a constriction of the energetically stable combinations of  $\phi$  and  $\psi$  (Ramachandran et al., 1963). In addition to the conformation of the peptide bonds (cis or trans) the different values for  $\phi$  and  $\psi$  define the backbone conformation of the polypeptide. In order to describe the entire conformation of the protein, the different conformations of all side chains have to be considered as well. Thus, there is an almost unlimited number of conformations even for small proteins and

the question arises of how an unfolded polypeptide chain can find its unique native and biologically active conformation.

### 2.1.2 The Thermodynamic Hypothesis

In 1972, Christian Anfinsen was awarded the Nobel Prize in Chemistry for his “studies on ribonuclease, in particular the relationship between the amino acid sequence and the biologically active conformation” (Anfinsen, 1973). His experiments were supporting the so-called “thermodynamic hypothesis”. According to this postulate, the native three-dimensional conformation of a protein is the one with the lowest free energy. This means that the native state of a protein is solely governed by its inter-atomic interactions and thus by its amino acid sequence and is not dependent on other cellular components (Anfinsen, 1973).

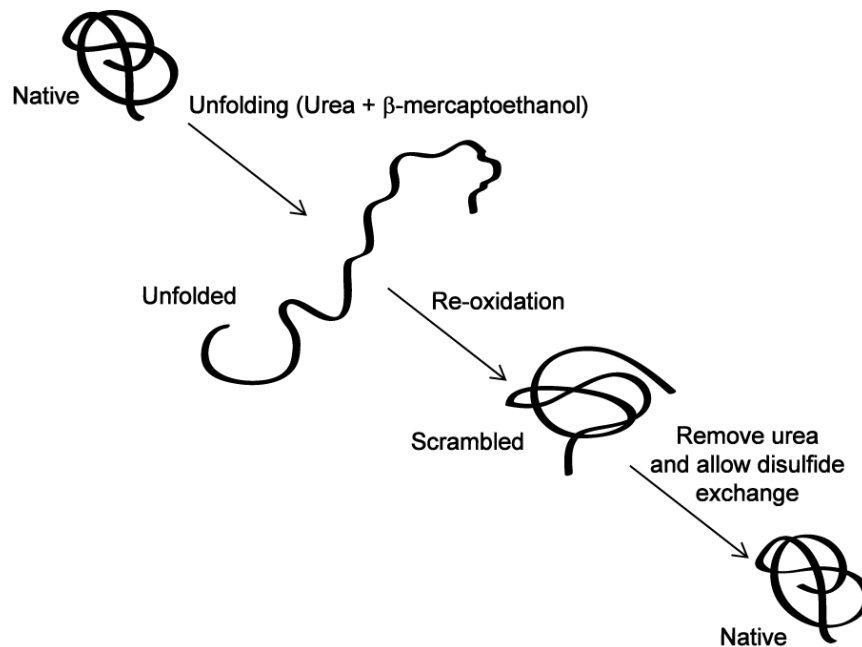


Figure 2: Scheme of experiments performed by Anfinsen and colleagues with ribonuclease; adapted from Anfinsen, 1973.

The bovine pancreatic ribonuclease is a protein of 154 amino acids which has four intramolecular disulfide bonds (Anfinsen, 1973). It was used in the 1950s and 1960s by many protein chemists for their experiments simply because it was available to them in large amounts (Richards, 1992). Anfinsen and his colleagues had denatured the protein in 8 M urea and reduced

the disulfide bonds with  $\beta$ -mercaptoethanol. Re-oxidation in the presence of urea resulted in the formation of non-native disulfide bonds and hence non-native and inactive ribonuclease. However, when the urea was removed and exchange of the disulfide bonds was enabled by addition of a small quantity of  $\beta$ -mercaptoethanol, the different non-native conformations were eventually converted into a homogeneous population of native ribonuclease (Figure 2), indicating that formation of the native state was not dependent on any external factors but was indeed determined by the amino acid sequence only (Anfinsen, 1973; Anfinsen et al., 1961). This statement holds in principle true also today, more than fifty years after Anfinsen's groundbreaking experiments.

### 2.1.3 Thermodynamics and Kinetics of Protein Folding

Even though folding is a specific process that differs not only between different proteins but also between the different unfolded states of one particular protein, several common principles have been postulated and confirmed experimentally. The energy landscape of a protein folding reaction is commonly depicted as a funnel, in which the thermodynamically stable native state is represented as the narrow bottom of the funnel while the unfolded state ensemble is represented as the broad edge at the top of the funnel (Dill and Chan, 1997). Any given point at the surface of the funnel depicts a particular conformation of the protein. Minimization of free energy drives the protein into the native conformation. Which are the factors that contribute to the low free energy of the native state?

The native state of most proteins is only marginally energetically stable (Dill et al., 2008). Several factors contribute to overcompensate the loss of entropy compared to the unfolded state ensemble. The most important factor seems to be the energetically favorable burial of hydrophobic side chains in the interior of the protein (Dill et al., 2008). Many proteins have a hydrophobic core, from which the surrounding aqueous solvent is excluded. Instead, polar and charged amino acid residues tend to cover the protein surface and increase the solubility of the respective protein by favorable interactions with the solvent. Another important factor contributing to protein stability is intramolecular hydrogen bonding (Dill et al., 2008). In fact, in folded proteins almost every amide and carbonyl group of the polypeptide backbone is involved

in hydrogen bonds that stabilize secondary structure elements such as  $\alpha$ -helices or  $\beta$ -strands. Also salt bridges between charged side chains contribute to protein stability.

The transition from the unfolded state ensemble to the native state is governed by thermodynamic parameters and is a reversible process. The kinetics of folding depend on the energy landscape of the folding reaction (Dill and Chan, 1997). In the simplest case, an unfolded protein is converted into the native state without the population of kinetically stable intermediates. However, not all protein folding reactions can be described as a simple two-state process. A more complicated scenario occurs when local energy minima exist on the way from the unfolded ensemble to the folded state. In this case, intermediate conformations are actually populated. A high energy barrier between the transition state ensemble and the native state slows down the folding process and can result in kinetically trapped intermediates that prevent the efficient accessibility of the native state (Baker and Agard, 1994; Kiefhaber, 1995). Furthermore, as long as a protein has not yet reached its native state, non-native intermolecular interactions can lead to the formation of protein aggregates (Dobson, 2003).

## 2.2 Molecular Chaperones Assist Protein Folding in the Cell

### 2.2.1 Many Molecular Chaperones are Heat Shock Proteins

The initial research on protein folding was carried out by refolding isolated and diluted small proteins *in vitro*. However, refolding experiments might only partially reflect the situation of *de novo* protein folding in the cell where co-translational folding during protein biosynthesis at the ribosomes plays a major role (Kramer et al., 2009). Additionally, protein folding in living cells is challenged by high intracellular macromolecule concentrations which favor non-native contacts of unfolded polypeptides (Ellis, 2001). Therefore, an elaborate molecular machinery has evolved throughout all three domains of life, which ensures that protein misfolding and aggregation is minimized and that protein folding to the native state occurs at a biologically relevant time scale (Hartl et al., 2011; Hartl and Hayer-Hartl, 2002). In fact, a sophisticated network of different

classes of proteins, termed molecular chaperones (Ellis, 1987), exists that accompanies a newly made protein from its formation at the ribosome until it has reached its native state (Figures 3 and 4).

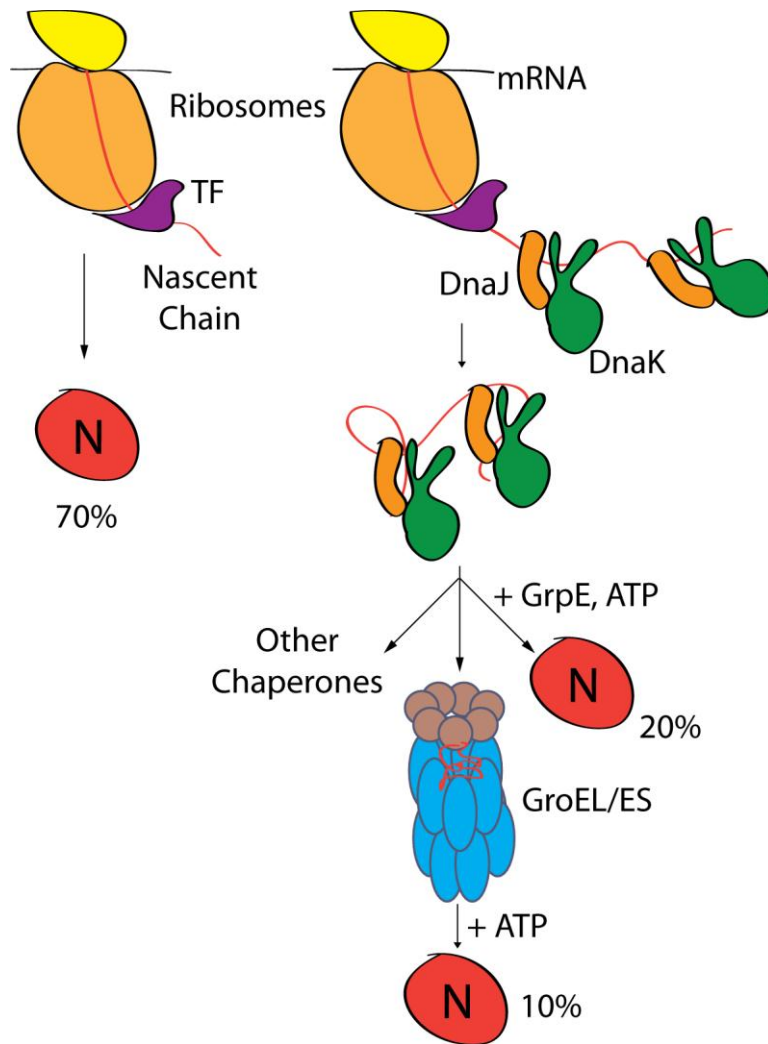


Figure 3: Simplified scheme of chaperone pathways in prokaryotes adapted from Hartl and Hayer-Hartl, 2002 and from Hartl et al., 2011

Many molecular chaperones are heat-inducible and they have thus originally been called “Heat shock proteins” (Hsps) (Lindquist and Craig, 1988; Schedl et al., 1978). In fact, various stress conditions lead to protein unfolding and the induction of Hsps during stress is highly important to deal with the increased load of unfolded proteins (Hageman et al., 2007). Heat shock proteins have been historically classified according to their rough molecular weight. The major groups are

small Hsps, Hsp40s, Hsp60s, Hsp70s, Hsp90s, Hsp100s and Hsp110s. Next to their role in dealing with unfolded proteins under stress conditions, different Hsps co-operate with other molecular chaperones in folding newly synthesized proteins along chaperone pathways in the cytosol (Hartl et al., 2011). Additionally, organelle-specific chaperones assist folding of their substrates within different organelles.

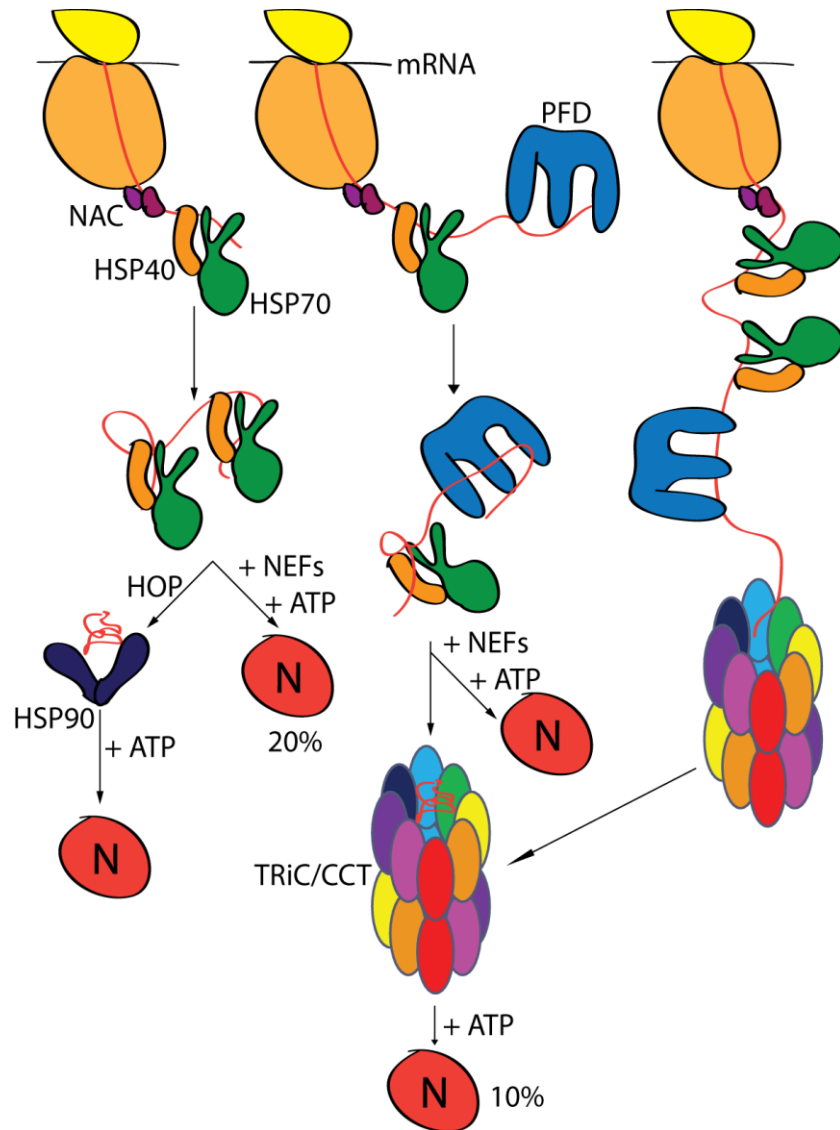


Figure 4: Simplified scheme of chaperone pathways in the eukaryotic cytosol adapted from Hartl and Hayer-Hartl, 2002 and from Hartl et al., 2011

### 2.2.2 Pathways of *de novo* Protein Folding in the Cytosol

A nascent polypeptide chain that emerges from the ribosomal exit tunnel is first recognized by ribosome-associated chaperones (Kramer et al., 2009), trigger factor (TF) in bacteria (Ferbitz et al., 2004) and nascent-polypeptide-associated complex (NAC) (Rospert et al., 2002) as well as the ribosome-associated complex (RAC) (Gautschi et al., 2001) in eukaryotes. Both TF and NAC work independently of nucleotides, but they do not share structural similarities. TF interacts with the ribosome as a monomer and the affinity of TF for the ribosome is drastically increased by ongoing translation and thus by the presence of a nascent chain, in which TF interacts with hydrophobic patches (Kaiser et al., 2006). NAC exists as a hetero-dimer and interacts with the ribosome via its  $\beta$ -subunit (Rospert et al., 2002). The mechanism of action of NAC is not well understood. In contrast to TF and NAC, RAC includes ATP-dependent molecular chaperones. In yeast, RAC consists of the Hsp70 protein Ssz1 and the Hsp40 protein zutin that build a stable hetero-dimeric complex (Gautschi et al., 2001). RAC stimulates the ATPase activity of Ssb1/2 (Huang et al., 2005), another ribosome-associated Hsp70 chaperone that directly contacts nascent polypeptide chains (Gautschi et al., 2002).

The interaction with Hsp70 is not sufficient for all proteins to reach the native state. Hsp90 and the Hsp60s, the latter also referred to as “chaperonins” (Hemmingsen et al., 1988), are specialized downstream chaperones that mediate folding of those proteins (Figures 3 and 4). The chaperonins are large ring-complexes that function as a cage for single protein molecules to fold unimpaired by aggregation. The mechanism of substrate delivery from Hsp70 to the downstream chaperones is not entirely understood. Nevertheless, some details are known about the respective chaperone pathways. For example, Hsp70 and Hsp90 interact via an adaptor protein called Hop that binds to both chaperones (Wegele et al., 2004). Transfer of substrates to the eukaryotic chaperonin TRiC (for TCP-1 Ring Complex, also called CCT for Chaperonin Containing TCP-1) seems to be mediated by the hexameric chaperone prefoldin (PFD) that was shown biochemically and structurally to be involved in delivery of actin and tubulin to TRiC (Hansen et al., 1999; Martin-Benito et al., 2002; Vainberg et al., 1998). However, a cryo-EM structure of the nucleotide-binding domain of Hsc70 in complex with TRiC suggests that transfer might be enabled also by a direct interaction between Hsp70s and TRiC (Cuellar et al., 2008).

## 2.3 Different Classes of Molecular Chaperones

The different classes of molecular chaperones are very diverse with regard to their structure. Hsp60s, Hsp70s and Hsp90s undergo ATP-dependent conformational changes that drive substrate binding and release. Other molecular chaperones like small Hsps as well as the ribosome-associated chaperones trigger factor and NAC work independently of ATP.

### 2.3.1 Small Heat Shock Proteins

The most prominent representative of small Heat shock proteins is  $\alpha$ -crystallin, a major component of the eye lens (Horwitz, 2003). Small Hsps are generally characterized by the presence of an  $\alpha$ -crystallin domain that is flanked by poorly conserved N- and C-terminal extensions (Sun and MacRae, 2005). The molecular weight of small Hsp monomers is low (approximately 10-40 kDa) but they assemble into large oligomeric complexes of up to 1 MDa. Small Hsps bind unfolded proteins and prevent their aggregation (Sun and MacRae, 2005). However, small Hsps do not actively refold denatured proteins; they rather keep their substrates in a folding competent state (Sun and MacRae, 2005).

### 2.3.2 Hsp70

Hsp70s are perhaps the most well-known group of all molecular chaperones. They consist of an N-terminal nucleotide-binding domain (NBD) of 45 kDa and a C-terminal substrate-binding domain of 25 kDa (Figure 5). The substrate-binding domain cycles between an open and a closed conformation depending on the nucleotide state of the NBD. In the ADP-bound conformation the lid over the substrate-binding domain is closed and Hsp70 forms a stable complex with its substrate (Mayer and Bukau, 2005). The ATPase cycle of Hsp70s is regulated by ATPase-activating proteins on the one hand and by nucleotide exchange factors (NEFs) on the other hand. NEFs catalyze the exchange of ADP for ATP, which results in an opening of the substrate-binding domain (Figure 5) and substrate release. Substrates that still expose hydrophobic patches

after release will rebind to Hsp70. The ATPase activity of substrate-bound Hsp70s is stimulated by Hsp40s that are also called J proteins following the bacterial Hsp40 DnaJ (Walsh et al., 2004).

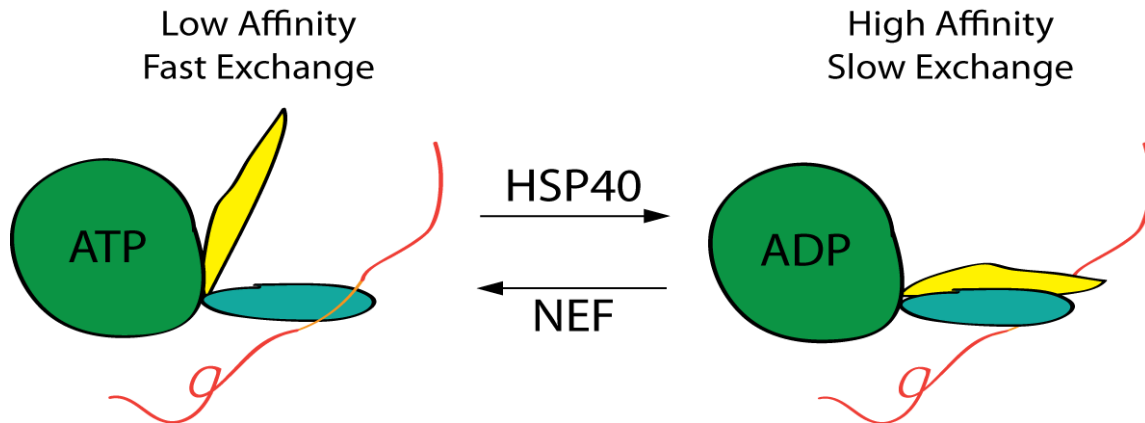


Figure 5: Simplified scheme of nucleotide-dependent changes in the substrate-binding domain of Hsp70s adapted from Hartl et al., 2011. The nucleotide-binding domain is shown in green. The substrate-binding  $\beta$ -sandwich domain is shown in turquoise and the  $\alpha$ -helical lid is shown in yellow. An unfolded substrate is shown in red, exposing a stretch a hydrophobic amino acids shown in orange.

### 2.3.3 Hsp70 Co-Chaperones

In bacteria, the NEF GrpE catalyzes the release of ADP from DnaK, thereby indirectly opening up the DnaK substrate-binding domain and enabling another cycle of substrate binding and release (Harrison et al., 1997; Packschies et al., 1997). The mammalian Hsp70s display a higher intrinsic dissociation rate of ADP than DnaK and can consequently function without a nucleotide exchange factor (Mayer and Bukau, 2005). However, their ADP release rate can also be increased by interaction with different structurally unrelated Hsp70 NEFs, namely BAG domain proteins (Hohfeld and Jentsch, 1997), HspBP1 homologs (Kabani et al., 2002) and Hsp110 proteins (Polier et al., 2008).

BAG-1 plays also a major role as a co-chaperone in chaperone-assisted protein degradation. This pathway leads to transfer of Hsp70 substrates to the proteasome or the lysosome. BAG-1 in conjunction with the chaperone-dependent ubiquitin E3 ligase CHIP connects Hsp70 with the ubiquitin-proteasome system. Different co-chaperones exist that link Hsp70 with the autophagy-

lysosome pathway (Kettern et al., 2010). Another Hsp70 co-chaperone called Hip stabilizes Hsp70 in the ADP-bound closed conformation (Hohfeld et al., 1995). Finally, Hsp110s are Hsp70 homologs that function as NEFs for Hsp70s (Polier et al., 2008; Schuermann et al., 2008; Shaner and Morano, 2007). Additionally, Hsp110 binds unfolded proteins and prevents their aggregation (Oh et al., 1997). However, refolding of denatured proteins cannot be achieved by Hsp110 alone. Instead, cooperation of Hsp110 with Hsp70 is required for refolding (Oh et al., 1997).

### 2.3.4 Hsp90

Hsp90 is a dimer in solution (Wandinger et al., 2008). In contrast to other molecular chaperones, Hsp90 has a fairly specialized and well defined set of substrates that fall mainly into the two major classes of signaling kinases and transcription factors, especially steroid hormone receptors (SHRs). Kinases and SHRs are transferred from Hsp70 to Hsp90 when both chaperones become connected by the co-chaperone Hop (Caplan et al., 2007; Wandinger et al., 2008). Hsp90 has moved into the focus of cancer research in the last decade because many of its substrates are signaling kinases that play important roles in the development of cancer. Small molecule inhibitors of the Hsp90 ATPase activity such as geldanamycin have an anti-tumor effect because inhibition of Hsp90 leads to degradation of the Hsp90 substrate proteins (Maloney and Workman, 2002).

### 2.3.5 Hsp100

The classes of molecular chaperones described above share a common function in preventing protein aggregation and assisting protein folding. In contrast, Hsp100 proteins come into play when protein aggregation has already occurred. They function as “disaggregases” and re-solubilize aggregated proteins in an ATP-dependent manner (Zolkiewski et al., 2012). Hsp100 proteins belong to the class of AAA+ ATPases. They form hexameric rings and re-solubilize aggregated proteins by threading them through the central pore of the hexamer (Zolkiewski et al.,

2012). Interestingly, Hsp100 proteins are found in bacteria (ClpB), yeast (Hsp104) and plants, but not in animal cells (Zolkiewski et al., 2012).

## 2.4 The Chaperonins

The chaperonins, also known as Hsp60s, are a class of evolutionary conserved molecular chaperones found in all domains of life. Chaperonins assemble into large oligomeric double-ring complexes whose rings are stacked back to back. The chaperonin monomers consist of three domains (Figure 6). The equatorial domain contains the ATP-binding site. The intermediate domains connect the equatorial domains with the apical substrate-binding domains, which are located at the ends of the double-ring complex (Braig et al., 1994). Folding of the substrate proteins is achieved upon encapsulation within the central cavity formed by one ring. Opening and closing of the cavity are driven by ATP binding and hydrolysis.

### 2.4.1 Differences between Group I and Group II Chaperonins

Chaperonins can be divided into two different groups (Kim et al., 1994). Group I chaperonins are found in bacteria (GroEL) and in organelles of prokaryotic origin, i.e. chloroplasts (Cpn60) and mitochondria (Hsp60). The best studied group I chaperonin is the tetra-decameric GroEL from *E. coli*. GroEL encapsulates its substrates with the help of the co-chaperone GroES (Hsp10). Homo-heptameric GroES serves as a lid that closes the GroEL cavity (Saibil, 1996). Group II chaperonins exist in the cytosol of archaea (Thermosome) and eukaryotes (TRiC). Structural studies have shown that they are independent of a GroES-like co-chaperone. Instead they have a built-in lid (Ditzel et al., 1998). The two groups of chaperonins differ in the inter-ring arrangement. While a single GroEL subunit contacts two subunits on the opposite side of the ring (Braig et al., 1994), in group II chaperonins each subunit contacts only one subunit across the ring (Ditzel et al., 1998; Gutsche et al., 1999).

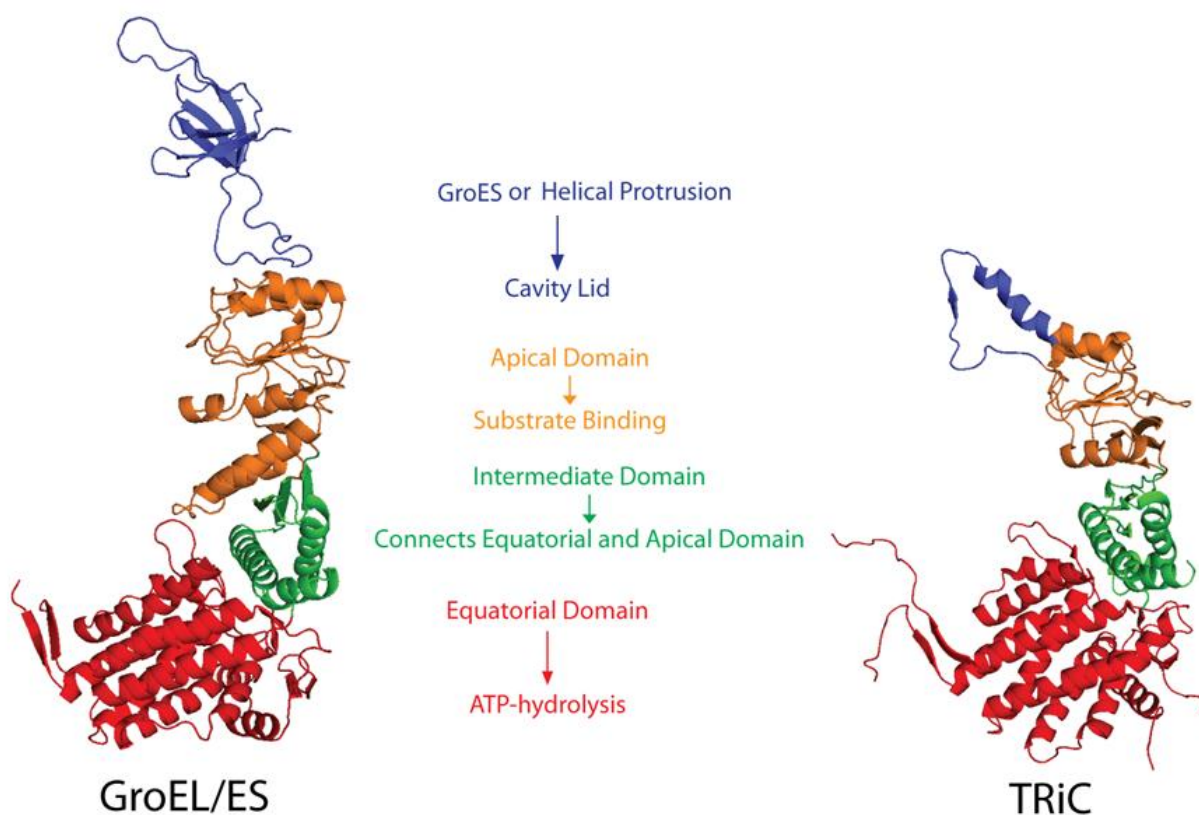


Figure 6: Comparison of single subunits of group I (GroEL/ES) and group II (TRiC) chaperonins. PDB files of respective crystal structures ((3P9D, Dekker et al., 2011) and (1AON, Xu et al., 1997)) have been modified using PyMOL (DeLano Scientific). The design of this figure was inspired by Gutsche et al., 1999. The subunits are not drawn to scale.

Another major difference between group I and group II chaperonins is the ATP-dependent rearrangement of the individual subunits that characterizes the cycles of opening and closing. The equatorial domains do not have high flexibility in group I chaperonins because of the staggered inter-ring arrangement. Thus, essentially only the intermediate and the apical domains move during ATP-driven cycling. Upon ATP-binding, the intermediate domain rotates downward by approximately 25°, thereby closing the ATP binding pocket. This movement induces and enables a clockwise rotation and a large upward tilt of the apical domain that is stabilized by binding of GroES (Ma et al., 2000). A stably closed GroEL/ES complex can be obtained by incubation with non-hydrolysable ATP analogs, AMP-PNP or ATP $\gamma$ S, indicating that ATP-binding to GroEL is sufficient to induce stable binding of GroES to GroEL.

Interestingly, the large movements of the apical domains are only easily achieved when all the subunits in the ring move in a concerted manner. Otherwise, sterical clashes would interfere with domain movement (Ma et al., 2000).

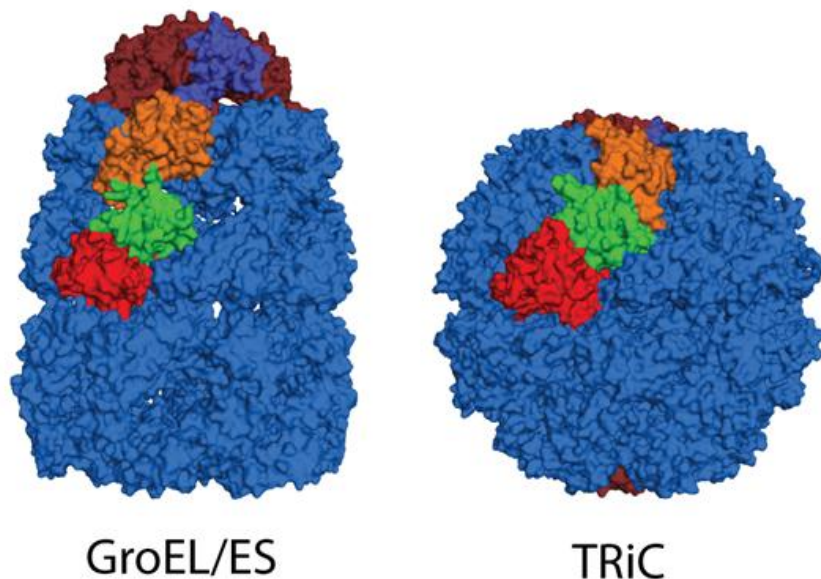


Figure 7: Structural comparison of group I (GroEL/ES) and group II (TRiC) chaperonins. PDB files of respective crystal structures ((3P9D, Dekker et al., 2011) and (1AON, Xu et al., 1997)) have been modified using PyMOL (DeLano Scientific). The design of this figure was inspired by Gutsche et al., 1999. The complexes are not drawn to scale. For better understanding one subunit of each complex was colored by domains using the same color code as in Figure 6. The other subunits are shown in blue. GroES and the helical protrusion region of TRiC were colored in brown.

In group II chaperonins the movements that are induced by ATP binding and hydrolysis are entirely different. ATP binding results in a 45° counterclockwise rotation of the apical domain. Upon ATP hydrolysis the entire subunit moves towards the center of the cavity by a large rocking motion hinged in the equatorial domain (Zhang et al., 2011). Thus, a stably closed group II chaperonin complex cannot be obtained by non-hydrolysable ATP analogs. Instead, a stably closed complex is achieved experimentally by analogs of the transition state of ATP hydrolysis, usually generated by incubation with ADP or ATP and aluminum fluoride (AlFx) (Chabre, 1990; Martin, 1988; Meyer et al., 2003). There are no structural constraints that would suggest that a concerted closure of the cavity would be preferred. Rather there is genetic and structural

evidence for a sequential mechanism of ring closure in group II chaperonins (Lin and Sherman, 1997; Rivenzon-Segal et al., 2005).

#### 2.4.2 Structural Characterization of Chaperonins

Chaperonins work as allosterically regulated “two-stroke” machines (Xu and Sigler, 1998), exhibiting negative cooperativity in ATP binding and hydrolysis between the two rings (Yifrach and Horovitz, 1995) thereby generating asymmetric complexes (Langer et al., 1992) with one ring closed (*cis* ring) and the other ring open (*trans* ring) during the functional cycle. Such a “bullet-like” (Ishii et al., 1992) complex has been characterized structurally at high resolution for the bacterial group I chaperonin GroEL (Xu et al., 1997) (Figure 7). The first crystal structure of a group II chaperonin was that of the symmetrically-closed thermosome from the archaeon *Thermoplasma acidophilum* (Ditzel et al., 1998). Structure determination of the eukaryotic group II chaperonin TRiC has proven to be more difficult. However, now crystal structures of TRiC in the open (Munoz et al., 2011) and in the closed (Dekker et al., 2011a) conformation as well as a high resolution cryo-EM structure of closed TRiC (Cong et al., 2010) are available. Additionally, the hexadecameric group II chaperonin from *Methanococcus maripaludis* (Mm-cpn) has gained attention for structure determination because its homo-oligomeric nature makes it a useful tool for introducing and studying point mutations and deletions. The open and the closed states have both been characterized by crystallography (Pereira et al., 2010) as well as cryo-EM (Zhang et al., 2010).

All the above mentioned structures show group II chaperonins in a symmetric conformation with either both rings closed (Figure 7) or both rings open. Structural indications for an asymmetric TRiC complex came mainly from low resolution cryo-EM (Llorca et al., 1999b) and small angle X-ray scattering (SAXS) (Meyer et al., 2003) data. Asymmetric structures of archaeal group II chaperonins have also been described (Clare et al., 2008; Schoehn et al., 2000). However, the observed negative cooperativity between the two rings suggested that the asymmetric complex might represent the physiologically more relevant conformation (Kafri et al., 2001; Reissmann et al., 2007; Yebenes et al., 2011). Finally, an asymmetric TRiC complex has recently been characterized structurally by symmetry-free cryo-EM reconstruction (Cong et al., 2011). The

asymmetric TRiC complex had been obtained by incubation with ADP and AlFx as described earlier (Meyer et al., 2003).

### 2.4.3 The Intra- and Interring Arrangement of TRiC Subunits

It is widely accepted that the individual TRiC subunits arrange in a fixed and unique orientation within one ring as well as between the rings. However, the exact intra- and inter-ring configuration was unclear during the last decade. Early experiments inferred the intra-ring subunit orientation from TRiC “micro-complexes” of 60-250 kDa that occurred upon sucrose density centrifugation and that had different subunit compositions (Liou and Willison, 1997). Based on cryo-EM structures of TRiC in complex with subunit-specific antibodies, an inter-ring orientation has been hypothesized under the assumption that the originally proposed intra-ring orientation was correct (Martin-Benito et al., 2007). Two recent higher resolution cryo-EM and crystal structures, which are not consistent among themselves, have challenged the original model (Cong et al., 2010; Dekker et al., 2011a). However, the limited resolution of both data sets has prevented an unambiguous assignment of the different subunits. In any case, the two-fold symmetry observed in both data sets clearly suggested two homotypic inter-ring contacts (Figure 8) at opposite sides of the ring, which has not been predicted by the earlier model. The definite intra- and inter-ring order of subunits was finally inferred from mass spectrometry detection of cross-linked peptides of different subunits (Kalisman et al., 2012; Leitner et al., 2012). The proposed subunit order differs from all previously suggested orientations, but has two homotypic inter-ring contacts as previously suggested. The fact that the same order of subunits has been found independently for both bovine and yeast TRiC makes it likely that the correct subunit order has been finally detected.

### 2.4.4 TRiC Co-Chaperones

For the eukaryotic chaperonin TRiC, several co-chaperones have been described that co-operate with TRiC. Delivery of the cytoskeletal proteins actin and tubulin to TRiC has been reported to be achieved by a hexameric jellyfish-like complex called prefoldin (Hansen et al., 1999; Martin-

Benito et al., 2002; Siegert et al., 2000; Vainberg et al., 1998). Another group of TRiC co-chaperones is the phospho-ucin-like proteins (PhLPs) (Willardson and Howlett, 2007). It is known that they build ternary complexes with TRiC and the substrate. The exact mechanism by which they modify and assist the TRiC-dependent folding reactions is still unclear. PhLP1 is essential for the folding of the G $\beta$  subunit of trimeric G-proteins (Lukov et al., 2006). PhLP3 has been reported to modulate the TRiC-dependent folding of actin and tubulin (Stirling et al., 2006).

## 2.5 Chaperonin-Substrate Interaction

The fate of chaperonin substrates during the interaction with the chaperonin has been investigated in great detail, especially for the bacterial GroEL/ES system. Substrates bind to hydrophobic residues in the apical domain of GroEL (Fenton et al., 1994). Binding of ATP to the equatorial domain of GroEL induces conformational changes that facilitate binding of GroES to the apical domain (Sigler et al., 1998). This in turn leads to release of the substrate from its GroEL binding sites and to encapsulation within the closed chaperonin *cis* ring. ATP hydrolysis results in a decreased stability of the GroEL/ES complex and finally ATP binding to the *trans* ring initiates release of GroES, substrate and ADP (Rye et al., 1997).

It has been discussed intensively whether the GroEL cavity would be essentially working as a so called “Anfinsen cage” (Saibil et al., 1993), i.e. by passively preventing aggregation of the substrate by encapsulation (Apetri and Horwich, 2008; Horwich et al., 2009), or whether GroEL would, in addition, actively change the folding landscapes of its substrates by confinement within the cavity, thereby preventing formation of extended conformations and thus accelerating the rate of folding (Baumketner et al., 2003; Brinker et al., 2001; Tang et al., 2006). Recently it has been shown that the acceleration in the rate of folding of the GroEL substrate DM-MBP by GroEL can be mimicked by introduction of disulfide bonds into DM-MBP, which reduces the conformational space of the protein during folding (Chakraborty et al., 2010). Thus, similar rate acceleration can be achieved by different conformational constraints, either by confinement inside GroEL/ES or by disulfide bonds, strongly suggesting that confinement of substrates plays a major role in the mechanism of rate acceleration by GroEL/ES.

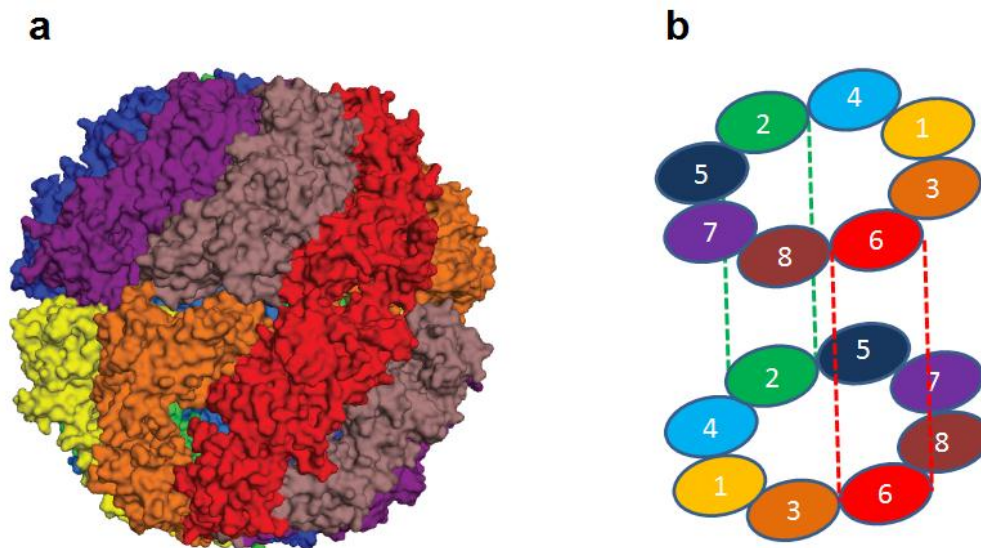


Figure 8: The subunit orientation of TRiC. **a)** PDB file of respective crystal structure ((3P9D, Dekker et al., 2011) has been modified using PyMOL. Each TRiC subunit is colored in an individual color. Note one of the two homotypic contacts across the equator (red subunit). **b)** Schematic representation of TRiC subunit orientation adapted from Leitner et al., 2012. Each subunit is colored in an individual color. The homotypic inter-ring contacts of subunits 2 and 6 are indicated by dashed lines.

The mechanism of folding of substrates by the eukaryotic chaperonin TRiC contains additional layers of complexity. In contrast to GroEL, TRiC is not homo-oligomeric. In fact, the octameric rings of TRiC contain eight different but paralogous subunits (Figure 8) with approximately 30% amino acid identity that have diverged very early in the evolution of eukaryotes (Archibald et al., 2001; Kubota et al., 1995). The different subunits are described by the Greek letters  $\alpha$ ,  $\beta$ ,  $\gamma$ ,  $\delta$ ,  $\epsilon$ ,  $\zeta$ ,  $\eta$  and  $\theta$  in mammalian TRiC and by the numbers 1-8 in yeast (Yebeles et al., 2011). Comparison of the mammalian orthologous subunits reveals a high degree of conservation with an amino acid identity of 95% between the orthologues. 60% identity remains even between mammalian and yeast orthologues (Kim et al., 1994), suggesting non-redundant functions of the individual subunits in the hetero-oligomeric TRiC complex. The identity of amino acids between the different subunits is not equally distributed. The equatorial ATPase domains are much more similar than the apical substrate binding domains (Kim et al., 1994). Divergence of the apical domains suggests a specialization of the different subunits in substrate binding.

### 2.5.1 Binding of Substrates to Chaperonins

In group I chaperonins, substrate binding is mediated by a hydrophobic groove between helices H and I in the apical domain (Chen and Sigler, 1999). It has been hypothesized that substrate binding in group II chaperonins takes place at a structurally related region between the apical helices H10 and H11 (Pereira et al., 2010). Strikingly, substrate specificity of different subunits for the known TRiC substrate VHL tumor suppressor can be transferred from one subunit to the other by exchanging the substrate binding motif in helix H11 (Spiess et al., 2006). Subunit specific binding of substrates to TRiC has also been shown for the most prominent substrates actin and tubulin (Llorca et al., 2000; Llorca et al., 1999a). It is well conceivable that the subunit specific binding of substrates plays an important role in the folding mechanism of TRiC-dependent substrates, especially considering the presumed sequential mode of cavity closure. Furthermore, it was shown by FRET measurements that binding of actin to TRiC opens the nucleotide binding cleft of actin substantially more than binding to GroEL (Villebeck et al., 2007a). Notably, GroEL can neither support folding of actin nor of tubulin (Tian et al., 1995).

### 2.5.2 The Size of the Chaperonin Cavity

The exact size of the TRiC cavity remains to be determined. Even before the high resolution structures were released, it was clear from lower resolution cryo-EM data (Booth et al., 2008) that the overall TRiC architecture is very similar to that of the thermosome from *T. acidophilum* whose cavity size was shown to be approximately 130,000 Å<sup>3</sup> (Ditzel et al., 1998). Indeed, the crystal structure of yeast TRiC in the closed state estimated the TRiC cavity volume to be approximately 145,000 Å<sup>3</sup> (Dekker et al., 2011a). This is only around 80% of the volume of the *cis* GroEL cavity which has a size of 175,000 Å<sup>3</sup> (Xu et al., 1997). However, a recent cryo-EM study captured an asymmetric state of TRiC induced by ADP and AlFx exhibiting an enlarged *cis* cavity (Cong et al., 2011), which is likely to represent a physiological intermediate of the folding cycle as suggested by the negative cooperativity between the two rings of TRiC (Kafri et al., 2001; Yifrach and Horovitz, 1995). The size of this enlarged cavity is approximately 180,000 Å<sup>3</sup> and thus theoretically large enough for encapsulation of proteins up to 70 kDa. Similarly, the GroEL *cis* cavity could accommodate substrate proteins of up to 70 kDa (Xu et al., 1997).

However, it has been shown by protease protection experiments that the actual upper size limit is approximately 60 kDa (Sakikawa et al., 1999).

## 2.6 Chaperonin Interactomes

### 2.6.1 Comparison of Prokaryotic and Eukaryotic Proteomes

Sequencing of whole genomes and subsequent assignment of protein coding regions has enabled the comparison of protein sequences from different kingdoms of life. Interestingly, eukaryotic proteins are on average approximately 50% longer than prokaryotic proteins (Zhang, 2000). However, protein domains have comparable average sizes of 200-250 amino acids in both eukaryotes and prokaryotes. Instead, the increased size of eukaryotic proteins (Figure 9) is caused by an increased number of domains per polypeptide in eukaryotes compared to prokaryotes (Brocchieri and Karlin, 2005). The different average size distributions of pro- and eukaryotic proteins are also reflected in the different interactomes of the respective representative chaperonins, GroEL and TRiC.

### 2.6.2 TRiC Interactors

In 2008, two independent studies have addressed the interactome of the eukaryotic chaperonin TRiC (Dekker et al., 2008; Yam et al., 2008). Dekker et al. investigated the TRiC interactome in yeast by both proteomic and genetic methods. Physical TRiC interactors were found by pull-downs of TRiC complexes carrying an affinity tag, followed by mass spectrometry. Genetic interactors were identified by a synthetic genetic array (SGA) (Tong et al., 2001). All viable yeast deletion mutants were combined with a temperature-sensitive TRiC mutant and the resulting double-mutants were analyzed for synthetic sickness/lethality. Notably, genetic TRiC interactors do not represent TRiC substrates but they are rather functionally overlapping with

TRiC substrates. The combination of the compromised function of a TRiC substrate with the deletion of a protein with overlapping function causes the synthetic defect (Dekker et al., 2008).

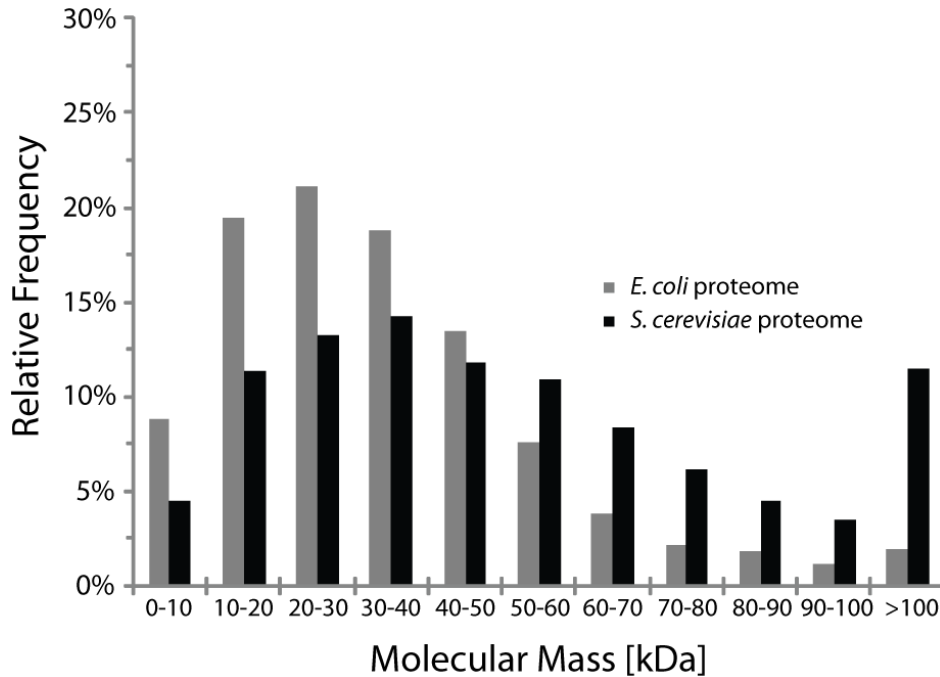


Figure 9: Size distribution of a prokaryotic and a eukaryotic proteome. The respective protein lists have been downloaded from <http://ecocyc.org/query.shtml> for *E. coli* and from [http://downloads.yeastgenome.org/curation/calculated\\_protein\\_info/](http://downloads.yeastgenome.org/curation/calculated_protein_info/) for *S. cerevisiae*.

When known co-chaperones are excluded, 150 physical TRiC interactors remain in the Dekker et al. study among them the well described TRiC substrates actin and tubulin (Figure 10). 79 of the interactions have been identified by Dekker et al. themselves in their mass spectrometry experiments. 47 interactors originate from various comprehensive yeast protein-protein interaction studies cited by Dekker et al. (Gavin et al., 2006; Graumann et al., 2004; Ho et al., 2002; Krogan et al., 2006). The remaining 24 interactors were described by Dekker et al. in the supplement without a precise indication of source.

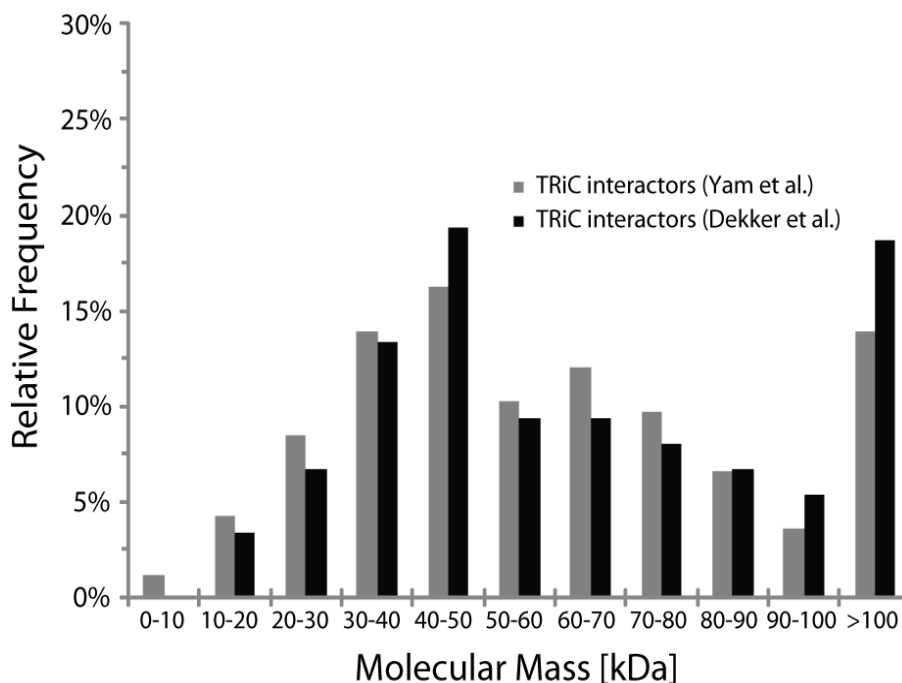


Figure 10: Comparison of TRiC interactomes described by Yam et al., 2008 (166 interactors) and Dekker et al., 2008 (150 interactors as described above).

An independent study conducted by Yam et al. identified TRiC interactors by expression of mouse cDNAs in an *in vitro* transcription/translation system – rabbit reticulocyte lysate (RRL) – followed by a pull-down using an antibody targeting the TRiC  $\beta$  subunit. The screen comprised 2600 cDNA clones, 1500 of which were estimated to result in detectable translation products. A list of 166 TRiC interactors is provided in the supplement of Yam et al., consisting of both interactors identified by Yam et al. themselves and of interactors described in the literature (Figure 10). Unfortunately, the sources of the interactions are not indicated and the list does not differentiate between mammalian and yeast proteins.

A one-to-one comparison of the TRiC interactomes of the two studies is not possible because interactors from different organisms are described. However, it is reasonable to assume that the TRiC-dependency for folding might be conserved for a given TRiC substrate from yeast to mammals. The list of 166 TRiC interactors provided by Yam et al. contains 127 proteins that are either yeast proteins or proteins for which a yeast homologue is known. Surprisingly, only 34 of these proteins were also described by Dekker et al. to be TRiC interactors. Moreover, 24 of these interactors described by both studies were actually cited from the literature and thus they do not

represent a real experimental overlap. Interestingly, among the remaining 10 proteins that were identified by both studies are actin and tubulin. Thus, it seems that the provided lists of TRiC interactors might on the one hand contain a substantial number of false positive interactors while on the other hand a number of authentic interactors might be missing. Despite the small overlap between the studies by Dekker et al. and Yam et al. on the TRiC interactome, the size distributions of the described TRiC interactors of both studies are remarkably similar (Figure 10), suggesting that the lists provide a good reflection of the size distribution of the authentic TRiC interactome regardless of their imperfection in detail.

### 2.6.3 GroEL Interactors

252 substrates of GroEL have been described in *E. coli* (Kerner et al., 2005), 22 (~9%) of which exceed 70 kDa (Figure 11). It is unclear how folding of these larger substrates is achieved. A cryo-EM study described an unusually expanded cavity of the single-ring mutant of GroEL encapsulating a 86 kDa protein (Chen et al., 2006). Another study suggested that folding of an 82 kDa substrate occurred *via* interaction with the GroEL *trans* ring without encapsulation by GroES (Chaudhuri et al., 2001). However, the physiological relevance of each of these mechanisms is not comprehensively understood so far.

### 2.6.4 Comparison of Interactors of GroEL and TRiC

Strikingly, the interactomes of the group I chaperonin GroEL and the group II chaperonin TRiC differ substantially with respect to their molecular weight distribution (Figure 11). Only 9% of the described GroEL interactors exceed the predicted upper size limit of the *cis* cavity of 70 kDa, essentially reflecting the size distribution of the *E. coli* proteome (<http://ecocyc.org/query.shtml>) with 7% of proteins larger than 70 kDa (Figure 9). Eukaryotic proteins have a higher average molecular weight than prokaryotic proteins (Brocchieri and Karlin, 2005; Netzer and Hartl, 1998; Zhang, 2000) (Figure 9). In fact, one quarter of all proteins from the baker's yeast *S. cerevisiae* are larger than 70 kDa, as estimated from genomic data ([http://downloads.yeastgenome.org/curation/calculated\\_protein\\_info/](http://downloads.yeastgenome.org/curation/calculated_protein_info/)). The relative amount of

large TRiC substrates even exceeds this number; almost 40% of the described TRiC interactors are larger than 70 kDa, indicating that especially larger proteins need the assistance of TRiC for proper folding (Figures 10 and 11).

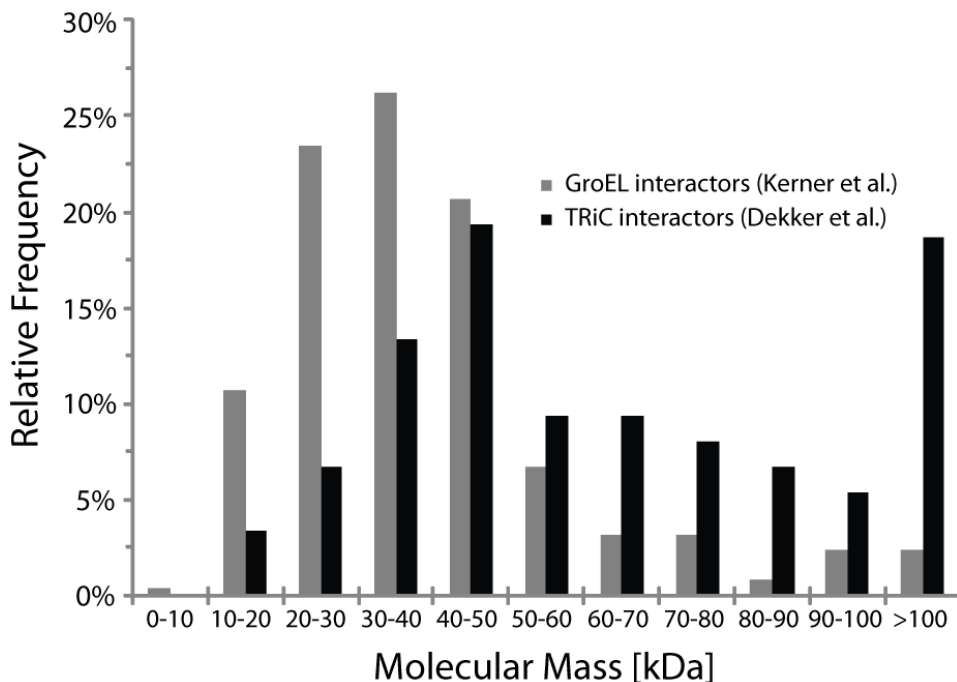


Figure 11: Size distributions of interactomes of GroEL and TRiC. 252 GroEL interactors as described by Kerner et al., 2005. 150 TRiC interactors from Dekker et al., 2008 modified as described above.

## 2.7 Aim of the Study

The mechanism by which chaperonins can assist the folding of proteins that are too large for encapsulation inside the central cavity is still unclear. It has been hypothesized that folding of large multi-domain substrates by TRiC might occur by partial encapsulation of the proteins (Spiess et al., 2004). This idea is especially interesting from an evolutionary perspective considering the sequential iris-like mechanism of lid closure (Pereira et al., 2010) that is found in group II chaperonins but not in group I chaperonins. It is tempting to speculate that this mechanism might have evolved to facilitate partial encapsulation of large multi-domain proteins,

which is not straightforward if a GroES-like co-chaperone is required for closing the cavity. However, it has never been investigated whether partial encapsulation of large substrates in TRiC occurs, and if so, whether it leads to productive folding.

The present work addressed these questions experimentally, using different fusion proteins of the well-described TRiC substrate actin with GFP and BFP as a model for large multi-domain proteins containing a TRiC-dependent domain. Actin folding was measured by two independent methods, its ability to bind to DNase I as well as the occurrence of a protease-resistant actin core in limited proteolysis experiments. Furthermore, the encapsulation of the actin fusion proteins or parts thereof inside the TRiC cavity was demonstrated by protection against proteolysis induced by closure of the chaperonin cage. In order to expand the study to a more physiological setting, various described TRiC interactors of large size were tested experimentally for interaction with TRiC and two strong interactors were tested for partial encapsulation.

## 3. Results

### 3.1 TRiC-dependent Folding of Actin Fusion Proteins

The cytoskeletal protein actin is well-suited to be used as a model TRiC substrate because it is strictly dependent on TRiC to reach its native state. It has been shown both *in vitro* (Gao et al., 1992; Stemp et al., 2005) and *in vivo* (Chen et al., 1994; Vinh and Drubin, 1994) that TRiC function is required for proper folding of actin. It has been suggested that the interaction with TRiC is required to overcome a high energy barrier in the folding landscape of actin that occurs on the way towards a conformation that is able to bind nucleotide (Altschuler and Willison, 2008). The folding of actin can be monitored by its ability to bind to DNase I (Lazarides and Lindberg, 1974; Mannherz et al., 1980). Actin and DNase I form a 1:1 complex via an interaction of a loop in sub-domain 2 of actin (Kabsch et al., 1990). Importantly, the interaction of actin with TRiC is sufficient for actin folding in contrast to folding of tubulin, which requires additional chaperones (Lewis et al., 1997).

The actin sequence is highly conserved among eukaryotic species (Korn, 1982). In contrast, actin has diverged from its prokaryotic homolog MreB so far (van den Ent et al., 2001) that the structural relationship between both proteins was not apparent with pairwise sequence alignment (Erickson, 2007). Instead, a combination of sequence and structural alignments of actin, hexokinase and Hsc70, which all share the “actin fold” (Kabsch and Holmes, 1995), has led to the discovery of homologous bacterial proteins (Bork et al., 1992). Thus, the evolution of actin involved very rapid divergence from its prokaryotic homologs at the origin of eukaryotes followed by virtual constancy throughout eukaryotic evolution (Doolittle, 1995). The same phenomenon is found for tubulin, the other major cytoskeletal protein in eukaryotes (Doolittle, 1995). Strikingly, the evolution of the TRiC substrates actin and tubulin resembles the evolution of the different TRiC subunits that have diverged rapidly after gene duplications at the origin of eukaryotes (Archibald et al., 2001) and have been much more conserved during the following eukaryotic evolution.

### 3.1.1 Actin Fusion Proteins as Model for Multi-Domain TRiC Substrates

For my studies, I have used yeast actin (Act1p) which has 375 amino acids and is 88% identical to rabbit cytoplasmic  $\beta$ -actin. It has a molecular weight of approximately 42 kDa and is thus too small to serve as a model for proteins that are exceeding the TRiC cavity, which can accommodate proteins of 50-60 kDa (Dekker et al., 2011a; Ditzel et al., 1998) or even up to 70 kDa (Cong et al., 2011). Therefore, I used fusion proteins, in which actin was connected with GFP alone or with BFP and GFP in different combinations (Figure 12) by flexible alanine-rich linkers. These linkers have all been derived from the 16 amino acid linker L16 (TSGSAASAAGAGEAAA) that has been described in an earlier publication from our group (Chang et al., 2005). Most of the constructs I used for the initial DNase I binding experiments had been cloned by Markus Stemp, a former PhD student in the lab. I have cloned the BGA construct.

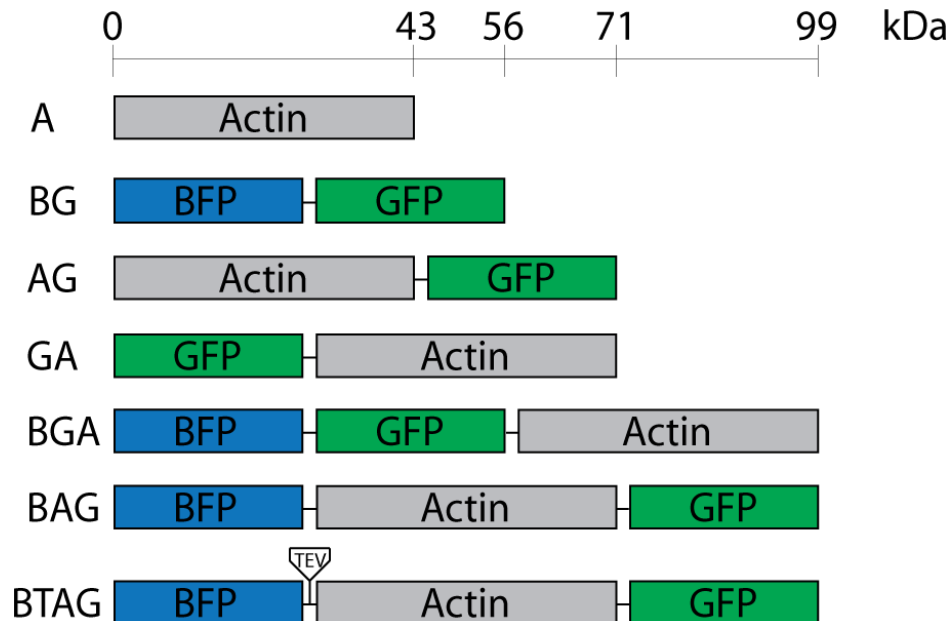


Figure 12: Schematic representation of different actin fusion constructs. The calculated molecular weight of the respective constructs is indicated on top. The TEV-cleavage site in the linker between BFP and actin in BTAG is shown schematically.

### 3.1.2 Actin Folding Estimated by DNase I Binding Experiments

The different actin fusion proteins were expressed in a coupled transcription/translation system from Promega, which is based on rabbit reticulocyte lysate (RRL), using plasmid DNA containing the respective genes as well as a T7 promoter. The proteins were labeled by L-[<sup>35</sup>S]-Methionine incorporation and detected by autoradiography after SDS-PAGE. All proteins were soluble after expression in RRL. The DNase I binding experiment was designed in a way that resulted in a ten times higher concentration of the “Eluate” sample compared to the “Input” sample in order to enable the detection of weak binding to DNase I. Consequently, “Eluate” bands can have a higher intensity than “Input” bands (Figure 13a). Bands of equal intensity correspond to 10% binding to DNase I.

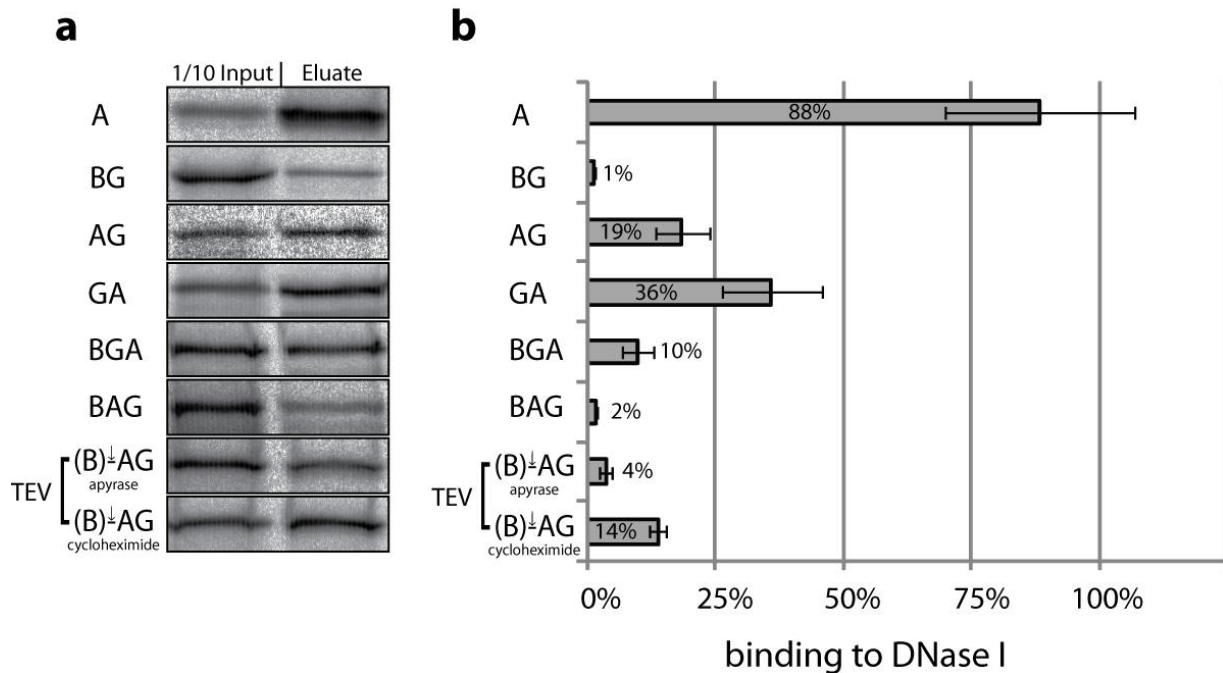


Figure 13: Binding of fusion proteins to DNase I. **a)** Representative autoradiographs after SDS-PAGE, showing the amount of DNase I bound protein in comparison with one tenth of the input material. **b)** Quantification of the respective bands using the AIDA software (raytest). Error bars indicate the standard deviation of N ≥ 3 independent experiments.

To perform the pull-down assays, commercial DNase I was immobilized on CNBr-activated Sepharose. Actin alone served as a positive control for binding to DNase I. On average of 88% of the actin produced in RRL was pulled down from the lysate by the DNase I Sepharose beads

(Figure 13). BFP-GFP (BG) served as a negative control to monitor unspecific binding to the beads, which was determined to be 1% of the total synthesized protein on average (Figure 13). Thus, the DNase I binding assay exhibits a high range between specific and background binding, making it an appropriate tool for determination of actin folding.

The amount of DNase I bound GA (36%) and AG (19%) in comparison to the BG background (1%) clearly indicates that a substantial fraction of actin in both fusion proteins reached the native DNase I binding competent conformation (Figure 13). However, DNase I binding was less efficient than for actin alone, indicating that the presence of GFP interferes with folding of actin. Apparently, the incompletely folded actin did not give rise to aggregates, as no insoluble protein was observed. The DNase I binding assay was always performed after 90 minutes of translation in RRL and the kinetics of occurrence of DNase I binding competent actin were not investigated. Therefore, it is possible that the rate of actin folding was decreased by the fusion with GFP and that more folded actin would have been produced after a longer period of incubation. There might be a change in the cycling rate of TRiC induced by the presence of a large substrate, leading to a slower turnover of the TRiC-GA and TRiC-AG complexes compared to the TRiC-actin complex. More likely, the efficiency of the actin folding reaction was reduced for the fusion protein due to interference between the actin moiety and the fused GFP/BFP domain.

Interestingly, the fraction of DNase I bound GA is almost twice as high as the fraction of DNase I bound AG (Figure 13). This is surprising because the N- and the C-terminus of actin are located in close proximity in sub-domain 1 (Kabsch et al., 1990) and thus GFP is expected to be in a similar position relative to actin in both GA and AG. However, both proteins differ obviously in their topological arrangement and the spatial constraints that are imposed on actin during the process of folding. Indeed, it has been suggested that the correct re-positioning of the actin C-terminus into its final location in sub-domain 1 is a late and essential step in the folding process of actin (Lee et al., 2012; Neiryneck et al., 2006). It is possible that the presence of GFP at the actin C-terminus is interfering with this re-positioning step, thus making folding of AG less efficient compared to folding of GA.

Both actin-GFP and GFP-actin fusion proteins are incorporated into cellular F-actin structures (Ballestrem et al., 1998; Doyle and Botstein, 1996; Fischer et al., 1998; Heidemann et al., 1999; Verkhusha et al., 1999; Yoon et al., 2002), indicating correct actin folding. However, it is not

clear if the GFP-actin fusion proteins are really too large for complete encapsulation inside the TRiC cavity. Thus, I analyzed a construct, in which two fluorescent proteins were fused to actin, namely BFP to the actin N-terminus and GFP to the actin C-terminus. DNase I binding of this construct (BAG) was close to the background level (Figure 13). In order to determine whether this was due to reduced folding of actin or due to impairment of DNase I binding by sterical reasons in presence of two fluorescent proteins, we prepared a construct, in which the linker between BFP and actin contained a TEV-cleavage site enabling selective removal of the N-terminal BFP. TEV-cleavage of this construct (BTAG) results essentially in production of AG. We tested DNase I binding of BTAG after cleavage with the TEV (tobacco etch virus) protease (Parks et al., 1994) under two different conditions. Before cleavage of BFP, translation was stopped with either apyrase (Komoszynski and Wojtczak, 1996) or cycloheximide (McKeehan and Hardesty, 1969). Cycloheximide is a specific inhibitor of translation and does not affect the function of TRiC or other chaperones in the lysate. DNase I binding of AG produced by TEV-cleavage of BTAG after translation stop with cycloheximide was comparable to DNase I binding of the regular AG construct described before, probably because TRiC was still active after cleavage. In contrast, addition of apyrase stops all ATP-dependent processes in the lysate, including TRiC function. The fact that DNase I binding of AG produced after cleavage of BTAG in presence of apyrase is not markedly different from DNase I binding of uncleaved BTAG indicates that actin was misfolded in the full-length BTAG protein (Figure 13). Thus, TRiC is unable to fold actin sided by GFP domains at both ends.

The impaired folding of actin in BAG does not necessarily mean that folding of such “middle-domains” by TRiC is impossible. Another explanation is that imposing constraints on both the N- and the C-terminus of actin is fatal for actin folding, especially considering the close proximity of both termini in the actin structure. To test this possibility, we prepared another large fusion protein, in which only one of the actin termini is attached to fluorescent proteins. We used GA as a starting point for this new construct because GA was folded more efficiently than AG. Fusion of BFP to the GA N-terminus resulted in the construct BGA (99 kDa). 10% of BGA bound to DNase I on average, demonstrating that TRiC can mediate the folding of actin in context with such a large protein, although with reduced efficiency.

### 3.1.3 Actin Folding Estimated by Protease-Resistant Actin Fragment

To confirm the results obtained by DNase I binding experiments, I used a different method to quantify actin folding. This method is based on the fact that fragments produced by limited proteolysis of native actin and of partially unfolded actin differ substantially (Kuznetsova et al., 1999). Digest of native actin with proteases of different specificity results in C-terminal protease-resistant fragments of 33-35 kDa dependent on the respective protease (Mornet and Ue, 1984). In contrast digest of non-native actin with various proteases does not result in production of a comparably stable protease-resistant fragment (Kuznetsova et al., 1999). Thus, it is conceivable that the relative amount of the protease-resistant actin fragment occurring upon digest of the different actin fusion proteins can be used as an inherent measure for the folding efficiency of each construct.

In order to find out whether the protease-resistant actin fragment was indeed a useful measure for actin folding, we quantified the intensity of the respective fragment from PK digest reactions of various actin fusion proteins and correlated it to the intensity of the corresponding full-length protein band (incubated without PK). Indeed, the estimation of the relative amount of properly folded actin based on the ratio of the intensities of the protease-resistant fragment and of full-length actin correlates well with the estimation of actin folding based on DNase I binding experiments (Figures 13 and 14). Thus, it appears that the relative intensity of the protease-resistant fragment is a good estimate for actin folding. The quantification of actin folding by the occurrence of the protease-resistant fragment is particularly advantageous for the actin fusion constructs because the GFP and/or BFP domains hinder DNase I binding sterically, resulting in an underestimation of folded actin.

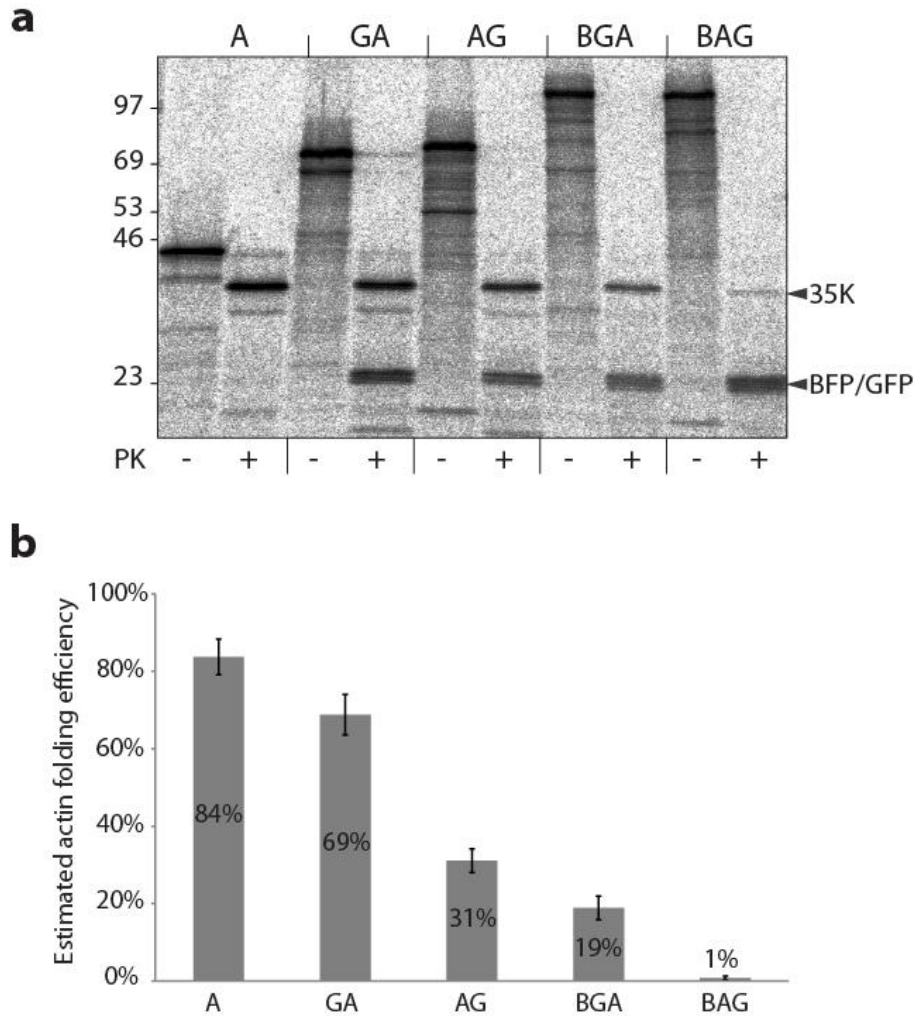


Figure 14: Actin folding estimated from protease-resistant actin fragment of 35 kDa. **a)** Representative autoradiograph of SDS-PAGE, showing PK digest of indicated actin fusion proteins. The molecular weight marker indicates the molecular weight in kDa. Protease-resistant BFP/GFP and the 35 kDa actin fragment (35K) are indicated on the right. **b)** Estimation of actin folding by quantification of the relative intensity of the 35 kDa actin fragment, corrected for number of methionine residues. The error bars indicate the standard deviation of N=3 independent experiments.

Comparison of the estimated folding efficiencies based on either the protease-resistant fragment or on DNase I binding reveals that in case of most actin fusion proteins, actin folding might have been indeed underestimated by DNase I binding (Figures 13 and 14). However, there is hardly any protease-resistant fragment detected upon digest of BAG (Figure 14), indicating once more that actin is not folded in the context of this particular fusion protein, as already inferred from DNase I binding experiments (Figure 13). Thus, despite the slightly different estimations of actin

folding by DNase I binding and by intensity of the protease-resistant fragment, the overall conclusions that were based on DNase I binding remain unchanged.

### 3.1.4 Depletion of TRiC from RRL

To formally demonstrate the TRiC dependence of actin folding (Chen et al., 1994; Gao et al., 1992; Stemp et al., 2005; Vinh and Drubin, 1994), TRiC was depleted from RRL. Depletion was achieved by Markus Stemp using the high affinity TRiC interactor PhLP1 that was purified after overexpression in *E. coli*. Purified PhLP1 was coupled to Dynabeads® TALON™ via an N-terminal 6xHis-tag and used for depletion of TRiC from RRL. Depletion of TRiC led to a strong decrease in DNase I binding of actin and the actin fusion proteins AG and GA translated in the TRiC-depleted RRL (Figure 15). Production of DNase I binding competent actin and GA was completely restored by addition of TRiC that was purified from bovine testes (Figure 15). Surprisingly, DNase I binding of AG was only partially restored. It seems possible that rabbit TRiC from RRL and purified bovine TRiC differ in their ability to fold the less efficiently folding AG construct.

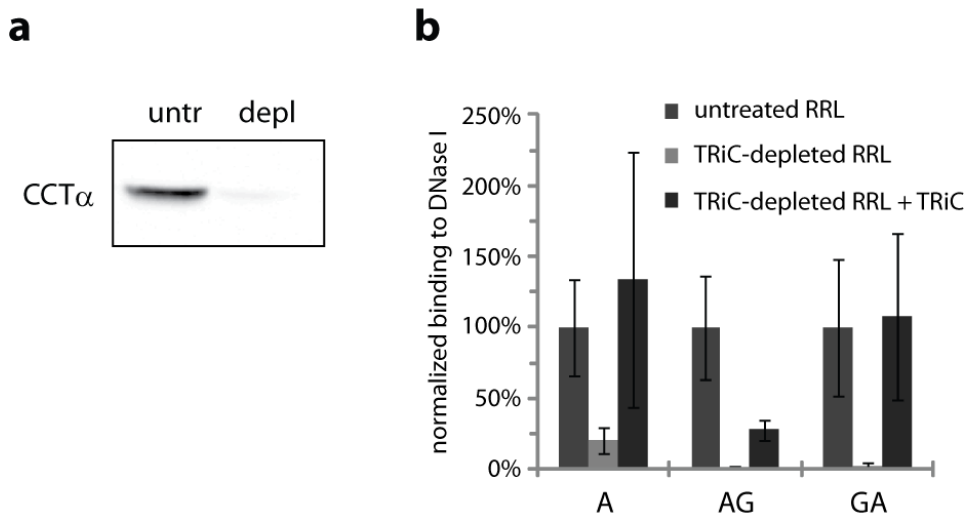


Figure 15: DNase I binding after depletion of TRiC from RRL. **a)** Representative Western Blot anti-CCT $\alpha$  showing successful depletion of TRiC from RRL. **b)** Quantification of DNase I binding. The error bars indicate the standard deviation N=3 independent experiments.

## 3.2 Stalling of Actin Fusion Proteins on the Ribosome

### 3.2.1 Stalling of Actin-GFP on the Ribosome

It has been shown by photo-crosslinking experiments that TRiC interacts co-translationally with ribosome-bound nascent chains (Etchells et al., 2005; McCallum et al., 2000). In order to test whether actin can be co-translationally folded into a native DNase I binding competent conformation, we prepared a shortened AG construct lacking a stop codon by PCR (AG219). This construct is translated in RRL like the full-length AG construct until the ribosome reaches the 3' end of the truncated mRNA, corresponding to amino acid 219 of GFP (Figure 16a). Because of the missing stop codon, a stalled ribosome nascent chain complex (RNC) is generated.

In SDS-PAGE, the stalled nascent chain migrates characteristically at a molecular weight that is approximately 20 kDa higher than that of the free polypeptide chain because of the attached peptidyl-tRNA (Figure 16b). This enables the quantification of the stalling efficiency by comparison between the intensities of stalled (+ tRNA) and released (- tRNA) chains. The stalling efficiency varied between 15% and 45% for AG219 in different experiments. DNase I binding can be quantified for the stalled nascent chain and the free polypeptide chain separately because of their different migration in SDS-PAGE. Interestingly, neither the stalled nor the released AG219 were binding to DNase I substantially more than the previously determined BFP-GFP background (Figure 16c). It is quite likely that actin folding is compromised by association with misfolded GFP folding intermediates, especially considering the  $\beta$ -barrel structure of GFP that is prone to misfolding while incomplete (Craggs, 2009; Richardson and Richardson, 2002).

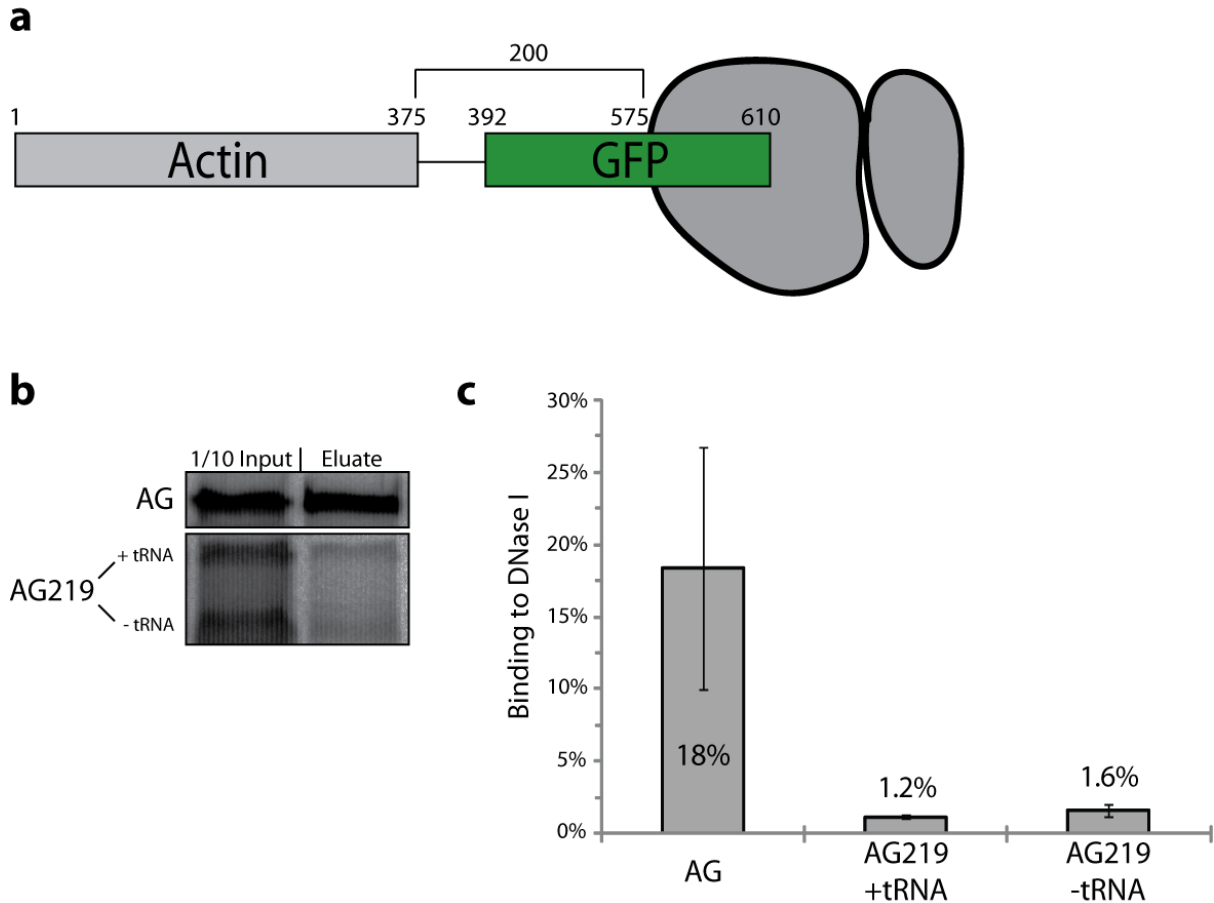


Figure 16: DNase I binding of stalled actin-GFP. **a**) Schematic representation of the stalled actin-GFP construct, not drawn to scale. Approximately 575 amino acids are outside the ribosomal exit tunnel, assuming that 35 amino acids span the distance from the peptidyl transferase center (PTC) until the end of the exit tunnel. The actin segment is thought to be separated from the ribosome by 200 amino acids in a stalled complex. **b**) Representative autoradiographs after SDS-PAGE. AG219  $\pm$  tRNA can be differentiated by different migration in SDS-PAGE. **c**) Quantification of the respective bands. The error bars indicate the standard deviation of  $N \geq 3$  independent experiments.

### 3.2.2 Stalling of Actin-Luciferase on the Ribosome

In order to generate actin stalling constructs that had a protein other than GFP fused to the actin C-terminus, we prepared an actin-luciferase construct. Using PCR we created three stalling constructs that differed in the length of the luciferase sequence (AL36, AL49 and AL61). The numbers indicate the number of luciferase amino acids that are included in the respective construct. The ribosomal exit tunnel has a length of approximately 100 Å and accommodates roughly 35 amino acids of the nascent chain, assuming a fully extended conformation (Lu and Deutsch, 2005). Thus, there are approximately 18, 31 or 43 amino acids in between actin and the

ribosome in AL36, AL49 and AL61 respectively, considering the 17 amino acid linker between actin and luciferase (Figure 17a).

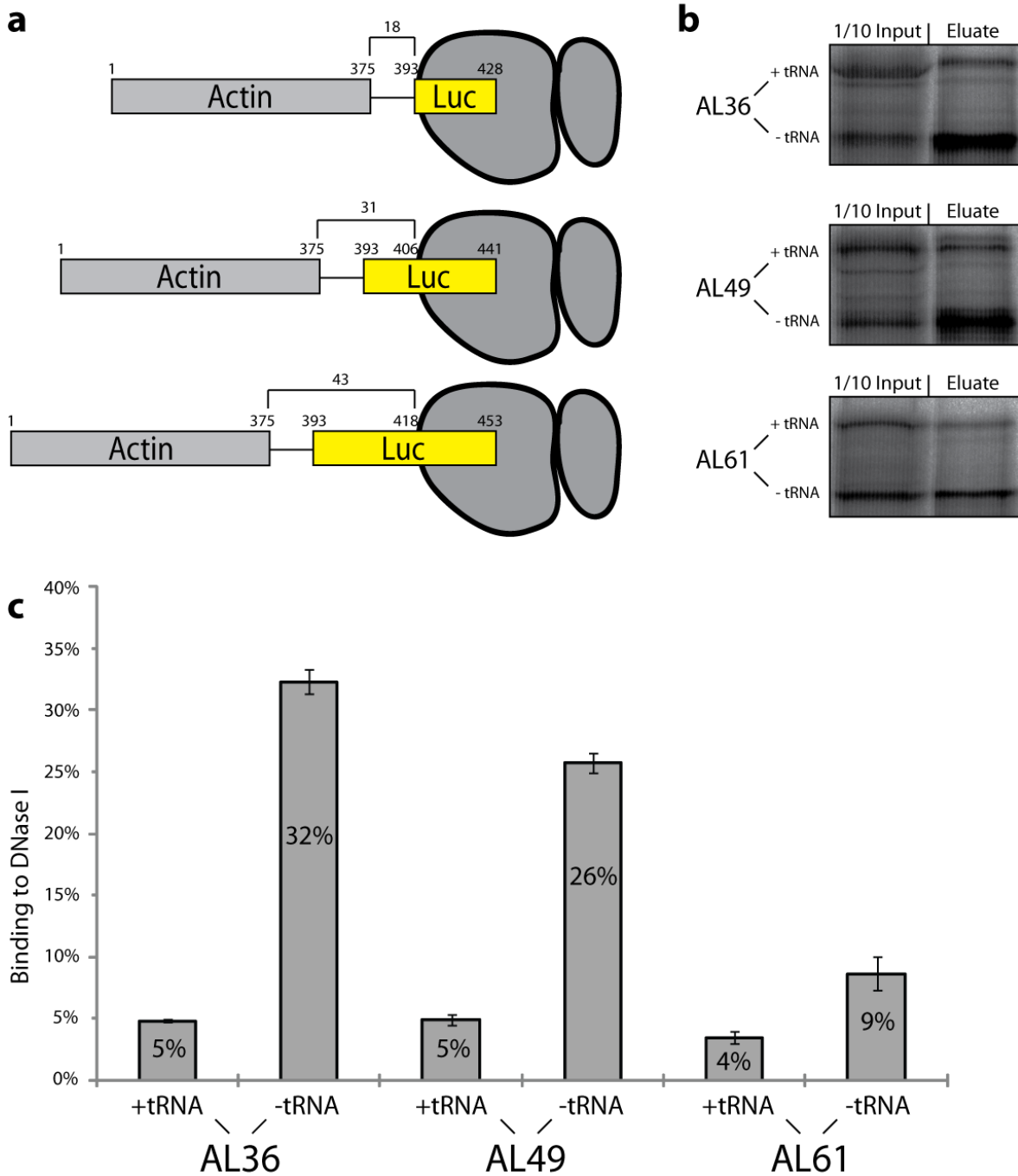


Figure 17: Stalling of actin-luciferase. **a)** Schematic representation of stalled actin-luciferase constructs, not drawn to scale. Calculation of amino acids outside the exit tunnel was done assuming that 35 amino acids span the distance from the PTC to the end of the exit tunnel. **b)** Representative autoradiographs after SDS-PAGE. **c)** Quantification of respective bands of N=2 independent experiments. The error bar indicates the standard deviation.

Folding of the free polypeptide chains is inversely dependent on the length of the luciferase fragment. The shorter the luciferase fragment, the more of the actin fusion protein is binding to DNase I (Figure 17). It is not implausible that the tendency of the incomplete luciferase chain to misfold is increasing with its length, which in turn might impair the folding of actin as observed for the truncated actin-GFP fusion protein. The DNase I binding ability of the ribosome-bound actin-luciferase chains is independent of the length of the luciferase fragment. Moreover, the values are only slightly increased compared to the background level (Figure 17). Thus, it is not possible to conclude that folding of ribosome-bound actin occurred.

### 3.2.3 Stalling of Actin with a Flexible Linker on the Ribosome

In order to exclude that actin folding was impaired by the adjacent luciferase fragment, a flexible linker of 97 amino acids consisting of GGGGS-repeats without a stop codon was attached to the actin C-terminus for stalling of translation (Figure 18a). The linker DNA sequence contained three unique motifs for binding of different primers to enable the creation of stalling actin constructs with different lengths of linkers by PCR (ActLink53, ActLink78 and ActLink97). Assuming that 35 amino acids span the ribosomal exit tunnel, actin is separated from the ribosome by flexible linkers of 18, 43 or 62 amino acids, respectively (Figure 18a).

Interestingly, DNase I binding of the ribosome-bound nascent chains again was close to the background level, independent of the length of the linker (Figure 18), suggesting that actin was not folded co-translationally into a DNase I binding competent conformation in either of the constructs. Thus, folding of actin at the ribosome appears generally impaired, independent of the linker length and sequence (Figures 16, 17, 18).

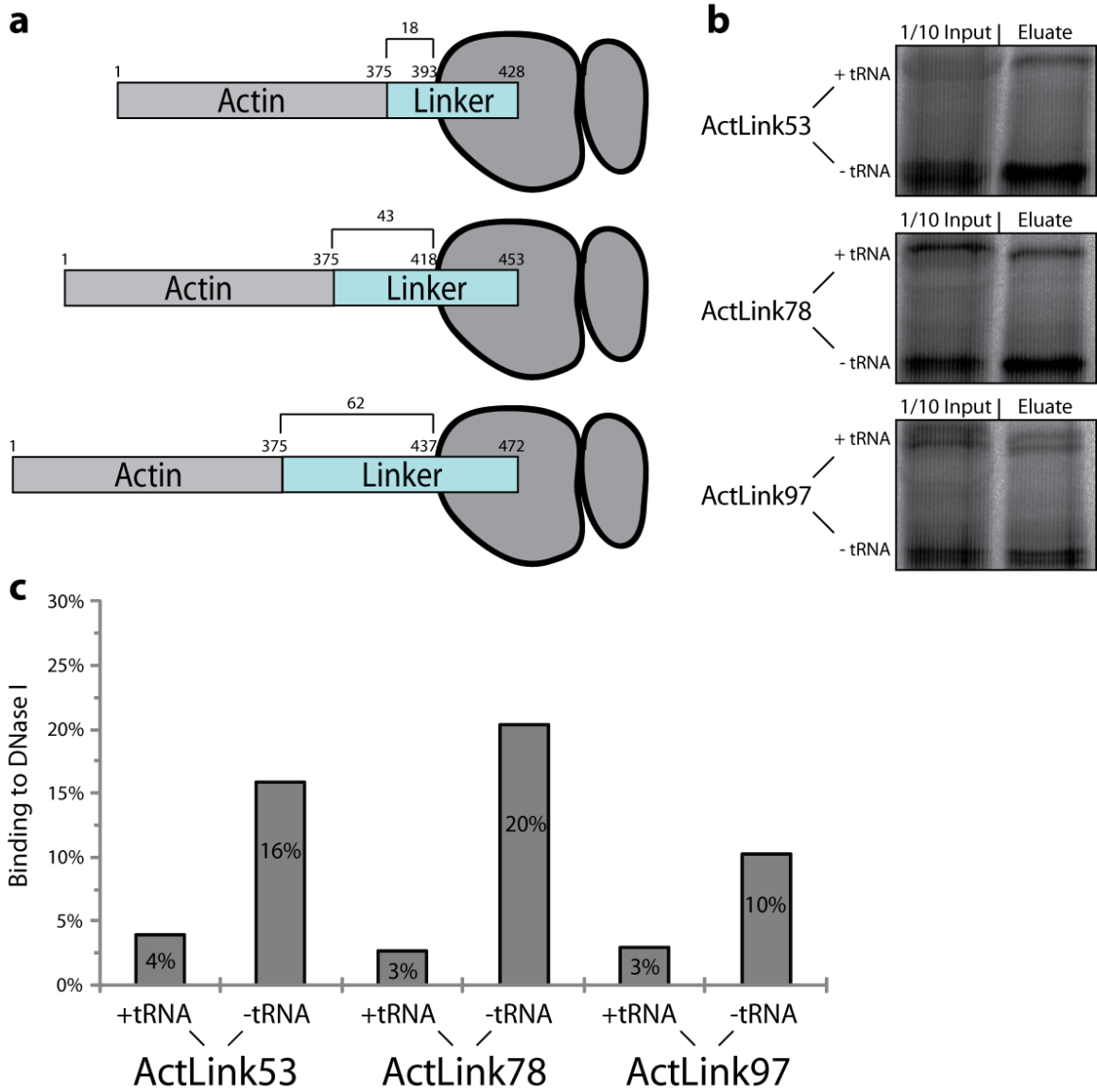


Figure 18: DNase I binding of stalled ActLink constructs. **a)** Schematic representation of ActLink constructs, not drawn to scale. Amino acids between actin and the ribosome were calculated assuming that 35 amino acids span the distance between the PTC and the end of the exit tunnel. **b)** Autoradiographs after SDS-PAGE showing the respective constructs  $\pm$  tRNA. **c)** Quantification of the respective bands of N=1 experiment.

In order to discern released translation product present before the DNase I binding step from material hydrolyzed during DNase I binding, separate DNase I binding reactions were performed for the free polypeptide and the ribosome-bound nascent chains. The two species were separated by ultra-centrifugation through a sucrose-cushion, resulting in sedimentation of ribosomes and ribosome-bound nascent chains (Figure 19).

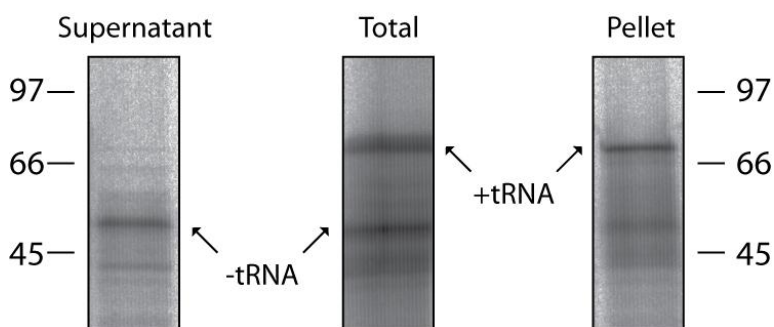


Figure 19: Separation of stalled from released ActLink78 by centrifugation through a sucrose cushion. Released ActLink78 is found in the supernatant. The ribosome-bound stalled nascent chains are enriched in the pellet fraction. The molecular weight in kDa is indicated.

To properly assess background binding, a folding-deficient version of actin carrying the point mutation G150P (McCormack et al., 2001a) was used. Alternatively, the translation reaction was supplemented with 5  $\mu$ M purified PhLP1, which is a high affinity interactor of TRiC that was shown to inhibit TRiC-dependent folding of actin (McLaughlin et al., 2002). The released polypeptide chains of both ActLink78 and ActLink97 bound to DNase I significantly more than the two background controls (Figure 20). In contrast, the ribosome-bound nascent chains of both constructs did not differ in DNase I binding from the background controls (Figure 20), suggesting once more that the stalled actin chains were not properly folded. It thus appears that the close environment of the ribosome hinders the ability of TRiC to mediate actin folding.

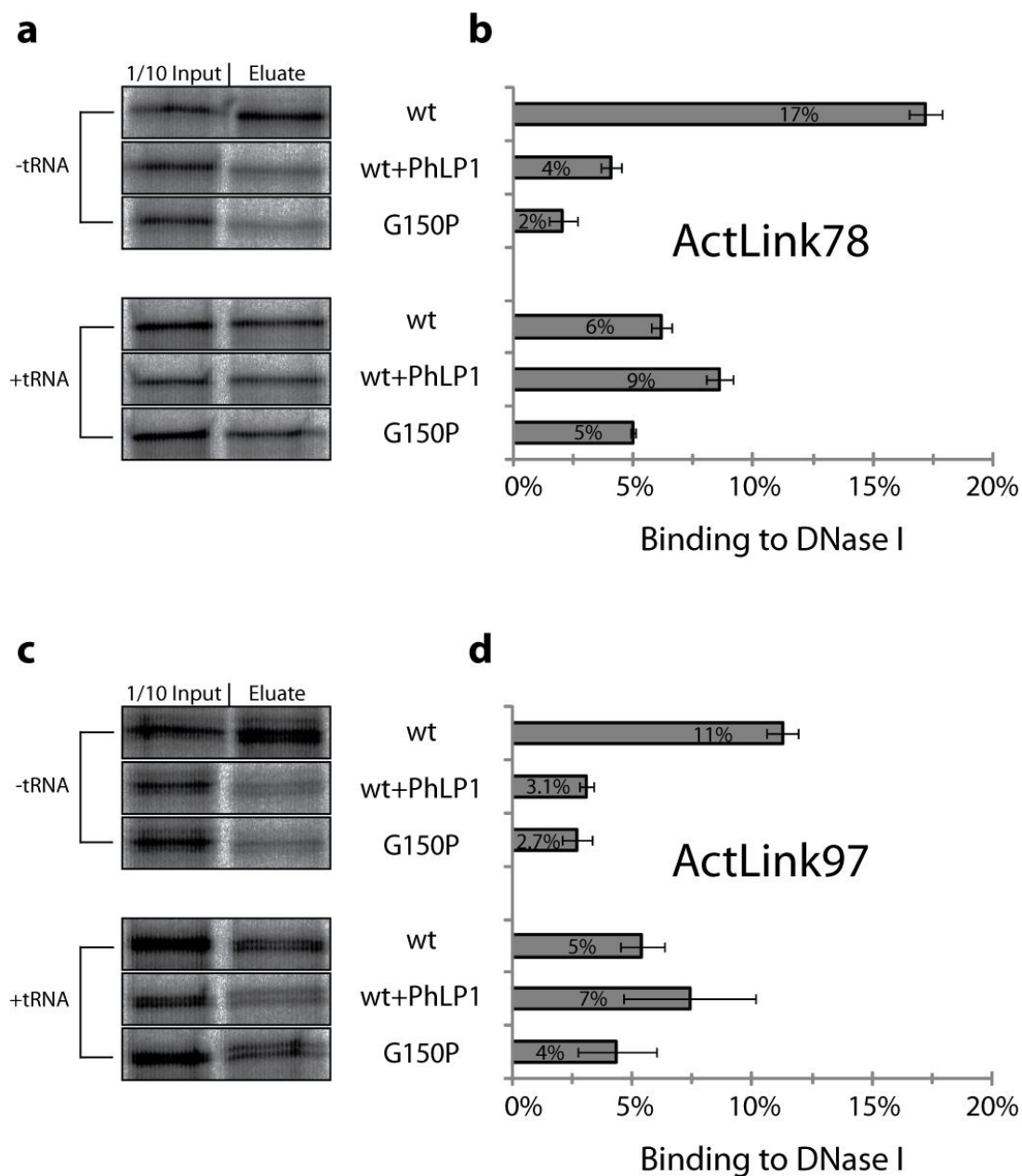


Figure 20: DNase I binding of ActLink78 and ActLink97. Prior to DNase I binding, stalled (+tRNA) nascent chains were separated from released chains (-tRNA) by centrifugation through a sucrose cushion. **a**), **c**) Representative autoradiographs after SDS-PAGE. **b**), **d**) Quantification of the respective bands of N=2 independent experiments. Error bars indicate the standard deviation. **a**), **b**) show experiments with ActLink78, **c**), **d**) show experiments with ActLink97.

### 3.3 Proteinase K Protection Experiments

Proteinase K (PK) is a rather unspecific protease from the fungus *Tritirachium album* (Ebeling et al., 1974). It cleaves flexible parts of proteins and is therefore often used to probe protein conformations. It has been shown that the TRiC subunits are sensitive to proteolytic digest at a flexible segment close to the helical protrusion at the tip of the apical domain (Szpikowska et al., 1998). Such cleavage results in fragments of a molecular weight of around 30 kDa. Importantly, in the closed TRiC conformation the TRiC subunits are not sensitive to protease digest. Additionally, actin encapsulated in the TRiC cavity is also protected from protease (Meyer et al., 2003). Thus, protease protection is an excellent tool to assess the extent to which a protein is encapsulated inside TRiC. Importantly, a stably closed TRiC complex can be generated by incubation with analogs of the transition state of ATP hydrolysis (Meyer et al., 2003). This is generally achieved by incubation of the protein of interest with ATP as well as aluminum and fluoride ions that build soluble aluminum fluoride complexes of different stoichiometries (AlF<sub>x</sub>) in solution (Chabre, 1990; Martin, 1988).

#### 3.3.1 PK Protection of Purified Bovine TRiC by ATP and AlF<sub>x</sub>

To establish a protease protection assay, we first confirmed the results concerning the insensitivity of closed TRiC to protease digest. In line with the results of Meyer et al. TRiC from bovine testis is indeed protected from protease digest in presence of ATP and AlF<sub>x</sub> (Figure 21, lanes 7 and 8)). In presence of ADP and AlF<sub>x</sub>, which leads to closure of only one of the TRiC rings (Meyer et al., 2003), approximately half of the full-length TRiC subunits were protected (Figure 21, lanes 3 and 4). As expected, the effect is dependent on the presence of Mg<sup>2+</sup> ions. Thus, no protection against PK digest is observed in presence of EDTA (Figure 21, lanes 11 and 12). Furthermore, AlF<sub>x</sub> alone does not have any protective effect (Figure 21, lanes 9 and 10). Interestingly, the 30 kDa fragments of TRiC seem to be more sensitive to further digestion in absence of Mg-ATP or Mg-ADP (Figure 21, lanes 10 and 12 vs. lanes 2 and 6). Mg-ATP alone leads to a slight protection of the complete TRiC subunits, probably because a fraction of the TRiC molecules remains in the closed state during the digest due to the slow ATPase rate of TRiC in the absence of substrate (Gao et al., 1994; Melki and Cowan, 1994). In summary, the

experiments with purified TRiC suggest that stable closure of the TRiC cavity can be achieved by treatment with ATP and AIFx, thus enabling PK digest experiments to monitor the encapsulation of protein substrates.

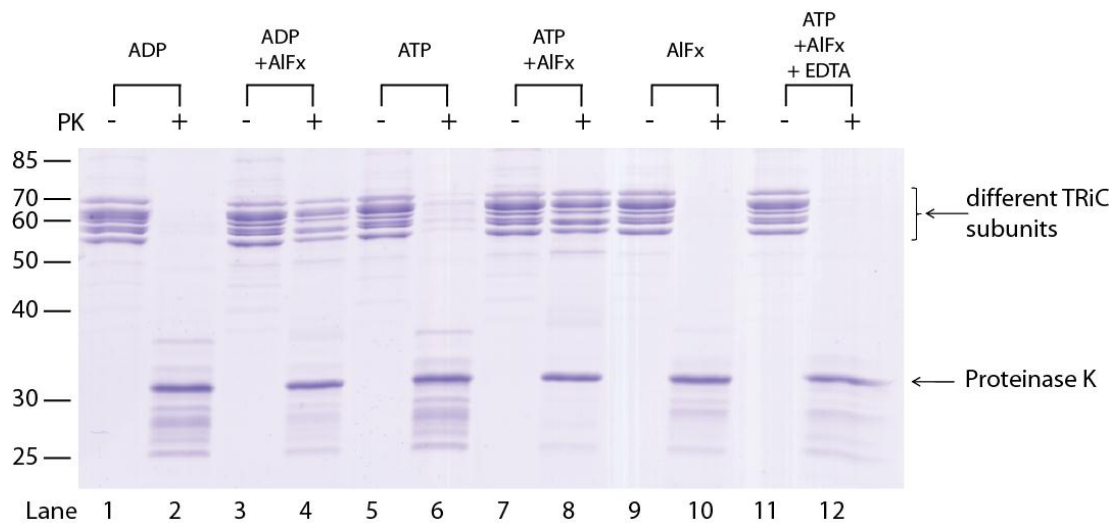


Figure 21: PK digest of purified bovine TRiC under different conditions. All reactions contained 5 mM  $Mg^{2+}$ . The figure shows a Coomassie stained gel after SDS-PAGE. The molecular weight standard given on the left side indicates the apparent molecular weight in kDa. Note the characteristic pattern of the different TRiC subunits around 60 kDa.

There are two principal strategies for obtaining TRiC-substrate complexes. First, purified unfolded substrate can be diluted from denaturant into a TRiC containing solution, followed by closure of the TRiC cavity with ATP and AIFx. Second, the substrate can be translated in RRL, which contains TRiC along with the cellular protein folding machinery, and the TRiC cavity is closed by addition of AIFx, providing a snapshot of encapsulated substrates at a given time. Most likely, binding of substrates to TRiC upon *in vitro* translation in RRL more closely resembles the *in vivo* situation of TRiC acting down-stream of ribosome-bound chaperones and the Hsp70 system (Yam et al., 2008). Thus, PK protection experiments were performed on *in vitro* translation reactions.

### 3.3.2 PK Protection of Actin Fusion Proteins in RRL by ATP and AIFx

Treatments of actin with various proteases were reported to result in production of a common C-terminal protease-resistant fragment of approximately 35 kDa (Graceffa and Dominguez, 2003; Higashi-Fujime et al., 1992; Jacobson and Rosenbusch, 1976; Schwyter et al., 1989). Such a fragment was also apparent in the present experiments with PK (Figures 14 and 22). Furthermore, a stable fragment of approximately 27 kDa was generated from actin fusion proteins but not from actin alone, suggesting that this fragment represents GFP and/or BFP respectively (Figure 22b-f).

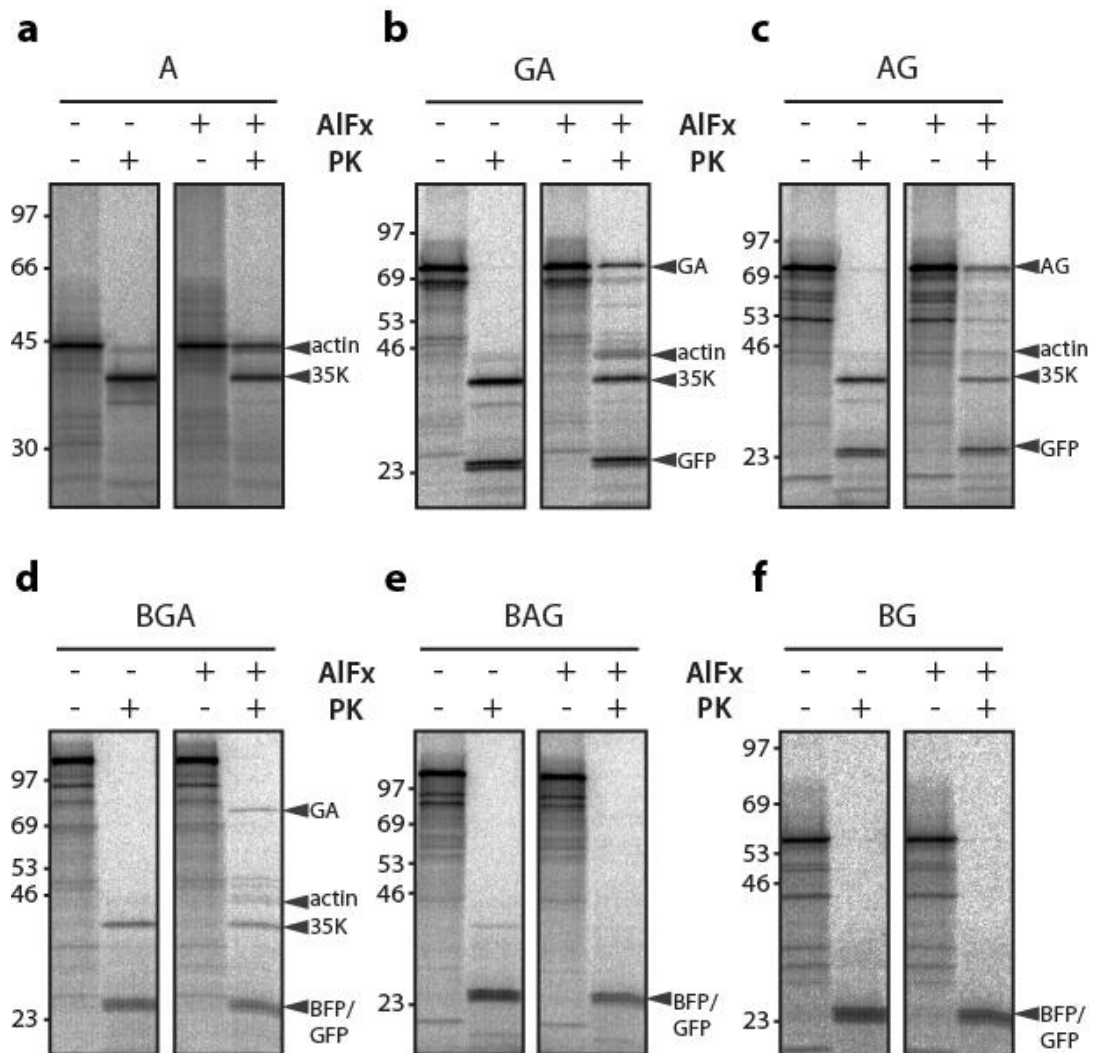


Figure 22: PK digest of actin fusion proteins in presence and absence of AIFx. The respective constructs have been transcribed and translated in RRL as described. Autoradiographs of gels after SDS-PAGE are shown. The molecular weight marker indicates the apparent molecular weight in kDa.

Additional bands were observed upon closure of the TRiC cavity induced by addition of AlFx to the RRL reaction (Figure 22). Presumably, these additional species were protected from PK digest by encapsulation inside the TRiC cavity. As expected, full-length actin was protected from PK digest upon treatment of RRL with AlFx, suggesting complete encapsulation of actin (Figure 22a). Interestingly, also full-length GA and AG were protected against PK digest in presence of ATP and AlFx (Figure 22b+c). In contrast, full-length BGA and BAG were not protected against PK digest (Figure 22d+e). Instead, a stable fragment of the size of GA was observed upon digest of BGA, suggesting that BGA was cleaved by PK within the flexible linker region between the BFP and the GFP moiety (Figure 22d). No protected actin-containing fragment was detected upon digest of BAG in presence of ATP and AlFx (Figure 22e), suggesting that BAG was not encapsulated inside TRiC. Digest of GA and BGA in presence of ATP and AlFx generates also fragments, which have approximately the molecular weight of actin (Figure 22b+d). Thus, the linker between actin and GFP was accessible to PK in a subset of TRiC-GA and TRiC-BGA complexes, indicating that TRiC-GA and TRiC-BGA complexes are heterogeneous with regard to their encapsulation inside the TRiC cavity.

### 3.4 Analysis of TRiC-bound Proteins by Native PAGE

Analysis of total RRL reactions was dominated by translation products that were not bound to TRiC and that gave rise to protease-resistant fragments independently of TRiC and AlFx (Figure 22). In order to concentrate on TRiC-dependent effects, TRiC-bound polypeptides were separated from the “free” proteins in solution prior to analysis. A gradient native PAGE ranging from 5-13% acrylamide in the separating gel was used to achieve this separation. To calibrate the gels, purified bovine TRiC was used with and without PK digest in presence and absence of AlFx. All TRiC complexes migrated in the upper quarter of the gel. Native PAGE was so sensitive that even the open and closed forms of TRiC were separated. The closed form was more compact and migrated faster than the open one (Figure 23). However, the AlFx-induced closed form of TRiC was not stable in absence of AlFx in the gel and thus several differently migrating species occurred during the gel run (Figure 23a). Including different amounts of AlFx into the gel mixture was used to control the mobility of the TRiC conformers: A high AlFx

concentration in the gel prevented opening of the AlFx-treated TRiC complexes but led in turn to closure of the not previously AlFx-treated complexes during the gel run (Figure 23b). Thus, a lower AlFx concentration was finally used for subsequent experiments as a trade-off between opening of AlFx-treated closed conformers and closure of untreated open conformers during the gel run (Figure 23c).

### 3.4.1 Native PAGE of Purified Bovine TRiC

Note that TRiC remained a hexadecamer upon treatment with PK in the absence of AlFx (Figure 23, lanes 2, 6, 10), even though the TRiC subunits were cleaved in the apical domain under these conditions (Figure 21, lane 6). The complexes containing the nicked subunits migrated slightly slower, suggesting a decreased compactness (Figure 23, lanes 2, 6, 10).

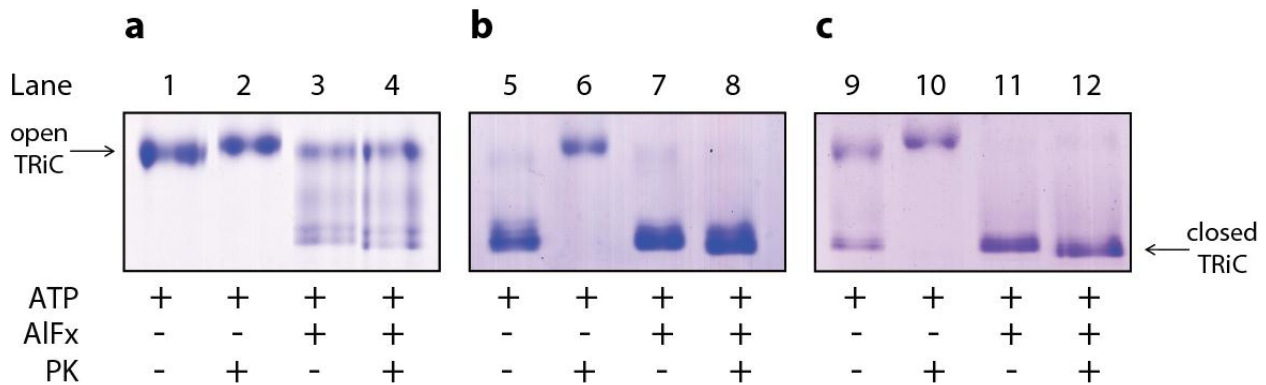


Figure 23: Native PAGE gels of purified bovine TRiC under different conditions. Sections of Coomassie stained native PAGE gels are shown. **a)** No AlFx in gel and in running buffers. **b)** 30 mM KF and 5 mM  $\text{Al}(\text{NO}_3)_3$  in gel and running buffers. **c)** 6 mM KF and 1 mM  $\text{Al}(\text{NO}_3)_3$  in gel and running buffers.

### 3.4.2 Native PAGE of RRL Reactions Translating Actin Fusion Proteins

When native PAGE gels of actin translation reactions were analyzed by autoradiography, a very similar band pattern was observed as for purified TRiC (Figures 23c and 24a). Notably, PK treatment in presence of AlFx did not alter the band pattern of TRiC-bound actin, suggesting that

actin was encapsulated inside TRiC and thus protected from digest (Figure 24a). Similarly, also the closed complexes of TRiC with the two smaller actin fusion proteins GA and AG appeared unchanged upon incubation with PK in presence of AlFx (Figure 24b+c). Interestingly, the closed TRiC-GA and TRiC-AG complexes populated also slightly slower migrating conformations compared to TRiC-A (Figure 24a-c) and thus appeared as more heterogeneous and less compact than TRiC-A.

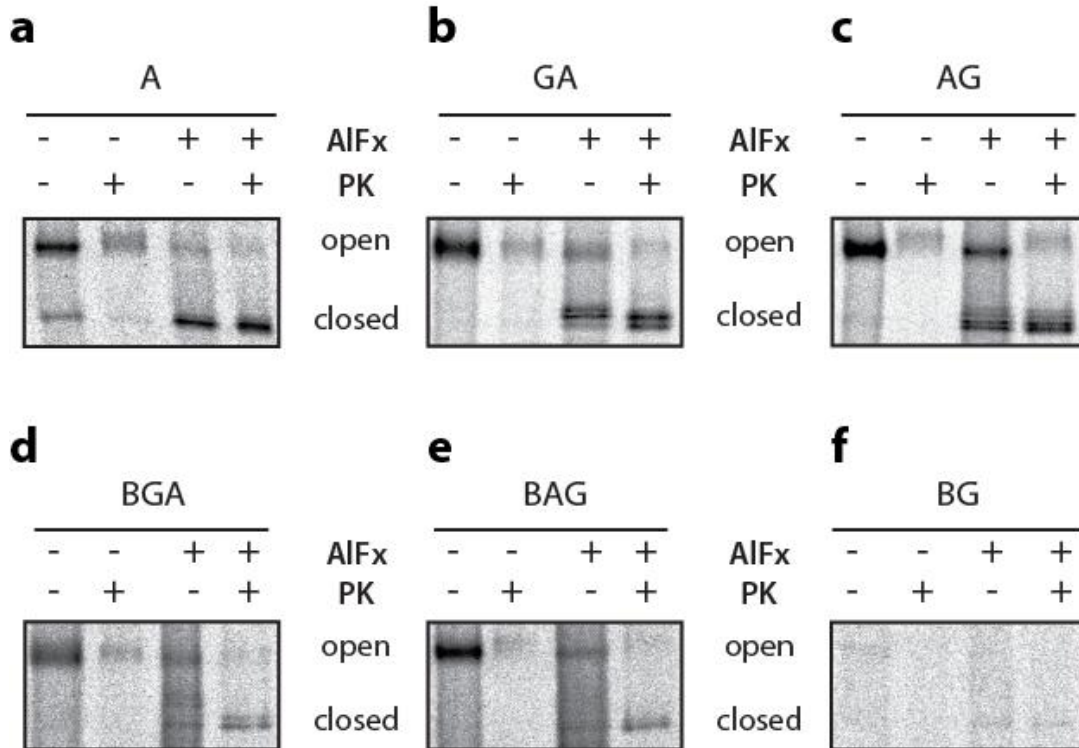


Figure 24: Native PAGE of TRiC-substrate complexes. The respective constructs have been transcribed and translated in RRL, as described. Autoradiographs after native PAGE are shown.

The migration pattern of the TRiC-BGA and TRiC-BAG complexes differed drastically from the migration of the TRiC-A, TRiC-AG and TRiC-GA complexes in presence of AlFx (Figure 24d+e). No distinct band at the position of closed TRiC was visible. Instead, the material migrated as a diffuse band. In case of TRiC-BGA, a stack of bands was visible between open and closed TRiC, which was not seen in case of BAG (Figure 24d+e). This stack of bands and the diffuse material disappeared upon treatment with PK and the remaining protease-protected protein migrated at the position of closed TRiC (Figure 24d+e).

Importantly, BG, which was used as a control throughout this study, did not bind to TRiC in any way comparable to the actin fusion proteins (Figure 24f) showing that the interaction of the actin fusion proteins with TRiC was indeed mediated by actin and not by BFP or GFP.

### 3.4.3 Elution of TRiC-bound Proteins from Native PAGE Gels

In order to determine the size of the protein species trapped on TRiC, the TRiC-bound proteins were eluted from the TRiC-containing region of the native gel with an SDS- and  $\beta$ -mercaptoethanol-containing buffer. Similar results were obtained upon elution from native gels irrespective of the AIFx content in the gel. The additional protected fragments seen in the total lysate upon addition of AIFx (Figure 22) were also found upon elution of proteins from TRiC-containing sections of native PAGE gels (Figure 25), indicating that their protection from PK digest was caused by encapsulation inside the TRiC cavity.

In contrast, the bands ascribed to GFP and the stable 35 kDa actin fragment were found upon elution from native PAGE gels. Thus, occurrence of these fragments in SDS-PAGE of the total lysate (Figure 22) results from their inherent protease-resistance as stable segments of the natively folded final products. Interestingly, in case of the folding-compromised BAG construct there was no ATP and AIFx induced protection against PK digest, neither of the full-length protein nor of any fraction (Figure 25e). This finding suggests that an inability of encapsulation of the actin domain of BAG by TRiC might be causing the severe folding problems of this fusion construct.

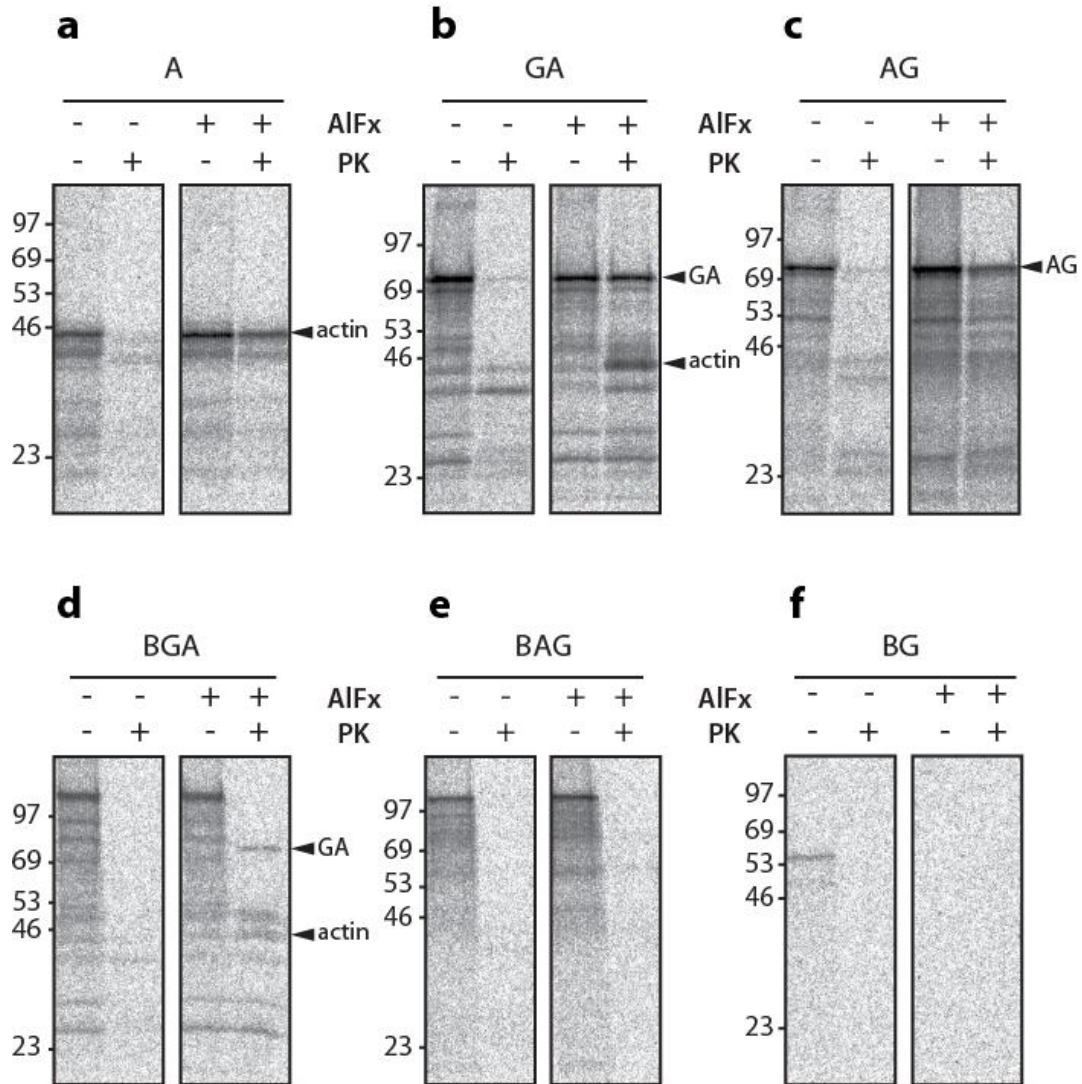


Figure 25: SDS-PAGE of TRiC-bound proteins eluted from Native PAGE slices. A native gel has been Coomassie stained and the TRiC containing regions were cut separately lane by lane. Proteins were eluted from the gel slices and subsequently analyzed by SDS-PAGE. The molecular weight marker indicates the apparent molecular weight in kDa.

## 3.5 A Protease-Sensitive GFP-Mutant

The AIFx-dependent protection of full-length GA and AG from PK digest suggests that these actin fusion proteins are completely encapsulated inside the TRiC cavity. However, it is formally not possible to conclude that a protein is completely encapsulated inside TRiC just because the full-length protein is protected from protease digest. In fact, a partially encapsulated protein whose protease-resistant parts protrude from the TRiC cavity would also be completely protected. GFP is resistant against PK digest (Figure 22) and thus it cannot be excluded that GA and AG are partially encapsulated inside TRiC with GFP protruding from the cavity.

### 3.5.1 $\Delta$ N-GFP-Actin is Completely Encapsulated inside the TRiC Cavity

To clarify this point, a protease-sensitive mutant of GFP was created by deletion of the N-terminal residues 3-38, which essentially reflect two adjacent  $\beta$ -sheets of the eleven-stranded GFP  $\beta$ -barrel (Figure 26a). PK digest of  $\Delta$ N-GFP-actin ( $\Delta$ N-GA) resulted in only one protease-resistant fragment, namely the stable 35 kDa actin fragment. A fragment of the size of  $\Delta$ N-GFP was absent, indicating that  $\Delta$ N-GFP is sensitive to digestion by PK. Nevertheless, full-length  $\Delta$ N-GA was protected from PK by TRiC in presence of ATP and AIFx (Figure 26b), thus suggesting complete encapsulation. The band pattern of the  $\Delta$ N-GA-TRiC complex in the native PAGE gel was very similar to the pattern observed for actin bound to TRiC (Figure 26c). Elution of TRiC-bound proteins from native gel slices, followed by SDS-PAGE of the eluted proteins (Figure 26d), revealed that the protected full-length  $\Delta$ N-GA was indeed bound to TRiC, suggesting that its protection from PK was caused by encapsulation inside the TRiC cavity. The complete encapsulation of  $\Delta$ N-GA does not necessarily imply that GA is also completely encapsulated, because the folded GFP  $\beta$ -barrel might behave differently from  $\Delta$ N-GFP.

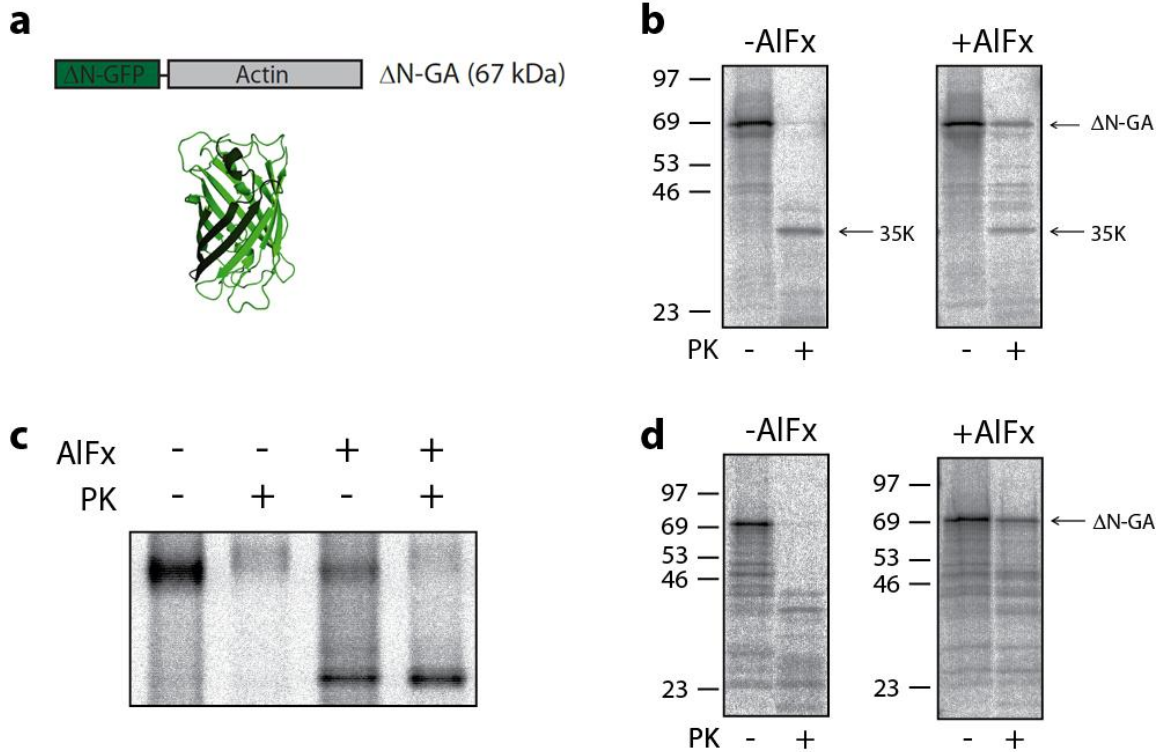


Figure 26: PK digest of  $\Delta$ N-GA.  $\Delta$ N-GA was translated in RRL as described. **a)** Top: Schematic representation of  $\Delta$ N-GA. Bottom: Crystal structure of GFP (1EMA) (Ormo et al., 1996). The deletion of the N-terminal two  $\beta$ -strands in  $\Delta$ N-GFP is indicated by dark color (done with PyMOL). **b)** Autoradiograph after SDS-PAGE of total RRL. **c)** Autoradiograph after Native PAGE. **d)** Autoradiograph after SDS-PAGE of TRiC-bound proteins eluted from native gel. The molecular weight markers indicate the apparent molecular weight in kDa.

### 3.5.2 Native PAGE Mobility Shift Assay

To analyze the encapsulation status of GA by a different experimental approach, the availability of the protein to an anti-GFP antibody upon closure of the TRiC cavity was tested. In fact, a mixture of two monoclonal anti-GFP antibodies was used. It has been described that binding of antibodies to protein complexes can be detected as a mobility shift in native PAGE (Swamy et al., 2007). The mobility of the open TRiC-substrate complex in absence of AIFx was shifted by anti-GFP in case of GA but not in case of A, indicating a specific binding to GFP (Figure 27a). The shift also occurred in case of  $\Delta$ N-GA, indicating that the epitope of at least one of the antibodies was not localized within the N-terminal 38 amino acids of GFP. Interestingly, a fraction of the TRiC-GA complex was shifted by anti-GFP even after closure of the TRiC cavity

by ATP and AIFx (Figure 27b). Thus, GFP seems to be outside the TRiC cavity in a subset of complexes, even though full-length GA is protected from PK digest upon closure of the TRiC cavity. It appears that GFP is located at the cavity entrance in a way that blocks access of PK to the protease-sensitive linker between GFP and actin. In contrast to TRiC-GA, TRiC- $\Delta$ N-GA was not shifted when the TRiC cavity was closed (Figure 27b), thus confirming the total encapsulation of  $\Delta$ N-GA.

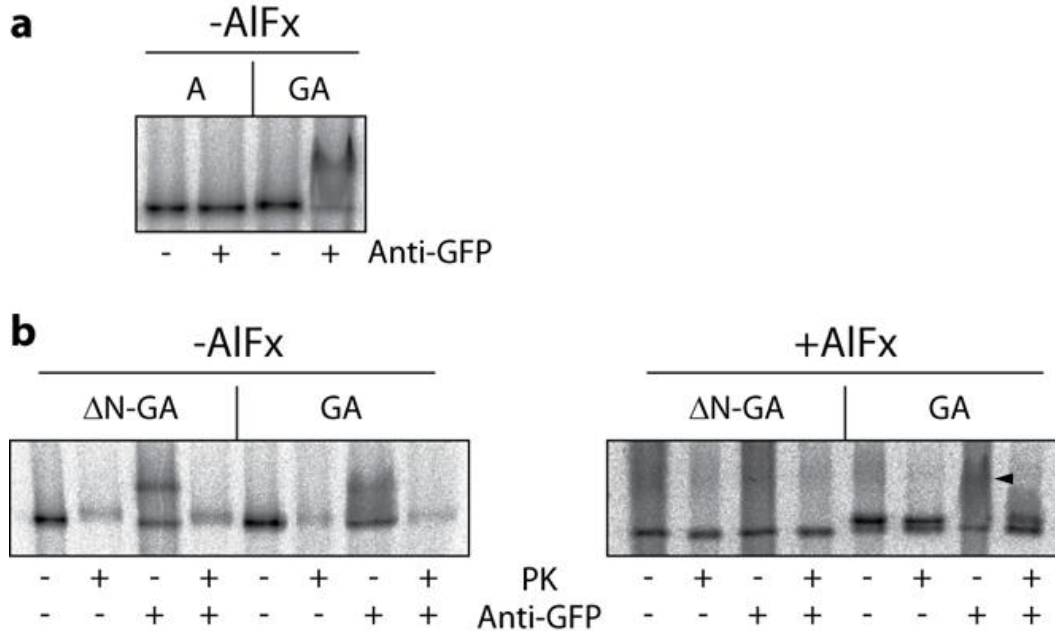


Figure 27: Antibody-based mobility shift. **a)** Autoradiograph after native PAGE. The respective proteins have been made in RRL as described and incubated with 10 ng/ $\mu$ l anti-GFP prior to native PAGE. **b)** Autoradiograph after native PAGE. Only samples and gel on the right side were treated with AIFx. The shifted TRiC-GA complex migrated as a diffuse band in presence of AIFx and is indicated by an arrowhead.

### 3.5.3 DNase I Binding of $\Delta$ N-GFP-Actin Fusion Proteins

Interestingly, DNase I binding experiments indicated that actin folding in  $\Delta$ N-GA is severely impaired (Figure 28). A possible explanation is that the folding incompetent  $\Delta$ N-GFP interfered with actin folding. If folding of actin occurred fast and co-translationally, the folding reaction would not be disturbed by  $\Delta$ N-GFP attached to the actin C-terminus. However, no substantial binding of Actin- $\Delta$ N-GFP (A $\Delta$ N-G) to DNase I was observed (Figure 28), once again supporting

the conclusion that folding of actin to the DNase I binding competent conformation is not completed co-translationally.

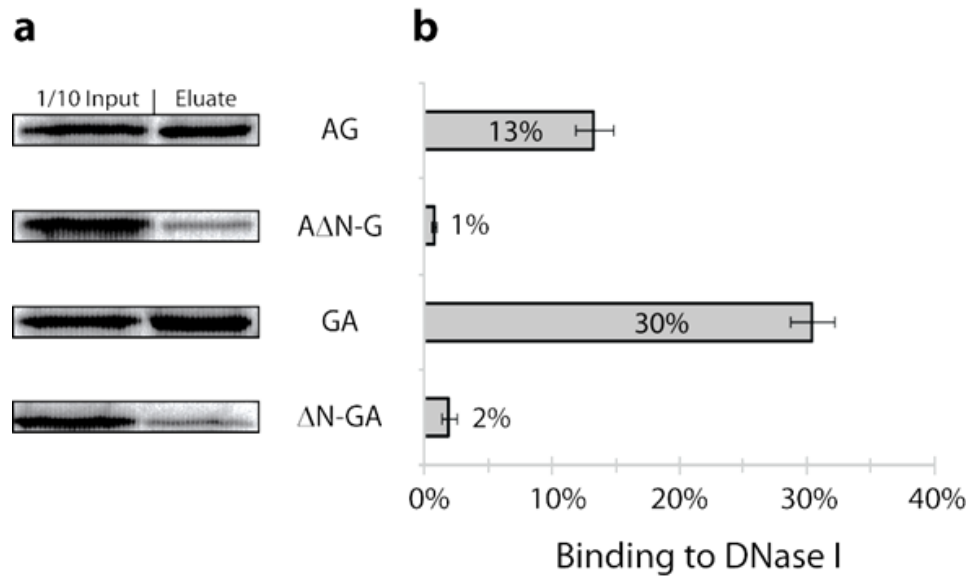


Figure 28: DNase I binding of  $\Delta$ N-GA and A $\Delta$ N-G. AG and GA have been tested as positive controls in parallel. **a)** Representative autoradiographs after SDS-PAGE. **b)** Quantification of the respective bands of N=3 independent experiments.

In summary, the experiments with different fusion proteins containing the TRiC-dependent protein actin and the fluorescent proteins BFP and GFP in various combinations led to the following conclusions:

1. TRiC can fold domains of multi-domain proteins that are in total too large for complete encapsulation (Figures 13 and 14).
2. Folding of actin is unlikely to be completed co-translationally, as stalled actin fusion proteins do not bind to DNase I (Figures 16, 17, 18 and 20).
3. TRiC is able to partially encapsulate large multi-domain proteins as shown by protease protection experiments (Figures 22, 24 and 25) and by an antibody-based mobility shift in native PAGE (Figure 27).

## 3.6 Investigating Naturally Occurring Large TRiC Substrates

### 3.6.1 Testing Human Homologs of Known TRiC Interactors

In order to test whether the principles governing the folding of actin fusion proteins are also valid for large natural substrates of TRiC, several known large TRiC interactors were expressed in RRL. In 2008, two independent studies investigated the interactome of the eukaryotic chaperonin TRiC (Dekker et al., 2008; Yam et al., 2008). Since a comprehensive human cDNA library was available in our institute, human homologs of the described interactors were tested. In case of the yeast interactors described by Dekker et al., the most suitable homologs were identified using BLAST. However, in some cases only a low degree of homology was identified. Three of the human genes (GANAB, MUC17 and DYNC1H1) were available only as 5'-deleted constructs, thus giving rise to N-terminally truncated proteins (Table 1). The smallest protein tested was 83 kDa in size and the largest had a molecular weight of 273 kDa (Table 1).

We expressed the constructs in RRL and probed the interaction with TRiC by native PAGE (Figure 29). Note that the band intensities are not absolutely comparable. For comparison the constructs with known TRiC-binding ability (BG, GA and BGA) are shown (Figure 29a). Four constructs (THNSL1, ATP6V0A1, NUP153, MUC17) were only poorly expressed in RRL (Figure 29). The product of the THNSL1 gene nevertheless bound strongly to TRiC. The translation products of most constructs were binding less well to TRiC than the model actin fusion proteins GA and BGA. The translation products of two constructs, EFTUD2 and COPB2, bound to TRiC with similar efficiencies as the actin fusion proteins tested before (Figure 29). Thus, we decided to focus on these two candidates.

Table 1: Putative TRiC substrates tested for binding to TRiC upon expression in RRL. The first column provides the name of the described TRiC interactor as given in the respective publication. The third column provides the name of the human gene corresponding to the described interactor.

TRiC Interactor	Described by	Human Gene	Construct	MW (kDa)
eEF2	Yam et al.	EEF2	Full-Length	95
Teashirt 3	Yam et al.	TSHZ3	Full-Length	99
SnRNP116	Yam et al.	EFTUD2	Full-Length	109
Met18	Yam et al.	MMS19	Full-Length	113
Uba1	Yam et al.	UBA1	Full-Length	118
LeuRS	Yam et al.	LARS	Full-Length	135
Skiv2l	Yam et al.	SKIV2L	Full-Length	138
Kip3	Yam et al.	KIF13A	Full-Length	199
Myosin	Yam et al.	MYH1	Full-Length	223
Fas2	Yam et al.	FASN	Full-Length	273
Aro1	Dekker et al.	THNSL1	Full-Length	83
Ubp3	Dekker et al.	USP10	Full-Length	87
Stv1	Dekker et al.	ATP6V0A1	Full-Length	96
Sec27	Dekker et al.	COPB2	Full-Length	102
Rot2	Dekker et al.	GANAB	$\Delta$ N (1-97)	96
Swi3	Dekker et al.	SMARCC2	Full-Length	133
Nup1	Dekker et al.	NUP153	Full-Length	154
Sla1	Dekker et al.	MUC17	$\Delta$ N (1-3270)	128
Dyn1	Dekker et al.	DYNC1H1	$\Delta$ N (1-3658)	112

### 3.6.2 hSnu114 – A Strong TRiC Interactor

The human gene EFTUD2 encodes a 972 amino acid protein with a molecular weight of 109 kDa (Figure 30) that is homologous to the essential yeast protein Snu114 (Fabrizio et al., 1997). The two proteins have 33% sequence identity and the human one is also called hSnu114 (Frazer et al., 2008). We will refer to this protein as hSnu114, although alternative names are used in the

literature, such as SnRNP116 (Yam et al., 2008) or U5-116kD (Fabrizio et al., 1997) because of its apparent molecular weight and its being a part of the U5 snRNP (Bach et al., 1989). Snu114 is a GTPase and it regulates the activity of the ATP-dependent helicase Brr2, dependent on whether GTP or GDP is bound (Small et al., 2006). In turn, active Brr2 unwinds the U4/U6 snRNAs (Maeder et al., 2009), which is required for activation of the spliceosome (Wahl et al., 2009).

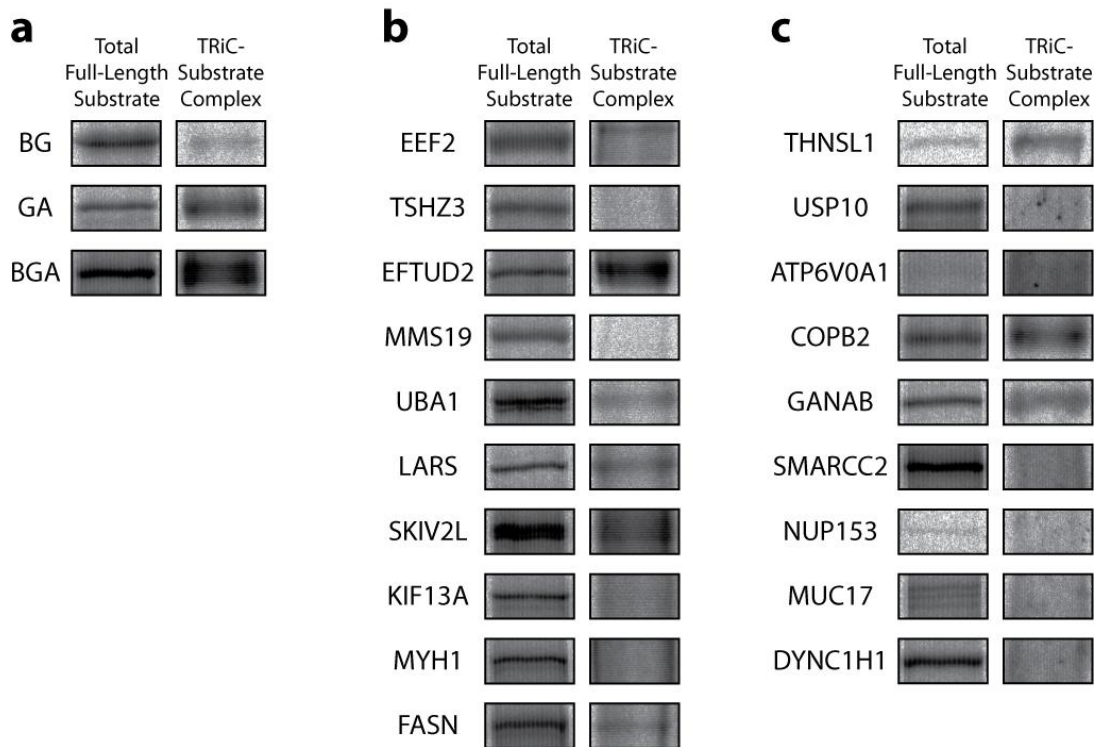


Figure 29: Binding of putative natural substrates to TRiC. The respective constructs were transcribed and translated in RRL and analyzed by SDS-PAGE (Total Full-Length Substrate) and native PAGE (TRiC-Substrate Complex). The gel sections entitled “Total Full-Length Substrates” show autoradiographs of gels after SDS-PAGE. Only a section of the gels corresponding to the respective full-length constructs is shown. Truncated translation products were observed as well for some of the constructs. The gel sections entitled “TRiC-Substrate Complex” represent autoradiographs of gels after native PAGE. The constructs in a), b) and c) are arranged according to the expected molecular weights of the respective full-length proteins from low (top) to high (bottom). **a)** Fusion proteins of fluorescent proteins and/or actin are shown as negative (BG) and positive (GA and BGA) controls for binding to TRiC. **b)** Human homologs of putative TRiC substrates described by Yam et al., 2008. **c)** Human homologs of TRiC substrates described by Dekker et al., 2008.

The 3D-structure of Snu114 is not known. However, sequence homology (Fabrizio et al., 1997) suggests that the structure of Snu114 is similar to that of eukaryotic elongation factor 2 (eEF2) (Jorgensen et al., 2006), for which several crystal structures are available (Jorgensen et al., 2005;

Jorgensen et al., 2003; Jorgensen et al., 2004; Soe et al., 2007). Elongation factor 2 is composed of six domains in total: G, G', II, III, IV and V. Domain G' is inserted into domain G (or I) and domain V is inserted into domain IV (Jorgensen et al., 2003). The N-terminal part of the protein, consisting of domains G, G' and II contains the GTP-binding module and resembles the prokaryotic EF-Tu and the eukaryotic EF1 $\alpha$  factors that deliver aminoacyl-tRNAs to the ribosome, while the C-terminal part, consisting of domains III, IV and V, is shaped similar to an aminoacyl-tRNA, providing an excellent example of molecular mimicry (Nissen et al., 1995). In addition to the described domains of eEF2, hSnu114 contains 110 mainly acidic amino acids at the N-terminus (Figure 30).

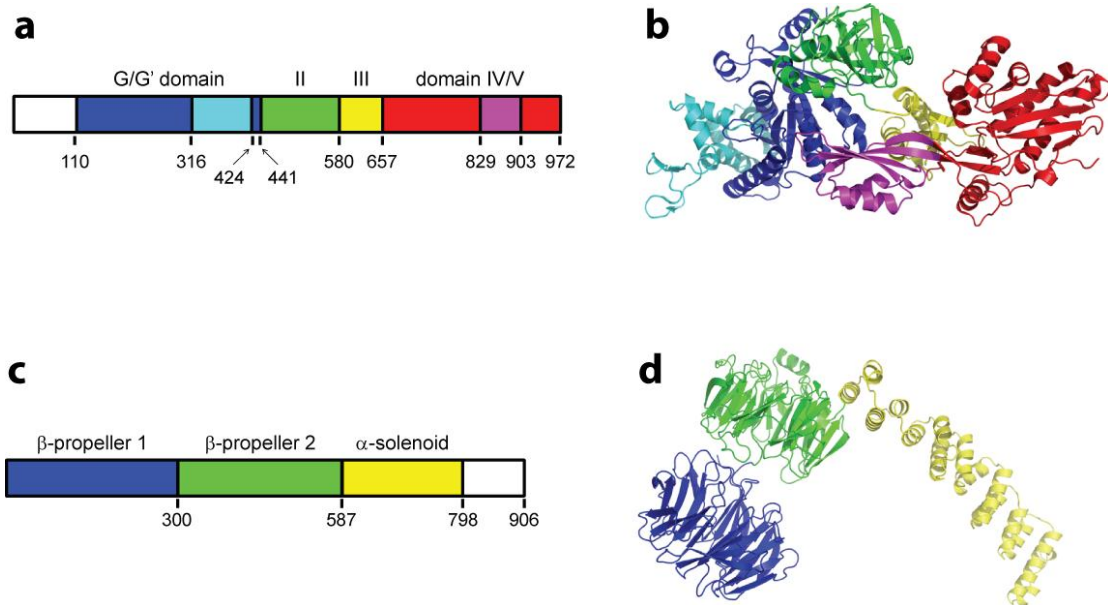


Figure 30: Structural models of the putative TRiC substrates hSnu114 (top) and  $\beta'$ -COP (bottom). White boxes in a) and c) indicate parts of the respective proteins not included in the crystal structures. **a)** Putative domain structure of hSnu114 based on homology to eEF2, whose structure is shown in **b)** based on the PDB file 1NOV (Jorgensen et al., 2003). **c)** Domain structure of human  $\beta'$ -COP based on the crystal structure of yeast  $\beta'$ -COP shown in **d)** (3MKQ, Lee and Goldberg, 2010).

### 3.6.3 $\beta'$ -COP – A WD40 Domain Containing Interactor of TRiC

The human gene COPB2 encodes a 906 amino acid protein with a molecular weight of 102 kDa that is homologous to the yeast protein Sec27 (Duden et al., 1994) and that is commonly called  $\beta'$ -COP (Figure 30). The protein is well conserved from yeast to humans, the sequences being 47% identical.  $\beta'$ -COP is involved in retrograde vesicular transport from the Golgi apparatus to the ER (Duden, 2003). It recognizes its cargo by specifically binding to di-lysine motifs via its N-terminal WD40 domain (Eugster et al., 2004). The crystal structure of the N-terminal 812 amino acids of yeast  $\beta'$ -COP has recently been solved (Figure 30d) in complex with the  $\alpha$ -solenoid domain of  $\alpha$ -COP (Lee and Goldberg, 2010).  $\beta'$ -COP contains two N-terminal WD40-repeat domains that form seven-bladed  $\beta$ -propellers (Smith et al., 1999), a domain that is often found in TRiC substrates (Valpuesta et al., 2002). However, it is not known whether the folding of  $\beta'$ -COP is actually dependent on TRiC.

### 3.6.4 Expressing N- and C-terminal hSnu114 and $\beta'$ -COP Parts separately

In order to identify TRiC-dependent domains in  $\beta'$ -COP and hSnu114, different constructs comprising either N- or C-terminal parts of the respective proteins were generated. Specifically, for hSnu114 an N-terminal construct (hSnu114-N, amino acids 1-580) comprising domains G, G' and II and a C-terminal construct (hSnu114-C, amino acids 581-972) comprising domains III, IV and V were produced (Figure 30a). Similarly, for  $\beta'$ -COP an N-terminal construct ( $\beta'$ -COP-N, amino acids 1-283) was designed to contain only the N-terminal propeller and a C-terminal construct ( $\beta'$ -COP-C, amino acids 284-906) comprising the rest of the protein. Unfortunately, the crystal structure of  $\beta'$ -COP, which was published after design of  $\beta'$ -COP-N and  $\beta'$ -COP-C, revealed that  $\beta'$ -COP-N misses the two  $\beta$ -strands 7B and 7C (Lee and Goldberg, 2010) of the N-terminal propeller blade. This potentially causes a severe folding defect.

We tested the interaction of the N- and C-terminal constructs of hSnu114 and  $\beta'$ -COP with TRiC by native PAGE. As judged from the TRiC-containing gel sections, the hSnu114-N construct barely interacted with TRiC, in contrast to the hSnu114-C construct that bound TRiC as strongly as the full-length protein (Figure 31a), suggesting that the TRiC-binding site of hSnu114 is

located in the C-terminal part. In the case of  $\beta'$ -COP, the N-terminal  $\beta'$ -COP construct ( $\beta'$ -COP-N) interacted more strongly with TRiC than  $\beta'$ -COP-C (Figure 31b).

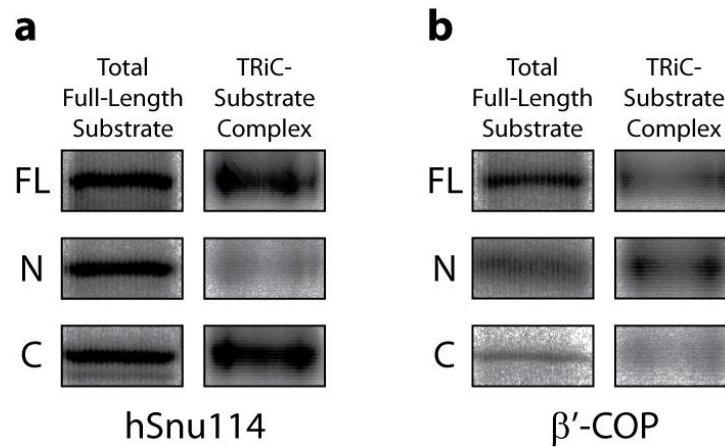


Figure 31: Binding of N- and C-terminal constructs of hSnu114 (a) and  $\beta'$ -COP (b) to TRiC. The respective constructs were transcribed and translated in RRL and the translation reactions were analyzed by SDS-PAGE and native PAGE as in Figure 29.

### 3.6.5 Partial Encapsulation of hSnu114

Next, we analyzed whether partial encapsulation of the two natural TRiC interactors occurred. PK protection experiments were performed as described for the actin fusion proteins. PK treatment of the total translation reactions resulted in a number of protease-resistant fragments for both constructs. Three fragments of major intensity appeared upon digest of hSnu114 and had apparent molecular weights of approximately 50 kDa, 55 kDa and 95 kDa (Figure 32a). For  $\beta'$ -COP, two major fragments of approximately 30 kDa and 70 kDa were observed (Figure 32a). These fragments might represent the N-terminal WD40-repeat domain and the remaining C-terminal part of the protein (Figure 30). Addition of AIFx had little effect on the fragmentation in total translation reactions (Figure 32a).

Probably, the autoradiographs (Figure 32) are dominated by protease-resistant fragments generated from proteins that are not bound to TRiC. Therefore, the TRiC-bound proteins were eluted from TRiC-containing slices of the native gel and separated by SDS-PAGE. Indeed, ATP and AIFx dependent protection of fragments was detected in the TRiC-bound fractions. These



### 3.6.6 The C-terminal Part of hSnu114 Binds Strongly to TRiC

The experiments above did not define which part of hSnu114 was encapsulated inside the TRiC cavity. To determine the identity of the encapsulated fragments, the N- and C-terminal constructs of hSnu114 (hSnu114-N (amino acids 1-580) and hSnu114-C (amino acids 581-972)) were expressed and analyzed for AIFx-induced protease protection.

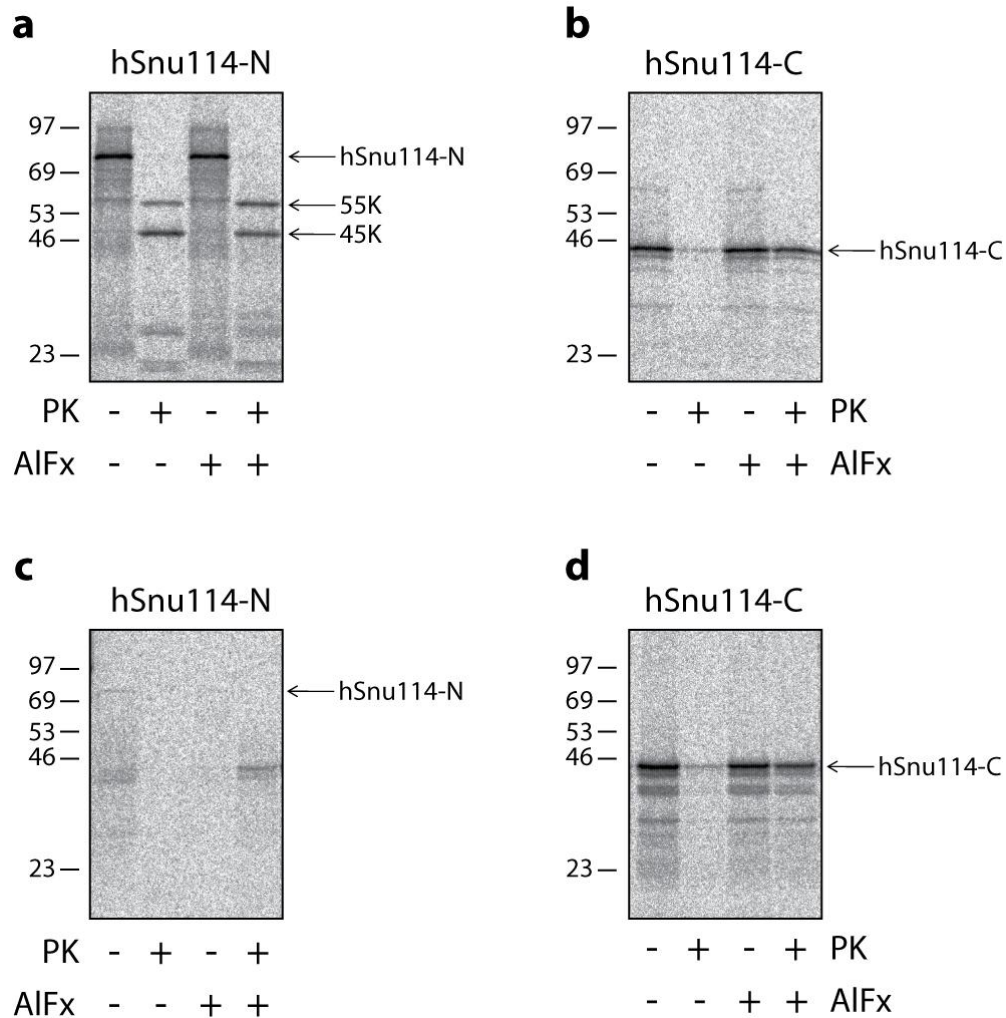


Figure 33: PK digest of hSnu114-N and hSnu114-C in presence and absence of AIFx. The respective constructs were transcribed and translated in RRL. **a), b)** Samples of the total lysate after SDS-PAGE. **c), d)** TRiC-bound proteins after elution from native gels and subsequent SDS-PAGE. The molecular weight markers indicate the apparent molecular weight in kDa. Smaller fragments after digest are indicated by arrows and the approximate apparent molecular weight.

PK treatment of hSnu114-N resulted in the formation of two major fragments of approximately 45 kDa and 55 kDa, regardless of whether AIFx was present or not (Figure 33a). Similar protease-resistant fragments were observed upon digest of full-length hSnu114 (Figure 32a). Previous experiments showed that hSnu114-N binds only very weakly to TRiC (Figure 31a). Indeed, elution of TRiC-containing sections of a native gel resulted in barely detectable amounts of hSnu114-N (Figure 33c), indicating that the N-terminus of hSnu114 is most likely not the TRiC-dependent part of the protein. In contrast, substantial amounts of TRiC-bound hSnu114-C were eluted from the TRiC-containing band of a native gel. Furthermore, TRiC-bound hSnu114-C was protected from PK digest in presence of ATP and AIFx (Figure 33d), suggesting complete encapsulation inside the TRiC cavity. Surprisingly, the observed TRiC-bound fragments of full-length hSnu114 that were protected against PK digest in presence of ATP and AIFx (Figure 32b) were not reproduced with hSnu114-C. Thus, the PK protection experiments indicate that hSnu114-C contains the high affinity TRiC-binding site of hSnu114 but that hSnu114-C and full-length hSnu114 nevertheless differ in the way they are encapsulated by TRiC. The 45 kDa hSnu114-C is completely encapsulated inside TRiC, while full-length hSnu114 gives rise to several smaller fragments between 15 kDa and 45 kDa (Figure 32b).

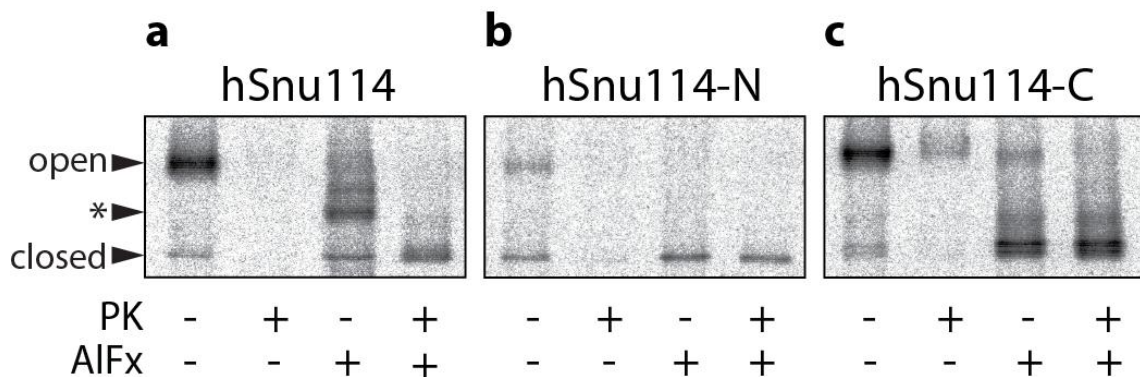


Figure 34: Native PAGE of different hSnu114 constructs showing TRiC-substrate complexes. The respective constructs were transcribed and translated in RRL. Autoradiographs of TRiC-containing sections of native gels are shown.

Partial encapsulation of full-length hSnu114 became also apparent in the migration pattern of the TRiC-hSnu114 complex during native PAGE. In presence of ATP and AIFx, the TRiC-hSnu114 complex migrated more slowly than closed TRiC (asterisk in Figure 34). Upon PK digest, a mobility similar to closed TRiC was observed (Figure 34a), probably because protruding parts of

hSnu114, which caused the aberrant migration properties, were cleaved by PK. A similar phenomenon was observed with the TRiC-BGA complex, which also migrated more slowly than TRiC alone in presence of ATP and AlFx and which was accelerated after cleavage of the BFP moiety by PK, indicating partial encapsulation of BGA (Figure 24). The TRiC-hSnu114-C complex exhibited the normal migration pattern (Figure 34c) in line with full encapsulation inside the TRiC cavity as supported by the protease protection experiments (Figure 33b+d).

### 3.6.7 Protected Fragments Originate from the C-terminus of hSnu114

Experiments with the N- and C-terminal parts of hSnu114 had suggested that the interaction with TRiC was mediated through the hSnu114 C-terminus (Figures 31, 33, 34). In order to determine the origin of the observed protease-protected fragments, either the N- or the C-terminus of hSnu114 was combined with an HA-tag, resulting in constructs HA-hSnu114 and hSnu114-HA, respectively, for detection by Western blot. Additionally, the constructs contained a FLAG-tag at the opposite chain terminus. However, the antibody directed against the FLAG epitope was not sensitive enough to detect the limited amounts of protein that were produced by *in vitro* translation in RRL.

PK treatment resulted in elimination of the HA-epitope of HA-hSnu114, both in the presence and absence of AlFx (Figure 35a). In contrast, a pattern of protected fragments similar to the original fragments of radiolabeled hSnu114 (Figure 32b) was detected by the anti-HA antibody in hSnu114-HA (Figure 35b), indicating that the observed fragments originated from the C-terminus of hSnu114. The 45 kDa fragment observed with the radiolabeled protein, was not detected on the anti-HA western blot, suggesting that encapsulation leading to this fragment excluded the HA-tag.

The same fragments observed in total RRL (Figure 35b) were also present in the TRiC-bound fraction (Figure 35d), indicating that protection of the HA-epitope was indeed caused by encapsulation of the C-terminus of hSnu114 inside the TRiC cavity.

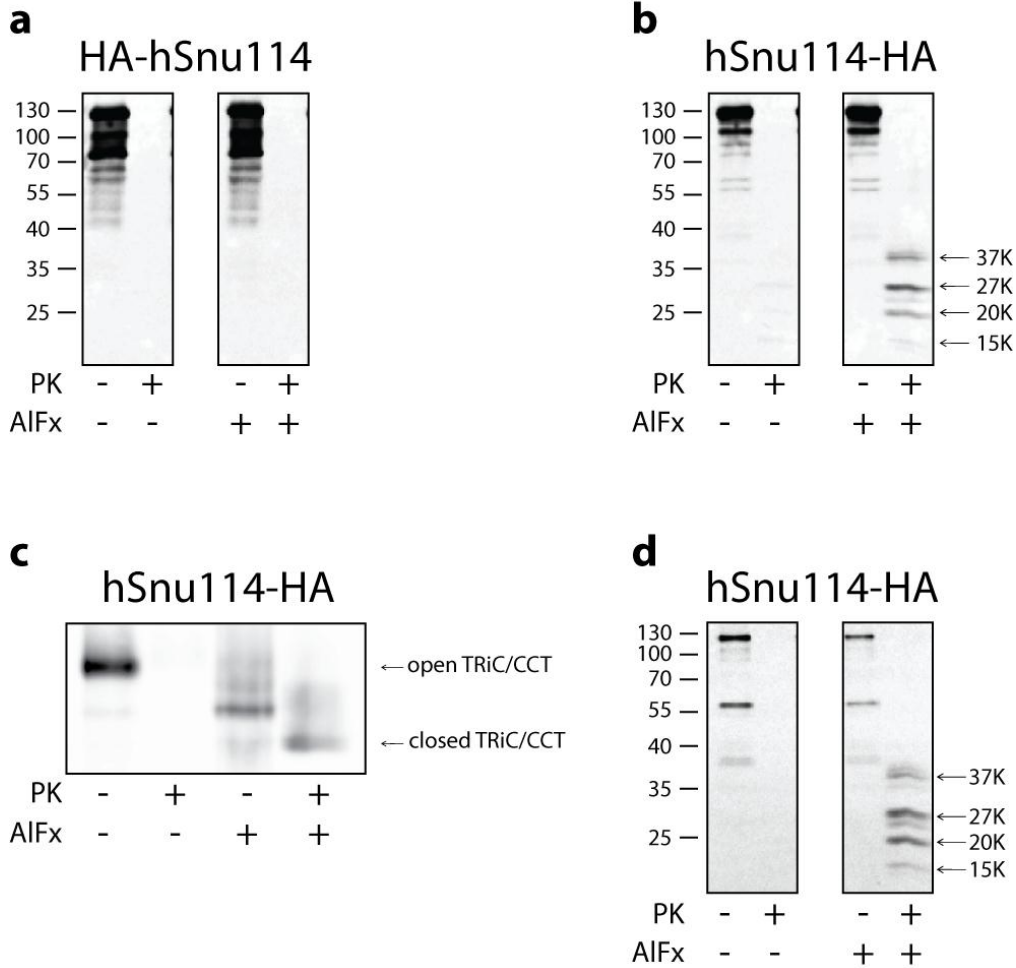


Figure 35: Detection of hSnu114 N- and C-terminus by Western blot. Transferred proteins were detected using an anti-HA antibody. The molecular weight markers indicate the apparent molecular weight in kDa. Protected fragments are indicated by arrows and the respective approximate apparent molecular weight in kDa. **a)** and **b)** Western blot after SDS-PAGE of samples of total RRL lysate. **c)** Western blot after native PAGE. **d)** Western blot after SDS-PAGE of TRiC-bound proteins eluted from native gels.

In order to relate the protease protected fragments to the hSnu114 domain structure, a homology model based on the structure of eEF2 (Jorgensen et al., 2003) was used. Note that domain V (purple) is inserted into domain IV (red) (Figure 30a).

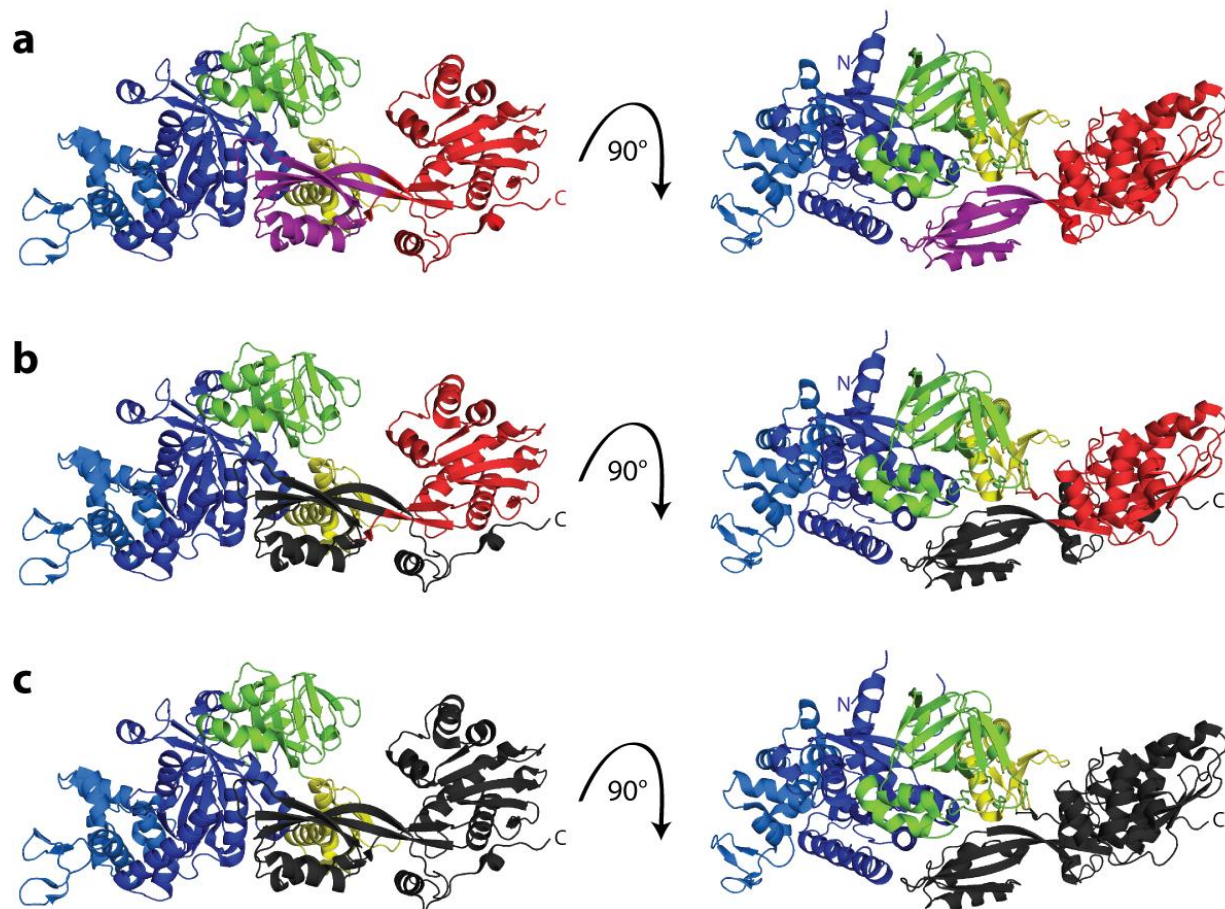


Figure 36: Structural analysis of partial encapsulation of hSnu114. The crystal structure of yeast eEF2 (1NOV, Jorgensen et al., 2003) was colored according to its domain structure using PyMOL. Domain G is shown in dark blue and domain G' in light blue. Domain II is shown in green, domain III in yellow, domain IV in red and domain V in purple. N- and C-termini are indicated when visible. The structures on the right represent a 90° rotated view. **b)** The C-terminal part of domain IV and additionally domain V were colored in dark grey to indicate parts of the corresponding hSnu114 structure, which likely gives rise to the protected 15 kDa fragment (Figures 32 and 35). **c)** Domain IV and domain V were colored in dark grey to indicate parts of the corresponding hSnu114 structure, which might give rise to the protected 35 kDa fragment.

The smallest observed fragment has a molecular weight of approximately 15 kDa and might correspond to domain V and the C-terminal part of domain IV (Figure 36b). The complete domains IV and V together are 315 amino acids in length and have an approximate molecular weight of 35 kDa (Figure 36c). This corresponds roughly to the largest observed C-terminal fragment. Interestingly, the two fragments with the highest intensity have apparent molecular weights of approximately 20 kDa and 27 kDa. Thus, they seem to originate from encapsulation

of the C-terminal part of domain IV plus domain V as well as parts of the N-terminal portion of domain IV. This is surprising, as it would be expected that all parts of the protein that are forming a single domain in the native protein should be encapsulated together to allow formation of the native structure during the time of encapsulation.

Furthermore, the sizes of the protected fragments were unexpected. All fragments were smaller than 50 kDa and thus the encapsulated segment of hSnu114 was not simply determined by the maximum capacity of the TRiC cavity. Rather, it appears that more specific mechanisms govern the selectivity for certain parts to be encapsulated inside the TRiC cavity. The results for the N- and C-terminal parts of hSnu114 are interesting in this regard. While hSnu114-N was not binding to TRiC and was therefore also not protected from PK digest upon closure of the TRiC cavity, hSnu114-C, which has a molecular weight of approximately 45 kDa, was completely protected from PK digest, suggesting total encapsulation of hSnu114-C. Thus, the occurrence of smaller protected fragments from the full-length protein is dependent on the presence of the N-terminal part of hSnu114. How this works mechanistically remains to be determined.

It is especially intriguing in this context that so many fragments of different sizes have been protected from PK digest by encapsulation inside the TRiC cavity. Possibly, the different fragments reflect snapshots of hSnu114 at different stages of folding. Assuming that the N-terminal domain folds independently into a stable structure, which is supported by stable fragments generated upon digest of hSnu114-N (Figure 33a), it is conceivable that folding of the C-terminal part of hSnu114 proceeds by stepwise addition of folding units onto a growing N-terminal core. According to this interpretation, the larger protected fragments reflect earlier stages of folding, in which the C-terminal part of hSnu114 is largely unfolded and consequently encapsulated inside TRiC. In contrast, the smallest fragment provides a snapshot of the final step of folding, in which the very C-terminal part is finally folded and combined with the remaining parts of the protein to form the folded hSnu114.

In summary, the experiments with the natural TRiC interactor hSnu114 led to the following insights:

1. The TRiC-hSnu114 interaction is most likely mediated by the C-terminal part of hSnu114 as suggested by the fact that a construct comprising the N-terminal amino acids 1-580 is hardly interacting at all with TRiC, in contrast to a construct comprising the C-terminal amino acids 581-972.
2. Consequently, TRiC encapsulates C-terminal fragments of hSnu114 upon closure of the cavity. The fragments have apparent molecular weights of approximately 15-45 kDa and are thus much smaller than the maximal capacity of TRiC.
3. Not all fragments are matching with the domain boundaries of hSnu114 as predicted by its homology to eEF2, suggesting that partial encapsulation of domains might occur.
4. The occurrence of multiple protected fragments suggests a stepwise folding mechanism of hSnu114, in which folding units are added sequentially onto a growing N-terminal core.

# 4. Discussion

## 4.1 Partial Encapsulation of Multi-Domain Proteins

The volume of the TRiC cavity was estimated to be large enough for complete encapsulation of substrates of 60-70 kDa (Cong et al., 2011; Dekker et al., 2011a). However, 30-50% of the known TRiC interactors exceed these size limits (Figure 10). Assuming that many of the large TRiC interactors represent authentic TRiC substrates, specific mechanisms must exist to enable folding of such large client proteins. Since productive folding requires protein encapsulation (Reissmann et al. 2007), the only logical mechanism to achieve the folding of large proteins is partial encapsulation. However, partial encapsulation of substrates inside TRiC has never been shown experimentally.

The mechanism of folding by partial encapsulation is especially interesting considering that more than 70% of eukaryotic proteins are multi-domain proteins (Han et al., 2007; Jacob et al., 2007). Typical domain sizes range from 50-300 amino acids (Netzer and Hartl, 1998). Thus, a typical domain would easily fit inside the TRiC cavity and partial encapsulation might occur in a domain-wise manner, in which the rest of the protein would be located outside the closed cavity where it cannot interfere with the folding process (Figure 37). The experiments with actin fusion proteins presented in this study confirm the importance of domain-wise encapsulation. By encapsulating only the actin moiety of the fusion protein, as in the case of GFP-actin, it is ensured that folding of actin can occur undisturbed. However, replacement of the stably folded GFP domain by the misfolded  $\Delta$ N-GFP in the fusion protein results in complete encapsulation (Figures 26 and 27) and consequently severely disturbs the folding of actin (Figure 28), probably because inappropriate contacts between actin and  $\Delta$ N-GFP occur.

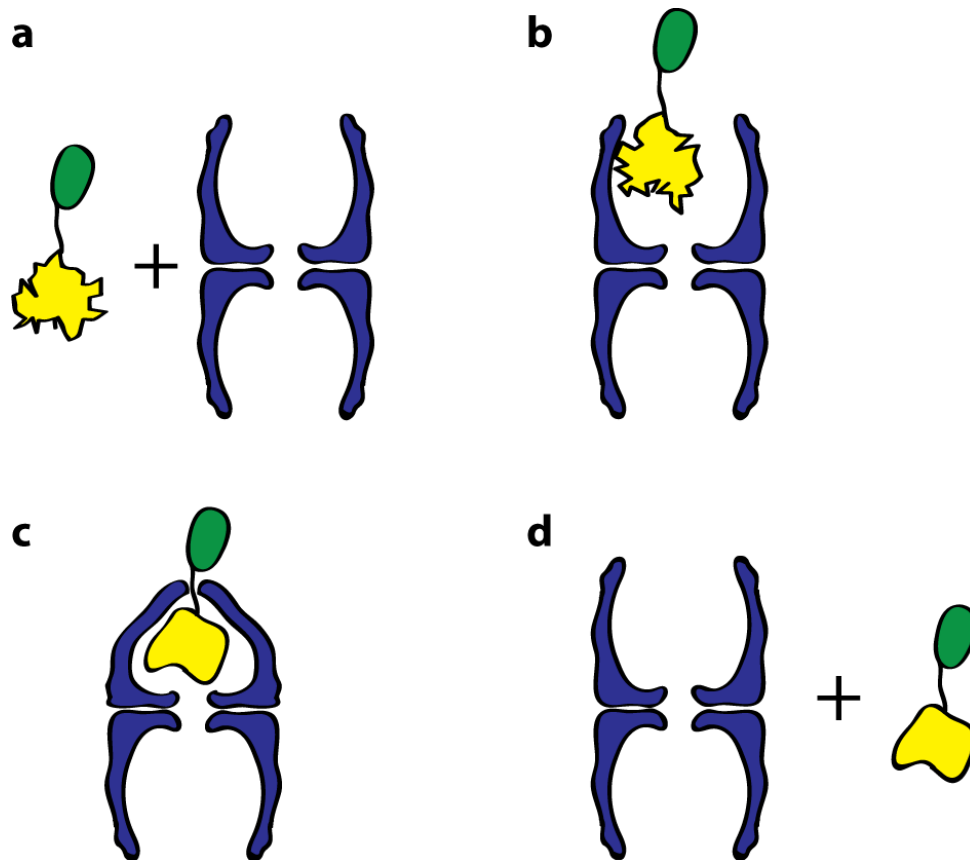


Figure 37: Simplified scheme of partial encapsulation of a two-domain protein by TRiC. The two rings of TRiC are shown in blue in a side-view, representing two opposite subunits of each ring. The model substrate has one TRiC-dependent (yellow) and one TRiC-independent (green) domain, connected by a flexible linker. The substrate binds to the apical domain of TRiC (b). Upon ATP hydrolysis the TRiC-dependent domain is encapsulated (c). The folded protein is released after ring opening (d).

Therefore, it is expected that TRiC would preferentially encapsulate only the TRiC-dependent domain of a multi-domain substrate, even if this domain is smaller than the maximum capacity of the cavity. Notably, this is exactly what was observed with the putative natural substrate hSnu114. The encapsulated fragments had molecular weights between 15 kDa and 45 kDa (Figures 32, 35, 36). Thus, it seems likely that partial encapsulation occurs not only for TRiC substrates exceeding the size limit, but for most multi-domain substrates with a single TRiC-dependent domain.

## 4.2 Factors Influencing Partial Encapsulation

It is not understood, how the selection of part of a substrate for encapsulation works in molecular detail. However, the experiments with actin fusion proteins suggested that the position of a domain within a multi-domain protein is influencing its encapsulation. Thus, the mode of encapsulation of a domain can be changed by the presence of a neighboring domain as seen for hSnu114, whose C-terminal part is completely encapsulated when expressed alone (Figure 33), but only partially encapsulated in the context of the full-length protein (Figure 32).

### 4.2.1 Initial Binding of Substrates to TRiC

Generally, encapsulation of a substrate is dependent on its initial binding to TRiC. Structural and biochemical data indicate that substrate binding to group II chaperonins is mediated by helices H10 and H11 within the apical domains of the chaperonin subunits (Pereira et al., 2010; Spiess et al., 2006). However, it is still not clear which determinants of the substrate proteins are generally mediating the binding to TRiC. It is still a matter of debate whether mainly hydrophobic or hydrophilic interactions occur in the initial substrate capturing by group II chaperonins (Huo et al., 2010; Jayasinghe et al., 2009; Kubota et al., 2006).

The interaction of actin with TRiC has been studied in great detail and is an excellent example of the complexity of the molecular events associated with substrate recognition, folding and release from the eukaryotic group II chaperonin. The tip of subdomain 4 of actin was found to be especially important for initial binding of actin to TRiC (McCormack et al., 2001b; Neiryneck et al., 2006). However, several other regions in the actin molecule have been shown to be involved in the interaction with TRiC at later folding stages (Neiryneck et al., 2006). Interestingly, a short peptide motif within subdomain 1 of actin, which is also present in the TRiC-substrate Cdc20, was found to be important for binding of Cdc20 to TRiC (Camasses et al., 2003), suggesting that at least some determinants might be of more general importance for TRiC-substrate interactions (Neiryneck et al., 2006). Nevertheless, no common sequence pattern for prediction of TRiC substrates has been identified so far. The present experiments with hSnu114 suggest that the binding determinants of this TRiC-interactor are localized within the C-terminal part of the

protein (Figures 33, 34, 35). Furthermore, based on the smallest detected fragment of 15 kDa (Figures 32b and 35b+d) it is likely that the binding determinants are present in the C-terminal 140 amino acids. Interestingly, this region is rich in  $\beta$ -strands (Figure 36b), consistent with previously reported data showing enrichment in regions of  $\beta$ -strand propensity among TRiC interactors (Yam et al., 2008).

#### 4.2.2 Sequential Release of Substrates into the TRiC Cavity

The way of encapsulation of a substrate within TRiC is furthermore determined by its release into the cavity. In group II chaperonins, release of the substrate was proposed to be mediated by a release loop in the apical domain that displaces the substrate bound to the neighboring subunit upon closure of the cage (Douglas et al., 2011). As seen for the TRiC-actin complex, substrates can interact with more than one TRiC subunit upon initial binding (Llorca et al., 1999a). Subunit specific binding across the apical pore might result in disruption of compact, non-productive folding intermediates and thus enable subsequent folding. TRiC is a hetero-oligomeric complex consisting of eight paralogous subunits. The inter-subunit sequence conservation is especially low within the substrate binding region in the apical domains (Kim et al., 1994), suggesting that specific TRiC subunits might interact with specific substrates or even specific regions within a given substrate. The proposed sequential mechanism of ring-closure (Lin and Sherman, 1997; Rivenzon-Segal et al., 2005) would result in a sequential release of the different binding determinants of a given substrate from TRiC and thus the encapsulation would occur for every substrate individually in a very defined space- and time-dependent manner that might be critical for productive folding.

#### 4.2.3 Position of the TRiC-dependent Domain

It is not yet clear, whether TRiC-dependent domains are preferentially located N- or C-terminally or whether no such preference exists. In fact, it is not known, which domains of the known large TRiC-interactors are dependent on TRiC for folding. N-terminal TRiC-dependent domains might be folded co-translationally by partial encapsulation while the folding of C-terminal domains can

be completed only post-translationally. A TRiC-dependent domain in the middle of a large multi-domain protein would create additional steric constraints because both the N- and the C-terminus of the substrate would have to protrude from the cavity and therefore two linker regions would have to pass through the opening of the cavity to connect the encapsulated middle-domain with the two termini. Indeed, actin as a middle-domain in between an N-terminal BFP and a C-terminal GFP was not folded by TRiC upon expression in RRL (Figures 13 and 14). However, some natural substrates might be evolutionarily optimized for partial encapsulation of a middle-domain in terms of the linker regions, in contrast to the BFP-actin-GFP construct used here.

In summary, encapsulation by TRiC is not only influenced by the size of the respective multi-domain substrate but also by various other factors. The domains adjacent to the TRiC-dependent domain in the substrate protein might substantially influence the encapsulation process. For example, TRiC encapsulates several different fragments between 15 kDa and 45 kDa of full-length hSnu114 (Figure 32). In contrast, the complete C-terminal part was encapsulated when it was expressed alone (Figure 33). Thus, it appears that the N-terminal part of hSnu114 is modulating the encapsulation of the C-terminal part, even though the N-terminal part itself is not interacting with TRiC (Figures 31 and 33). Possibly, the N-terminal part serves as a core for stepwise addition of C-terminal folding units. The position of the TRiC-dependent domain within a multi-domain protein is important for the efficiency of folding. At least, the actin fusion proteins that were tested clearly showed context-dependent differences in folding: C-terminal actin was more efficiently folded than N-terminal actin. Folding failed completely when actin was not localized at either of the termini (Figures 13 and 14). However, it is not clear whether this observation can be generalized to natural TRiC substrates. Finally, the complex interplay between different binding determinants and the sequential release upon cavity closure is accompanied by a high structural flexibility of the open TRiC complex (Cong et al., 2011), resulting in heterogeneity of TRiC-substrate complexes upon encapsulation. Heterogeneity of encapsulation was observed for the natural substrate hSnu114 (Figures 32 and 35). Digest of the TRiC-bound GFP-actin fusion protein resulted mainly in protection of full-length GFP-actin because GFP is itself protease-resistant. However, different fragments with the size of actin were generated when the linker between GFP and actin was accessible to PK, indicating heterogeneity of TRiC-bound GFP-actin as well (Figures 22 and 25).

## 4.3 Structural and Evolutionary Aspects of Partial Encapsulation

### 4.3.1 The Built-in Lid in Group II Chaperonins

Each subunit of a group II chaperonin contains a helical protrusion of approximately 30 amino acids at the tip of the apical domain (Klumpp et al., 1997). The protrusions of the different subunits come together at the center of the cavity upon ATP hydrolysis to seal off the cavity from the surrounding environment, in contrast to group I chaperonins such as GroEL which make use of a detachable co-chaperone to close the cage. Conceptually, it is very difficult to imagine how partial encapsulation would be achieved if encapsulation occurred with a GroES-like co-chaperone. By contrast, the iris-like closure of the built-in lid in group II chaperonins is perfectly suited for partial encapsulation. The different TRiC subunits would sequentially move towards the center of the ring upon ATP hydrolysis, thereby scanning the substrate until they reach their final position. The proposed scanning movement of the subunits would also help to explain the observed heterogeneity of closed TRiC-substrate complexes. Obviously, the flexibility of the different TRiC subunits would not always result in exactly the same portion of the substrate to be encapsulated. It is also conceivable that the TRiC complex would not adopt a conformation that is as tightly closed as the structures of the symmetrically closed group II chaperonins suggest (Cong et al., 2010; Dekker et al., 2011a; Ditzel et al., 1998). However, the closure of the cavity is tight enough to prevent protease from accessing parts of the substrate inside the cavity as well as to protect the protease-sensitive helical protrusion of TRiC from digest, as the experiments with large partially encapsulated substrates show clear protection of encapsulated parts.

### 4.3.2 Evolution of Different Lids in Group I and II Chaperonins

Based on structural alignments and comparison of the specific tertiary structure of different protein folds, it has been proposed that the apical domain of chaperonins originates evolutionary from peroxiredoxins (Dekker et al., 2011b). Interestingly, the authors furthermore suggest that the Ur-chaperonin was completely lidless and that the development of the different encapsulation mechanisms in group I and group II chaperonins took place only after their evolutionary

separation rather than that the GroES-like co-chaperone would have been lost during evolution of archaea and eukaryotes. If the need for encapsulation of chaperonin-dependent protein-domains has occurred after the appearance of larger multi-domain proteins in eukaryotes, it is logical to assume that only a mechanism of encapsulation like the built-in lid could evolve because it was compatible with partial encapsulation. If on the other hand the different mechanisms of encapsulation have evolved early after separation of the different kingdoms of life, it is clear that larger multi-domain proteins with chaperonin-dependent domains could not evolve in eubacteria because their co-chaperone dependent encapsulation mechanism did not support partial encapsulation.

The correlation of the chaperonin type present in a specific domain of life with the proportion of multi-domain proteins in that domain suggests a clear interdependency of both factors as long as only eubacteria and eukaryotes are analyzed. However, archaea possess group II chaperonins with built-in lids, even though their proteomes are very similar to bacterial proteomes with regard to the fraction of multi-domain proteins (Ekman et al., 2005). Therefore, it is more likely that the folding of large multi-domain proteins by partial encapsulation is not enabled by the built-in lid as such, but by the sequential closure of the cavity, which is dependent on the hetero-oligomeric nature of the eukaryotic chaperonin. Future studies should address, which other large TRiC interactors are encapsulated partially by the chaperonin and how partial encapsulation works in mechanistic detail.

# 5. Materials and Methods

## 5.1 Materials

### 5.1.1 Chemicals

Table 2: List of chemical compounds used in this study.

<b>Chemical compound</b>	<b>Purchased from</b>
6-aminohexanoic acid	Sigma-Aldrich
Acetic acid	Sigma-Aldrich
Acetone	VWR
ADP	Sigma-Aldrich
Agarose LE	Biozyme
Al(NO <sub>3</sub> ) <sub>3</sub>	Sigma-Aldrich
Ampicillin	Carl Roth
APS	Sigma-Aldrich
ATP	Sigma-Aldrich
Bis-Tris methane	Sigma-Aldrich
Bromophenol blue	Sigma-Aldrich
CaCl <sub>2</sub>	Merck
Chloramphenicol	Sigma-Aldrich
Cycloheximide	Sigma-Aldrich
DTT	Roche
EDTA	Merck
EDTA-free protease inhibitor cocktail tablets	Roche
EGTA	Sigma-Aldrich
Glycerol	Merck
Glycine	Carl Roth
HCl	VWR
HEPES	Biomol
Kanamycin	Sigma-Aldrich
KCH <sub>3</sub> CO <sub>2</sub>	Carl Roth
KCl	Sigma-Aldrich
KF	Sigma-Aldrich
KH <sub>2</sub> PO <sub>4</sub>	Carl Roth
β-mercaptoethanol	Sigma-Aldrich
Mg(CH <sub>3</sub> CO <sub>2</sub> ) <sub>2</sub>	Merck
MgCl <sub>2</sub>	Sigma-Aldrich

MnCl <sub>2</sub>	Merck
MOPS	Sigma-Aldrich
Na <sub>2</sub> HPO <sub>4</sub>	Merck
NaCH <sub>3</sub> CO <sub>2</sub>	Sigma-Aldrich
NaCl	VWR
NaHCO <sub>3</sub>	Sigma-Aldrich
(NH <sub>4</sub> ) <sub>2</sub> SO <sub>4</sub>	Sigma-Aldrich
PMSF	Sigma-Aldrich
Ponceau S	Sigma-Aldrich
RbCl	Sigma-Aldrich
SDS	SERVA
Sodium deoxycholate	Sigma-Aldrich
Sucrose	Sigma-Aldrich
SYBR® Safe	Invitrogen
TCEP	Thermo Scientific Pierce
TEMED	Sigma-Aldrich
Trichloroacetic acid	Sigma-Aldrich
Tris	Sigma-Aldrich
Triton X-100	Sigma-Aldrich
Tween 20	Sigma-Aldrich

### 5.1.2 Media and Buffers

Table 3: List of media and buffers used in this study.

Medium/Buffer	Composition
LB medium	10 g/l NaCl 5 g/l yeast extract (BD) 10 g/l tryptone (BD)
Buffer Tfb1	30 mM KCH <sub>3</sub> CO <sub>2</sub> 100 mM RbCl 50 mM MnCl <sub>2</sub> 10 mM CaCl <sub>2</sub> 15% glycerol Adjust to pH 5.8 with acetic acid
Buffer Tfb2	10 mM MOPS-NaOH, pH 6.8 10 mM RbCl 75 mM CaCl <sub>2</sub> 15% glycerol

TAE Buffer	40 mM Tris 40 mM acetic acid 1 mM EDTA
Homogenization Buffer	20 mM HEPES-NaOH, pH 7.4 50 mM NaCl 5 mM MgCl <sub>2</sub> 1 mM EDTA 1 mM DTT 40 tablets/l EDTA-free protease inhibitor cocktail
Buffer A	20 mM HEPES-NaOH, pH 7.4 50 mM NaCl 5 mM MgCl <sub>2</sub> 1 mM EDTA 1 mM DTT 10% glycerol 4 tablets/l EDTA-free protease inhibitor cocktail
Buffer B	20 mM HEPES-NaOH, pH 7.4 1 M NaCl 5 mM MgCl <sub>2</sub> 1 mM EDTA 1 mM DTT 10% glycerol
Storage Buffer	20 mM HEPES-NaOH, pH 7.4 100 mM NaCl 5 mM MgCl <sub>2</sub> 1 mM DTT 10% glycerol 2 tablets/l EDTA-free protease inhibitor cocktail
Coupling Buffer	100 mM NaHCO <sub>3</sub> , pH 8.3 500 mM NaCl
Low pH Washing Buffer	100 mM acetic acid / sodium acetate, pH 4.0 500 mM NaCl
High pH Washing Buffer	100 mM Tris-HCl, pH 8.0 500 mM NaCl
1x PBS	137 mM NaCl 2.7 mM KCl 10 mM Na <sub>2</sub> HPO <sub>4</sub> 2 mM KH <sub>2</sub> PO <sub>4</sub> pH 7.4
Dilution Buffer	1x PBS 5 mM EDTA 1 mM DTT 0.1% Tween 20 20 tablets/l EDTA-free protease inhibitor cocktail

Washing Buffer 1	50 mM Tris-HCl, pH 7.4 150 mM NaCl 5 mM EDTA 1% Triton X-100
Washing Buffer 2	50 mM Tris-HCl, pH 7.4 500 mM NaCl 5 mM EDTA 1% Triton X-100
Sucrose Buffer	20 mM HEPES-KOH, pH7.5 500 mM sucrose 10 mM KCl 5 mM MgCl <sub>2</sub> 2 mM β-mercaptoethanol 1 mM EGTA 10% glycerol
Buffer Lid	20 mM HEPES, pH 7.4 100 mM KCH <sub>3</sub> CO <sub>2</sub> 5 mM Mg(CH <sub>3</sub> CO <sub>2</sub> ) <sub>2</sub>
2x SDS Loading Buffer	120 mM Tris-HCl, pH 6.8 20% glycerol 5% β-mercaptoethanol 4% SDS 0.01% bromophenol blue
2x Native Loading Buffer	100 mM Bis-Tris methane, pH 8.0 1 M 6-aminohexanoic acid 10 mM KCl 2 mM MgCl <sub>2</sub> 30% glycerol 0.008% Ponceau S 10 tablets/l EDTA-free protease inhibitor cocktail
Transfer Buffer	48 mM Tris 39 mM glycine 20% methanol 0.037% SDS
TBS-T	10 mM Tris-HCl, pH 7.5 150 mM NaCl 0.1% Tween 20
Blocking Buffer	TBS-T 5% skimmed milk powder (Saliter)

### 5.1.3 Plasmids

The pMS vector was derived from the pCH vector, a modified pET-22b vector (Novagen) described earlier by our group (Chang et al., 2005). The vector contains an ampicillin resistance gene. The gene of interest is under the control of a T7 promoter. All constructs except pMS-ActLink and pMS-ActLink-G150P encoded for proteins with a C-terminal 6xHis-tag.

Table 4: List of actin-fusion expression plasmids used in this study. The linkers between the different “domains” are described by “L” followed by the number of amino acids of the respective linker. The linker sequences can be found in Table 5. Xa stands for the four amino acid factor Xa protease cleavage site “IEGR” (Nagai and Thogersen, 1984). The myc-tag sequence “EQKLISEEDL” is indicated by “myc”.

Plasmid	Encodes for	Source
pMS-BG	BFP-L15-GFP-L3-6xHis	Markus Stemp
pMS-A	Actin-L9-6xHis	Markus Stemp
pMS-AG	Actin-L16a-GFP-L3-6xHis	Markus Stemp
pMS-GA	GFP-L17-Actin-L2-6xHis	Markus Stemp
pMS-BAG	BFP-L16b-Actin-L16a-GFP-L3-6xHis	Markus Stemp
pMS-BTAG	BFP-L23-Actin-L16a-GFP-L3-6xHis	Markus Stemp
pMS-BTAG-G150P	BFP-L23-Actin(G150P)- L16a-GFP-L3-6xHis	Markus Stemp
pMS-AL	Actin-L17-Luciferase-Xa-L14-myc-6xHis	Markus Stemp
pMS-BGA	BFP-L15-GFP-L17-Actin-L2-6xHis	This work
pMS-ActLink	Actin-L97	This work
pMS-ActLink-G150P	Actin(G150P)-L97	This work
pMS-ΔN-GA	ΔN-GFP-L17-Actin-L2-6xHis	This work
pMS-AΔN-G	Actin-ΔN-GFP-L3-6xHis	This work

The actin amino acid sequence used was from *Saccharomyces cerevisiae* and is accessible under the UniProt ID “P60010” (www.uniprot.org). In pMS-BTAG-G150P and pMS-ActLink-G150P, glycine at position 150 of actin was mutated to proline. The GFP amino acid sequence used differed in five positions from the sequence of wild-type GFP of *Aequorea victoria*, as described under the UniProt ID “P42212”. Specifically, the sequence contained the three cycle 3 mutants F99S, M153T and V163A, which reduce the hydrophobicity of GFP and thereby cause less aggregation upon heterologous expression (Crameri et al., 1996). Additionally, the GFP sequence contains the two point mutations S2G and Q80R compared to the *Aequorea victoria*

sequence, which is a known sequence conflict (see the GFP UniProt entry and the respective reference (Rouwendal et al., 1997)). In the constructs with a C-terminal GFP (BG, AG, BAG and BTAG), the starting methionine of GFP was exchanged to isoleucine. The BFP sequence differed in two positions from the wild-type GFP sequence of *Aequorea victoria* as described in UniProt entry “P42212”. The two mutations are Y66H and Q80R. Y66H is the necessary chromophore mutation to convert GFP into BFP (Heim et al., 1994). The luciferase sequence in pMS-AL is the sequence from *Photinus pyralis*, which can be found under the UniProt ID “P08659”.

In order to clone the BGA construct, pMS-BG and pMS-GA were cut with XhoI and DraIII. XhoI cuts within the GFP sequence but not within the BFP sequence. DraIII cuts downstream of the coding region within the pMS vector. After purification of the respective fragments from an agarose gel, a ligation was set up comprising the GFP-actin part of pMS-GA and the BFP-GFP part of pMS-BG. The resulting product is pMS-BGA, where the 5' region of the GFP sequence originates from pMS-BG and the 3' region of the GFP sequence originates from pMS-GA.

Construction of pMS- $\Delta$ N-GA was started with a PCR reaction to create a respective  $\Delta$ N-GFP-actin DNA sequence. pMS-GA was used as plasmid DNA. The respective forward and reverse primers were GFPdeltaN38NcoIf and T7Terminator r. Both the PCR product and pMS-GA were cut with NcoI and NdeI. The cut PCR product encoding  $\Delta$ N-GFP was inserted into the cut pMS-GA construct, thereby replacing wild-type GFP with  $\Delta$ N-GFP and creating pMS- $\Delta$ N-GA.

In order to generate pMS-A $\Delta$ N-G, an NcoI restriction site was introduced just upstream of the GFP encoding sequence in pMS-AG by site-directed mutagenesis using the primers AG G1214C C1217Gfor and AG G1214C C1217Grev. The new pMS-AG that contains the NcoI restriction site and pMS- $\Delta$ N-GA were both digested with NcoI and XhoI. The fragment containing the  $\Delta$ N-GFP encoding sequence was then inserted into pMS-AG, replacing the wild-type GFP encoding sequence and thus creating pMS-A $\Delta$ N-G.

The ribosome stalling constructs were created by PCR, resulting in a truncated message without an in-frame stop codon. AG219 was made using pMS-AG as template DNA. The forward primer was T7pIVEX27f that binds 20-40 base pairs upstream of the T7 promoter in the pMS vector. The reverse primer was G219r. The resulting PCR product encodes for a truncated nascent chain



The plasmid DNA, encoding for the different natural TRiC interactors, was obtained from different human cDNA libraries containing IMAGE cDNA clones ([www.imagenes-bio.de](http://www.imagenes-bio.de)) available within the core facility of the Max Planck Institute of Biochemistry (MPIB). I have used the following constructs (Table 6).

Table 6: Putative TRiC substrates tested for binding to TRiC upon expression in RRL.

Gene Name	IMAGE ID	Vector	Promoter
ATP6V0A1	IRATp970F1251D	pCMV-SPORT6	SP6
COPB2	IRAUp969D082D	pOTB7	SP6
DYNC1H1	IRAUp969G0774D	pOTB7	SP6
EEF2	IRCMp5012E0117D	pCR4-TOPO	T3
EFTUD2	IRAUp969B023D	pOTB7	SP6
FASN	IRATp970A1078D	pCMV-SPORT6	SP6
GANAB	IRATp970G0786D	pCMV-SPORT6	SP6
KIF13A	IRCMp5012B0136D	pCR-BluntII-TOPO	SP6
LARS	IRATp970C01140D	pCMV-SPORT6	SP6
MMS19	IRCMp5012D0412D	pCR4-TOPO	T3
MUC17	IRCMp5012B0117D	pCR4-TOPO	T3
MYH1	IRCMp5012C1031D	pCR-BluntII-TOPO	T7
NUP153	IRATp970E0675D	pCMV-SPORT6	SP6
SKIV2L	IRAUp969E0173D	pOTB7	SP6
SMARCC2	IRATp970H0938D	pCMV-SPORT6	SP6
THNSL1	IRATp970D0960D	pBluescriptR	T7
TSHZ3	IRCMp5012A1036D	pCR-BluntII-TOPO	SP6
UBA1	IRAUp969B0950D	pOTB7	SP6
USP10	IRAUp969G1012D	pOTB7	SP6

The constructs for separate expression of the N- and C-terminal parts of  $\beta'$ -COP ( $\beta'$ -COP-N (amino acids 1-283) and  $\beta'$ -COP-C (amino acids 284-906)) and hSnu114 (hSnu114-N (amino

acids 1-580) and hSnu114-C (amino acids 581-972)) were generated by PCR. The template DNA was pOTB7-COPB2 for  $\beta$ '-COP and pOTB7-EFTUD2 for hSnu114, respectively.

In a first PCR reaction, constructs that have the Kozak consensus sequence (Kozak, 1987) directly 5' of the start codon and a 12 base pair Poly(A) tail directly 3' of the stop codon were created. The respective primer pairs were:

KozakStartCOPB2(1)for + PolyTStoppCOPB2(283)rev,

KozakStartCOPB2(284)for + PolyTStoppCOPB2(906)rev,

KozakStartEFTUD2(1)for + PolyTStoppEFTUD2(580)rev and

KozakStartEFTUD2(581)for + PolyTStoppEFTUD2(972)rev.

The respective PCR products were purified from an agarose gel and used as template DNA for the second PCR, in which the T7 promoter sequence was added 5' to the Kozak consensus sequence. The reverse primers in the second PCR were the same as in the first PCR, but T7KozakStartfor was used as a forward primer in all 4 PCRs to add the T7 promoter.

Two different versions of HA- and FLAG-tagged hSnu114 were created, one with an N-terminal HA- as well as a C-terminal FLAG-tag and another one with an N-terminal FLAG- and a C-terminal HA-tag. In a first step, the sequences of the respective tags were added by PCR. pOTB7-EFTUD2 was used as template DNA. The respective primer pairs were:

FLAG-EFTUD2 for + HA-EFTUD2 rev and HA-EFTUD2 for + FLAG-EFTUD2 rev.

In order to add a 5' NdeI restriction site and a 3' NheI restriction site, the respective PCR products were used as template DNA for a second PCR after purification from an agarose gel. The respective primer pairs were:

Spacer-NdeI-FLAG for + Spacer-NheI-Stop-HA rev and

Spacer-NdeI-HA for + Spacer-NheI-Stop-FLAG rev

The PCR products were then cut with NdeI and NheI and inserted into pMS-AG, which was also cut with NdeI and NheI, thereby replacing AG with the sequences encoding for the different tagged hSnu114 constructs.

#### 5.1.4 Oligonucleotides

Table 7: List of primers used in this study. All oligonucleotides have been purchased from metabion international AG (Martinsried, Germany).

Primer	Nucleotide sequence (5'→3')	Source
T7pIVEX27f	CCGGCGTAGAGGATCGAGATC	Florian Brandt
G219r	GGACCATGTGGTCTCTCTTTTC	Markus Stemp
Luc36r	GAACCAGGGCGTATCTCTTC	This work
Luc49r	TCACCTCGATATGTGCATCTG	This work
L61r	GAACGGACATTTCGAAGTATTC	Markus Stemp
G4SLinker53r	CCACTGTAGCTCCACCAGC	This work
G4SLinker78r	CGACGTTCAGCAGAAGGAG	This work
G4SLinker97r	ACACCTGGATGATGATGATGC	This work
GFPdeltaN38NcoIf	ACTGAGTCCATGGGTTACGGAAAACCTT ACCCTT	This work
T7Terminator r	GCTAGTTATTGCTCAGCGG	This work
AG G1214C C1217Gfor	GCTGGCGAAGCGGCCCGCCATGGGTAAA GGAGAAGAACTT	This work
AG G1214C C1217Grev	AAGTTCCTTCTCCTTTACCCATGGCGGCCGCT TCGCCAGC	This work
KozakStartCOPB2(1)for	TAGGGAACAGCCACCATGCCTCTGCGA CTTGAT	This work
PolyTStoppCOPB2(283)rev	TTTTTTTTTTTTTCATGACCCTCTTAGAC TGGC	This work
KozakStartCOPB2(284)for	TAGGGAACAGCCACCATGAACAATGTC GCTTTGGGCT	This work
PolyTStoppCOPB2(906)rev	TTTTTTTTTTTTTCAATCATCCAAAATAT CTTCATC	This work
KozakStartEFTUD2(1)for	TAGGGAACAGCCACCATGGATACCGAC TTATATGAT	This work
PolyTStoppEFTUD2(580)rev	TTTTTTTTTTTTTTCACAAGGGTCGGAAA ATCTGA	This work
KozakStartEFTUD2(581)for	TAGGGAACAGCCACCATGAAGTTCAAT ACCACATCT	This work
PolyTStoppEFTUD2(972)rev	TTTTTTTTTTTTTTCACATGGGGTAATTGA GC	This work

T7KozakStartfor	GGATCCTAATACGACTCACTATAGGGA ACAGCCACCATG	This work
FLAG-EFTUD2 for	CTACAAGGACGACGATGACAAGATGGA TACCGACTTATATGATG	This work
HA-EFTUD2 rev	GTAGTCTGGGACGTCGTATGGGTACAT GGGGTAATTGAGCACAAC	This work
HA-EFTUD2 for	ATACGACGTCCCAGACTACGCTATGGA TACCGACTTATATGATG	This work
FLAG-EFTUD2 rev	GTCATCGTCGTCCTTGTAGTCCATGGGG TAATTGAGCACAAC	This work
Spacer-NdeI-FLAG for	GAACAGCATATGGACTACAAGGACGAC GATGAC	This work
Spacer-NheI-Stop-HA rev	GAACAGGCTAGCTTAAGCGTAGTCTGG GACGTCGTAT	This work
Spacer-NdeI-HA for	GAACAGCATATGTACCCATACGACGTC CCAGACTAC	This work
Spacer-NheI-Stop-FLAG rev	GAACAGGCTAGCTTACTTGTCATCGTCG TCCTTGTAG	This work

## 5.2 Molecular Biology Methods

### 5.2.1 Preparation of Chemically Competent Cells

To obtain sufficient amounts of plasmid DNA for subsequent experiments, the respective plasmids were multiplied in chemically competent *E. coli* of the DH5 $\alpha$  strain. Chemically competent cells were generated with the RbCl method. 3 ml of autoclaved LB medium were inoculated with DH5 $\alpha$  cells and the cells were incubated for 16 hours overnight at 37°C and 220 rpm shaking. This culture was diluted 100-fold into 100 ml LB to obtain an OD of approximately 0.05. The DH5 $\alpha$  cells were then incubated again at 37°C and 220 rpm until the OD reached 0.5. After incubation for 15 minutes on ice, the cells were centrifuged at 4820 rpm for 15 minutes in the C0650 rotor in an Avanti 30 centrifuge (both from Beckman). The pellet was resuspended in 32 ml buffer Tfb1. After 15 min incubation on ice the DH5 $\alpha$  cells were again centrifuged for 15 min at 4820 rpm. The pellet was resuspended in 8 ml buffer Tfb2. The resuspended cells were divided into aliquots of 50  $\mu$ l volume, snap-frozen in liquid nitrogen and stored at -80°C.

### 5.2.2 Transformation of Chemically Competent Cells

Transformation of the chemically competent cells was performed by the following procedure: A 50  $\mu\text{l}$  aliquot of DH5 $\alpha$  cells was thawed on ice for 10 min. Then 1  $\mu\text{l}$  of plasmid DNA with a concentration of 15 ng/ $\mu\text{l}$  (in H<sub>2</sub>O) was added. After 30 min incubation on ice, the DH5 $\alpha$  cells were heat-shocked at 42°C for 45 sec. After 2 min incubation on ice, 800  $\mu\text{l}$  LB medium was added and the cells were incubated for 1 h at 37°C under shaking at 600 rpm. The cells were then pelleted by centrifugation at 16100 g for 15 sec. 650  $\mu\text{l}$  of the supernatant were removed, the pellet was resuspended in the remaining supernatant and distributed on an LB agar plate containing the respective antibiotic. The plate was incubated at 37°C for 16 h.

### 5.2.3 Preparation of Plasmid DNA

To amplify plasmid DNA, a single colony was used to inoculate 3 ml LB medium containing 100  $\mu\text{g}/\text{ml}$  ampicillin or 10  $\mu\text{g}/\text{ml}$  kanamycin, or 25  $\mu\text{g}/\text{ml}$  chloramphenicol depending on the resistance conferred by the respective plasmid.

For a Miniprep, the cells were grown for 16 h at 37°C and 220 rpm shaking. The Minipreps were done using the Wizard® Plus SV Minipreps DNA Purification System from Promega according to the manufacturer's instructions, except that addition of Alkaline Protease Solution, which was interfering with subsequent *in vitro* translation reactions, was omitted. Elution from the Spin Columns was generally done with 50  $\mu\text{l}$  H<sub>2</sub>O.

For a Midiprep, the cells were incubated for 8 h at 37°C and 220 rpm shaking after inoculation of 3 ml LB-ampicillin. Then 100  $\mu\text{l}$  were diluted into 50 ml LB-ampicillin and incubated for 16 h at 37°C and 220 rpm shaking. The Midiprep was done using the PureYield™ Plasmid Midiprep System from Promega according to the manufacturer's instructions. Elution from the PureYield™ Binding Column was generally done with 550  $\mu\text{l}$  H<sub>2</sub>O. The DNA concentration was determined by absorbance at 260 nm using the NanoDrop 1000 spectrophotometer (Thermo Fisher Scientific). Plasmid DNA was stored at -20°C.

#### 5.2.4 Gel Electrophoresis of DNA

Gel electrophoresis of DNA was generally done for 20 min at 90 V using 1% agarose LE gels in TAE buffer (Table 3). For visualization of DNA, SYBR® Safe was diluted 1:10000 into the gel mixture. As a molecular weight marker, GeneRuler™ 1 kb DNA Ladder from Fermentas was used. Visualization was done using a UV-transilluminator system from MVG-Biotech and the BioCaptMW software. When DNA fragments were to cut from the agarose gel for subsequent applications, the Safe Imager™ 2.0 Blue Light Transilluminator from Invitrogen was used. Purification of DNA from agarose gel slices was done using the Wizard® SV Gel and PCR Clean-Up System from Promega according to the manufacturer's instructions.

#### 5.2.5 Polymerase Chain Reaction

Generally, PCR reactions were performed in a volume of 50 µl and contained 15 ng template DNA. The final concentration of each primer was 400 nM and the final concentration of each dNTP was 200 µM. As polymerase, generally Herculase Enhanced DNA Polymerase from Stratagene was used at a final concentration of 0.1 U/µl. The PCR reactions were done in a T3 Thermocycler from Biometra. An initial denaturation step was included in all PCR conditions for 3 min at 95°C. Within each cycle, the denaturation step was generally at 95°C for 30 sec, the annealing temperature was dependent on the respective primers and was generally between 50-60°C for 30 sec, and the elongation step was at 72°C for 1 min per kb of expected PCR product. Generally, each cycle was repeated 30-35 times, followed by a final elongation step at 72°C that was approximately 1.5 times as long as the elongation step within the cycle. For site directed mutagenesis, the cycle was typically repeated only 15 times. PCR purification was done using the Wizard® SV Gel and PCR Clean-Up System from Promega according to the manufacturer's instructions.

#### 5.2.6 Restriction Digest

All restriction enzymes were purchased from New England Biolabs. Restriction digests were done in a final volume of 10 µl containing typically 1-2 µg DNA in the buffer best suited for the

respective restriction enzymes (NEBuffer 1, 2, 3 or 4, New England Biolabs). When suggested for the respective restriction enzymes, the reactions contained additionally 100 µg/ml BSA. Normally, 0.5 µl of each restriction enzyme were used. The reactions were incubated at 37°C for 90 min. When the respective fragment was to be used as the vector in a subsequent ligation, the reaction was incubated for another 30 min at 37°C after addition of 5 units of Calf Intestinal Alkaline Phosphatase (New England Biolabs) to prevent vector re-ligation.

### 5.2.7 DNA Ligation

Ligation was done after purification of the respective fragments from agarose gels. The total volume of a ligation reaction was 10 µl and the ligation was done in T4 DNA Ligase Reaction Buffer (New England Biolabs). The molar insert:vector ratio was typically 3-5 and the total DNA mass in the reaction was normally 100-150 ng. Generally, a ligation reaction contained 200 cohesive end units T4 DNA Ligase, purchased either from New England Biolabs or from the core facility of MPIB. The ligation reactions were incubated for 40 min at room temperature followed by incubation for 40 min at 4°C. Prior to transformation of chemically competent DH5α, the T4 DNA ligase was inactivated by incubation at 60°C for 10 min. Typically, 2.5 µl of a ligation reaction were used for transformation of 50 µl DH5α.

The DNA sequence of all constructs was verified by DNA sequencing in the Core Facility of MPIB.

## 5.3 Biochemical Methods

### 5.3.1 Purification of TRiC from Bovine Testes

TRiC from bovine testes was purified with minor modifications following a published protocol (Villebeck et al., 2007b). The whole purification procedure was performed at 4°C. 200 g bovine testes were homogenized in 300 ml homogenization buffer. Homogenization was done using the

PT-DA 3012/2TM dispersing tool connected to the POLYTRON PT 3100 homogenizer (both from Kinematica) with up to 6000 rpm. The homogenate was clarified by centrifugation at 20,000 g for 40 min using the JA 25.50 rotor in an Avanti™ J-25I centrifuge (both from Beckman) at 4°C. The supernatant was further processed by ultracentrifugation at 118,000 g for 60 minutes using the Type 70 Ti rotor in an Optima™ L-90K centrifuge (both from Beckman) at 4°C.

**Salt fractionation:** ATP was added to a final concentration of 1 mM to the supernatant. Subsequently, a saturated stock solution of  $(\text{NH}_4)_2\text{SO}_4$  was added to the supernatant to 25% saturation (3 parts supernatant + 1 part  $(\text{NH}_4)_2\text{SO}_4$  stock solution). Precipitated material was removed by centrifugation at 20,000 g for 30 min at 4°C using the JA 25.50 rotor in an Avanti™ J-25I centrifuge. Then  $(\text{NH}_4)_2\text{SO}_4$  was added to 55% saturation to the supernatant (6 parts supernatant + 4 parts  $(\text{NH}_4)_2\text{SO}_4$  stock solution). Precipitated material was sedimented by centrifugation at 20,000 g for 40 minutes at 4°C using the JA 25.50 rotor in an Avanti™ J-25I centrifuge. The resulting pellet was resuspended in 70 ml buffer A. Insoluble material was removed by centrifugation at 20,000 g for 20 minutes at 4°C.

**Heparin chromatography:** Before loading the supernatant onto a HiTrap™ Heparin HP column (GE Healthcare) ATP was added to a final concentration of 1 mM. Five 5 ml HiTrap™ Heparin HP columns were connected in series to an ÄKTA™purifier system (GE Healthcare). The columns were equilibrated in buffer A (Table 3). After loading the supernatant onto the columns, a wash step with 40 ml of 12% buffer B (Table 3) was applied. Then, a gradient from 12% buffer B to 25% buffer was applied within the next 30 ml. Another gradient from 25% buffer B to 60% buffer B was applied within the next 200 ml. Finally, the column was washed with another 50 ml of 100% buffer B. 9 fractions of 8 ml volume each were collected during the initial washing until 25% buffer B was reached. Then fractions of 5 ml each were collected during the gradient from 25-60% buffer B and during the final wash with 100% buffer B. TRiC eluted in fractions 40-55 towards the end of the 25-60% buffer B gradient, as judged by a dot blot probed with an antibody against CCT $\alpha$ . The respective fractions were further analyzed by SDS-PAGE followed by Coomassie staining. Most TRiC was found in fractions 47-53 and thus these fractions were pooled.

**Size exclusion chromatography:** Before loading onto a HiLoad™ 16/60 Superdex 200 gel filtration column (GE Healthcare), the pooled fractions were concentrated to a final volume of 7 ml using a Vivaspin 20 centrifugal concentrator (Sartorius) with a molecular weight cutoff of 100 kDa. The column was equilibrated and run with storage buffer. Fractions of 4 ml volume were collected and analyzed by SDS-PAGE followed by Coomassie staining. TRiC was eluting in fractions 11-13. Thus, fractions 11-13 were pooled and concentrated with a Vivaspin 20 centrifugal concentrator to a final volume of 3 ml.

The concentration of TRiC was determined using the Coomassie Protein Assay Kit (Thermo Scientific Pierce), which works based on the assay described by Bradford (Bradford, 1976). The final concentration of the TRiC preparation was approximately 4.7 mg/ml, which corresponds to 5  $\mu$ M. Thus, in total approximately 14 mg of TRiC were obtained from 200 g of bovine testes. The purified TRiC was stored in aliquots at -80°C.

### 5.3.2 *In vitro* Translation in Rabbit Reticulocyte Lysate

Different TNT® Coupled Reticulocyte Lysate Systems by Promega were used depending on the expression construct. All of these systems were coupled transcription/translation systems based on a lysate of rabbit reticulocytes. Plasmid DNA that was to be transcribed by the T7 RNA polymerase or the SP6 RNA polymerase was typically expressed using the TNT® T7 Quick Coupled Transcription/Translation System or the TNT® SP6 Quick Coupled Transcription/Translation System, respectively. Plasmid DNA that was to be transcribed by the T3 RNA polymerase was expressed using the TNT® T3 Coupled Reticulocyte Lysate System. Finally, when PCR products served as DNA source instead of plasmids, TNT® T7 Quick for PCR DNA was used for expression.

Generally, the coupled transcription/translation reactions were done at 30°C using the Thermomixer Comfort 1.5 ml (Eppendorf) in a total volume of 50  $\mu$ l containing 1  $\mu$ g of DNA. The protein of interest that was produced was typically radioactively labeled by addition of 10  $\mu$ Ci of EasyTag™ L-[<sup>35</sup>S]-Methionine (PerkinElmer).

### 5.3.3 Depletion of TRiC from Rabbit Reticulocyte Lysate

To investigate the TRiC dependence of actin folding in RRL, TRiC was depleted from RRL using the high affinity TRiC interactor PhLP1. Human PhLP1 was purified upon overexpression in BL21 *E. coli* cells (provided by Markus Stemp). The protein contains additionally the following 27 N-terminal amino acids, including a 6xHis-tag and a TEV cleavage site: MSYYHHHHHDYDIPTTENLYFQGAMG. The purified protein had a concentration of 11.3 mg/ml. PhLP1 was coupled to Dynabeads<sup>®</sup> TALON<sup>™</sup> via its N-terminal 6xHis-tag. The PhLP1 buffer contained DTT, which is suggested to be removed prior to coupling to Dynabeads<sup>®</sup> TALON<sup>™</sup> (Invitrogen) by the manufacturer. Therefore, buffer exchange to PBS was done using Micro Bio-Spin<sup>®</sup> columns filled with Bio-Gel<sup>®</sup> P-6 (both from Bio-Rad) according to the manufacturer's instructions. 500 µl Dynabeads<sup>®</sup> TALON<sup>™</sup> solution with a concentration of 40 mg/ml were washed three times with 1.5 ml PBS. Separation of the beads from the supernatant was possible by immobilizing the beads on one side of a reaction tube using a magnet. Then the beads were resuspended in 700 µl PBS, mixed with 60 µl of PhLP1 and incubated for 2 h at 4°C rotating with 11 rpm. After three washes with each 1.5 ml PBS to remove unbound PhLP1, the PhLP1-beads were resuspended in 500 µl PBS and stored at 4°C. For depletion of TRiC from RRL, the beads were washed twice with 1 ml RNase free H<sub>2</sub>O. Then the beads were incubated with 125 µl TNT<sup>®</sup> Rabbit Reticulocyte Lysate for 2 h at 4°C rotating with 11 rpm. Simultaneously, a control TNT<sup>®</sup> Rabbit Reticulocyte Lysate was kept at 4°C for 2 h. Both lysates were subsequently used for translation reactions. Samples of untreated and depleted RLL were taken to monitor the depletion efficiency by Western Blot using an antibody against CCT $\alpha$ . To check if actin folding was restorable by addition of purified TRiC, half of the depleted translation reactions were supplemented with 1 µM purified bovine TRiC prior to translation.

### 5.3.4 Preparation of DNase I - Sepharose

DNase I (grade II from bovine pancreas, Roche) was coupled to CNBr-activated Sepharose<sup>™</sup> 4B (GE Healthcare). 1 g of CNBr-activated Sepharose<sup>™</sup> 4B powder was hydrated in 10 ml of 1 mM HCl, yielding approximately 3.5 ml Sepharose medium. The medium was washed three times by centrifugation for 2 min at 1000 rpm in a GH-3.8 rotor in a GS-6R centrifuge (both from

Beckman) and removal of the supernatant followed by addition of 10 ml fresh 1 mM HCl. DNase I was dissolved in 5 ml coupling buffer and added to the washed Sepharose medium. The mixture was incubated by constant rocking at room temperature for 90 min. The DNase I beads were subsequently washed three times with 10 ml coupling buffer. The excessive amine binding sites were blocked by incubation for 2 h with 10 ml of 100 mM Tris-HCl, pH 8.0 at room temperature without rocking. Then the DNase I beads were washed three times with alternating low pH and high pH buffer (10 ml each). The washed beads were stored in 20% ethanol at 4°C.

### 5.3.5 DNase I Binding Assay

Typically, the DNase I binding assay was performed with 3-6 RRL reactions in parallel that were translating different constructs. 150-300 µl of a 1:1 suspension of DNase I beads were used depending on the number of RRL reactions to be processed. The beads were washed two times with 1 ml dilution buffer by centrifugation at 1,000 g for 3 min at 4°C using an FA-45-24-11 rotor in a 5415 R centrifuge (both from Eppendorf) followed by removal of the supernatant and addition of fresh buffer. Finally, the beads were resuspended in 75-150 µl dilution buffer depending on the initial volume of beads in order to restore a 1:1 suspension. The translation reaction in the 50 µl RRL mixtures was stopped after 90 min by addition of 0.5 U apyrase (grade VII from potato, Sigma-Aldrich) followed by incubation at 30°C for 2 min. A 4 µl sample was taken as an input reference and diluted into 26 µl of 2x SDS loading buffer. 40 µl of the RRL reaction were diluted into 400 µl dilution buffer and subsequently mixed with 40 µl of the 1:1 suspension of washed DNase I beads. After continuous rocking at 4°C for 2 h, the beads were washed with 500 µl dilution buffer, 500 µl washing buffer 1, 2 x 500 µl washing buffer 2 and finally with 500 µl PBS using a Mobicol “classic” spin column (Mobicol) connected to a QIAvac 24 vacuum manifold (QIAGEN). After a short spin (3 sec, 5,000 rpm using an FA-45-24-11 rotor in a 5415 D centrifuge (both from Eppendorf)) to remove excessive buffer, the proteins bound to the beads were eluted with 30 µl 2x SDS loading buffer by incubation for 2 min at 95°C followed by centrifugation at 16,100 g for 2 min, resulting in an effective ten-fold higher concentration of the eluate sample compared to the input sample. 12 µl of both the input and the eluate samples were analyzed by SDS-PAGE followed by autoradiography.

**DNase I binding of BTAG:** In case of translation of the cleavable BTAG construct, translation was stopped after 90 min either by addition of 0.5 U apyrase or by addition of cycloheximide to a final concentration of 140  $\mu$ M. A 4  $\mu$ l sample was taken to ensure that full-length BTAG was indeed made. The reaction was then incubated with a final concentration of 500 U/ml TEV protease (Invitrogen) for 30 min at 30°C followed by the DNase I binding assay as described.

**DNase I binding after separating stalled and free nascent chains:** In order to separate stalled ActLink78 and ActLink97 nascent chains from free released chains prior to DNase I binding, centrifugation through a sucrose cushion was used. After translation at 30°C for 60 min the translation was stopped by addition of 0.5 U apyrase and incubation for 2 min at 30°C. After taking a 2  $\mu$ l total sample, 20  $\mu$ l of the RRL reactions were added on top of 130  $\mu$ l sucrose buffer in a 7x20 mm Open-Top Thickwall Polycarbonate Tube (Beckman). After centrifugation at 75,000 rpm for 60 min using a TLA-100 rotor in an Optima TLX centrifuge (both from Beckman) the supernatant (150  $\mu$ l) was removed and the pellet was resuspended in 150  $\mu$ l sucrose buffer. After taking a 12  $\mu$ l input sample from both the supernatant and the resuspended pellet fraction, 120  $\mu$ l of the respective fractions were diluted into 400  $\mu$ l dilution buffer. DNase I binding was done as described above using 40  $\mu$ l washed DNase I beads.

### 5.3.6 Protease Protection Assay

**PK protection of purified TRiC:** PK digest of purified bovine TRiC was done in buffer lid (Table 3) that was described previously by Booth et al., 2008. TRiC was diluted 1:20 into buffer lid containing 1 mM TCEP yielding a final TRiC concentration of 250 nM in a total volume of 50  $\mu$ l. In order to convert TRiC into defined conformational states, TRiC was incubated at 30°C in presence of either 1 mM ADP or 1 mM ATP or without addition of any nucleotide. As a control, one reaction contained 10 mM EDTA in addition to 1 mM ATP. After 30 min ADP or ATP was added to a final concentration of 2 mM to the reactions containing the respective nucleotide. AlFx was produced by adding KF to a final concentration of 30 mM and Al(NO<sub>3</sub>)<sub>3</sub> to a final concentration of 5 mM. After incubation for another 60 min at 30°C each reaction was split into two parts and transferred to ice. One part served as an input control. The other was incubated in presence of a final concentration of 83 ng/ $\mu$ l PK for 10 min on ice. The input

control received the same volume of H<sub>2</sub>O instead of PK. The protease was inactivated by addition of PMSF to a final concentration of 8 mM. The samples were diluted into 2x SDS loading buffer prior to SDS-PAGE and into 2x native loading buffer prior to native PAGE.

**PK protection of proteins translated in RRL:** PK digest of RRL translation reactions was done under varying conditions. For quantification of the intensity of the protease-resistant 35 kDa actin fragment, the digest was done after translation of the respective constructs for 90 minutes at 30°C. Translation was stopped by addition of cycloheximide to a final concentration of 140 µM followed by incubation at 30°C for 2 min. Typically, RRL reactions were incubated at 30°C for 30-60 min prior to addition of AlFx, which was done as described above. Control reactions received the same volume of H<sub>2</sub>O instead of AlFx. Generally, the reactions were kept at 30°C for another 30-60 min before they were split into two parts and transferred to ice. The PK digest was done as described above for purified TRiC.

**Analysis of PK protection of TRiC-bound proteins:** Elution of TRiC-bound proteins from native gels was achieved by incubation of TRiC-containing gel slices in 150 µl 2x SDS loading buffer without SERVA Blue R for 2 hours at 68°C and 1,400 rpm shaking in the Thermomixer Comfort 1.5 ml followed by incubation at 95°C for 10 min and centrifugation for 10 min at 16,100 g using the FA-45-24-11 rotor in the 5415 D centrifuge. The TRiC-containing regions of the native gel were identified after Coomassie staining and comparison with the position of purified bovine TRiC run in parallel as control. Typically, the eluted proteins were precipitated prior to analysis by SDS-PAGE. 125 µl of the 2x SDS loading buffer containing the eluted proteins was incubated on ice in presence of 0.02% sodium deoxycholate for 45 min. Then trichloroacetic acid was added to a final concentration of 10% and the mixture was incubated for another 75 min on ice. After centrifugation at 16,100 g using the FA-45-24-11 rotor in the 5415 R at 4°C for 20 min, the supernatant was discarded and the pellet was resuspended in 180 µl ice-cold (-20°C) acetone and kept at -20°C for 15 min. After another centrifugation at 16,100 g for 15 min at 4°C, the supernatant was again discarded and the pellet was resuspended in 20 µl 2x SDS loading buffer. 15 µl of the sample were analyzed by SDS-PAGE.

### 5.3.7 Native PAGE Mobility Shift Assay

To detect a mobility shift in native PAGE, RRL reactions translating actin, GFP-actin or  $\Delta$ N-GFP-actin were incubated with an anti-GFP antibody (Roche). The antibody provided by Roche is actually a mixture of two monoclonal antibodies (clones 7.1 and 13.1). The different translation reactions were either treated with AIFx as described above or received the corresponding volume of H<sub>2</sub>O instead of AIFx. 45-60 min after addition of AIFx or H<sub>2</sub>O the samples were transferred to ice and incubated in presence of 10 ng/ $\mu$ l anti-GFP for 90 min. Then the samples were split into two parts for PK digest as described above. Prior to SDS-PAGE and native PAGE, parts of the samples were diluted into the respective loading buffers. Samples that were treated with AIFx were analyzed by Blue Native PAGE containing 30 mM KF and 5 mM Al(NO<sub>3</sub>)<sub>3</sub> within the native gel as well as within the cathode and anode buffer. Samples that were not treated with AIFx were analyzed by Clear Native PAGE without any AIFx.

### 5.3.8 Electrophoresis of Proteins

A discontinuous (Davis, 1964; Ornstein, 1964) SDS polyacrylamide gel system was used similar in composition to the one described by Laemmli (Laemmli, 1970). The composition of the electrode buffer and of the separating gel was exactly as described. The stacking gel used had a higher acrylamide concentration than the one of Laemmli, namely 5% compared to 3% and a lower concentration of Tris, namely 60 mM instead of 125 mM. The 30% acrylamide stock solution was purchased from SERVA and contained acrylamide and N,N'-Methylenebisacrylamide in a 37.5:1 ratio. Polymerization was done with 0.0625% APS and 0.0625% TEMED in case of the separating gel and with 0.05% APS (Sigma-Aldrich) and 0.1% TEMED (Sigma-Aldrich) in case of the stacking gel. SDS-PAGE was normally done with an initial voltage of 120 V for 10 min followed by another 50 minutes with 180 V.

Native PAGE was also done using a discontinuous system similar to the one described by Schagger and von Jagow (Schagger and von Jagow, 1991). Native PAGE was performed at 4°C with an initial voltage of 100 V for 2 h followed by 14-16 h at 200 V. The composition of the anode buffer as well as the gel buffer was exactly as described. The cathode buffer was identical to cathode buffer A described by Schagger and von Jagow except for the Bis-Tris concentration,

which was 12 mM. Typically, electrophoresis was done as Clear Native PAGE, thus omitting SERVA Blue G in the cathode buffer. The dimensions of the gels were 20 cm x 20 cm x 1 mm. The bottom of the gel was plugged by 2 ml of a 9% acrylamide solution (0.6 ml of the 30% acrylamide stock solution + 1.4 ml H<sub>2</sub>O) polymerized by 0.1% APS and 0.1% TEMED to avoid leaking of liquid upon pouring the separating gel. The separating gel formed a continuous gradient from 13% acrylamide at the bottom to 5% acrylamide on top. The gradient was produced by mixing two different solutions of 12 ml volume each using the gradient maker SG50 (Hoefer). The solution that was filled into the chamber closer to the outlet valve contained 13% acrylamide and approximately 17% glycerol in gel buffer plus 0.035% APS and TEMED for polymerization. The solution that was filled into the other chamber contained 5% acrylamide and 5% glycerol in gel buffer plus approximately 0.048% APS and TEMED for polymerization. After the outlet valve and the valve connecting the two chambers were opened, the solutions were pumped into the assembled glass plates using the peristaltic Pharmacia pump LKB P-1, thus forming the continuous gradient. During the pumping, the solutions were continuously mixed by magnetic stirring bars. After polymerization of the separating gel, 5 ml stacking gel were added on top of the gradient separating gel. The stacking gel contained 3.25% acrylamide in gel buffer.

Typically, 6 mM KF and 1 mM Al(NO<sub>3</sub>)<sub>3</sub> were included in the gel buffer as well as the anode and cathode buffer, in order to prevent opening of TRiC complexes during the gel run, which had been pre-treated with AlFx. However, gels were also run in absence of AlFx. Additionally, in case of the antibody gel shift assay, gels were run including 30 mM KF and 5 mM Al(NO<sub>3</sub>)<sub>3</sub> in gel buffer and anode and cathode buffer to ensure complete closure of TRiC complexes during the gel run. In this case the native gel had to be run as Blue Native PAGE to obtain separation of appropriate quality.

Both SDS gels and native gels were stained as follows. The gels were subjected to constant shaking during the whole staining and destaining procedure. Coomassie staining of gels was done using 0.25% SERVA Blue R in 45% ethanol and 10% acetic acid generally for approximately 30 min at room temperature. Destaining was done using destain solution (10% acetic acid, 40% ethanol) at room temperature for several hours. The gel was then incubated in H<sub>2</sub>O for at least 15 min prior to scanning using the Epson Expression 1680 scanner. Incubation

with H<sub>2</sub>O was also done prior to excision of slices from native gels for subsequent elution of proteins from TRiC-containing slices.

When the gel was to be analyzed by autoradiography only, the staining, destaining and watering procedure was substantially shortened to approximately 5-10 min for each step. The gel was then dried at 76°C for 1 h (SDS gels) or 2 h (native gels) using an SGD 2000 slab gel dryer embedded in an SGD 300 stacker gel dryer system (both from Savant). A BAS-MS 2025 imaging plate (Fujifilm) was then exposed to the dried gel for varying times in an FBXC 810 autoradiography cassette (Fisher Biotech), generally between 1 and 24 h depending on the intensity of the signal. The signal was recorded using the FLA-2000 scanner (Fujifilm) and analyzed using the AIDA software version 4.15 (raytest).

### 5.3.9 Western Blotting

If proteins were to be detected by specific antibodies after native PAGE or SDS-PAGE, they were transferred electrophoretically to a Protran™ nitrocellulose membrane (Whatman). Transfer of proteins from SDS gels was done using a Mini Trans-Blot Cell (Bio-Rad) filled with transfer buffer. Typically, the transfer was done for 1 h using 200-300 mA per gel. Proteins from native gels were transferred by semi-dry transfer for 1 h using 0.8 mA per cm<sup>2</sup> of gel. Prior to transfer, native gels were incubated for 30 min in transfer buffer containing additional 0.2% SDS.

After transfer, the nitrocellulose membranes were blocked by incubation in blocking buffer, generally for approximately 30 min at room temperature. Primary and secondary antibodies were diluted into blocking buffer as well, prior to incubation with the nitrocellulose membrane. The incubation of the membrane with the respective antibodies was done in a rotating chamber to ensure even coverage of the membrane with the antibody solution. Incubation with the primary antibody was done for approximately 16 h at 4°C or alternatively for approximately 2 h at room temperature. The nitrocellulose membrane was washed three times with TBS-T between incubations with primary and secondary antibody. Typically, the membrane was incubated with secondary antibody for approximately 2 h at room temperature. Prior to detection, the membrane was washed three times with TBS-T. Secondary antibodies coupled to horseradish peroxidase

were used. For detection, the membrane was incubated with the USB Rodeo™ ECL Detection Reagents (Affymetrix). The emitted light was detected using the LAS-3000 imaging system (Fujifilm).

TRiC was detected using a rat monoclonal antibody directed against CCT $\alpha$  (CTA-191, Stressgen) at a final concentration of 1  $\mu$ g/ml. The HA-tagged hSnu114 was detected using a rat monoclonal anti-HA antibody (Anti-HA High Affinity, clone 3F10, Roche) at a final concentration of 0.2  $\mu$ g/ml. Both primary antibodies were detected by anti-rat IgG (whole molecule) peroxidase conjugate (A 9037, Sigma-Aldrich) diluted 1:1000 into blocking buffer.

## 6. References

- Altschuler, G.M., and Willison, K.R. (2008). Development of free-energy-based models for chaperonin containing TCP-1 mediated folding of actin. *J R Soc Interface* 5, 1391-1408.
- Anfinsen, C.B. (1973). Principles that govern the folding of protein chains. *Science* 181, 223-230.
- Anfinsen, C.B., Haber, E., Sela, M., and White, F.H., Jr. (1961). The kinetics of formation of native ribonuclease during oxidation of the reduced polypeptide chain. *Proc Natl Acad Sci U S A* 47, 1309-1314.
- Apetri, A.C., and Horwich, A.L. (2008). Chaperonin chamber accelerates protein folding through passive action of preventing aggregation. *Proc Natl Acad Sci U S A* 105, 17351-17355.
- Archibald, J.M., Blouin, C., and Doolittle, W.F. (2001). Gene duplication and the evolution of group II chaperonins: implications for structure and function. *J Struct Biol* 135, 157-169.
- Bach, M., Winkelmann, G., and Luhrmann, R. (1989). 20S small nuclear ribonucleoprotein U5 shows a surprisingly complex protein composition. *Proc Natl Acad Sci U S A* 86, 6038-6042.
- Baker, D., and Agard, D.A. (1994). Kinetics versus thermodynamics in protein folding. *Biochemistry* 33, 7505-7509.
- Ballestrem, C., Wehrle-Haller, B., and Imhof, B.A. (1998). Actin dynamics in living mammalian cells. *J Cell Sci* 111 ( Pt 12), 1649-1658.
- Baumketner, A., Jewett, A., and Shea, J.E. (2003). Effects of confinement in chaperonin assisted protein folding: rate enhancement by decreasing the roughness of the folding energy landscape. *J Mol Biol* 332, 701-713.
- Booth, C.R., Meyer, A.S., Cong, Y., Topf, M., Sali, A., Ludtke, S.J., Chiu, W., and Frydman, J. (2008). Mechanism of lid closure in the eukaryotic chaperonin TRiC/CCT. *Nat Struct Mol Biol* 15, 746-753.
- Bork, P., Sander, C., and Valencia, A. (1992). An ATPase domain common to prokaryotic cell cycle proteins, sugar kinases, actin, and hsp70 heat shock proteins. *Proc Natl Acad Sci U S A* 89, 7290-7294.
- Bradford, M.M. (1976). A rapid and sensitive method for the quantitation of microgram quantities of protein utilizing the principle of protein-dye binding. *Anal Biochem* 72, 248-254.

Braig, K., Otwinowski, Z., Hegde, R., Boisvert, D.C., Joachimiak, A., Horwich, A.L., and Sigler, P.B. (1994). The crystal structure of the bacterial chaperonin GroEL at 2.8 Å. *Nature* *371*, 578-586.

Brinker, A., Pfeifer, G., Kerner, M.J., Naylor, D.J., Hartl, F.U., and Hayer-Hartl, M. (2001). Dual function of protein confinement in chaperonin-assisted protein folding. *Cell* *107*, 223-233.

Brocchieri, L., and Karlin, S. (2005). Protein length in eukaryotic and prokaryotic proteomes. *Nucleic Acids Res* *33*, 3390-3400.

Camasses, A., Bogdanova, A., Shevchenko, A., and Zachariae, W. (2003). The CCT chaperonin promotes activation of the anaphase-promoting complex through the generation of functional Cdc20. *Mol Cell* *12*, 87-100.

Caplan, A.J., Mandal, A.K., and Theodoraki, M.A. (2007). Molecular chaperones and protein kinase quality control. *Trends Cell Biol* *17*, 87-92.

Chabre, M. (1990). Aluminofluoride and beryllofluoride complexes: a new phosphate analogs in enzymology. *Trends Biochem Sci* *15*, 6-10.

Chakraborty, K., Chatila, M., Sinha, J., Shi, Q., Poschner, B.C., Sikor, M., Jiang, G., Lamb, D.C., Hartl, F.U., and Hayer-Hartl, M. (2010). Chaperonin-catalyzed rescue of kinetically trapped states in protein folding. *Cell* *142*, 112-122.

Chang, H.C., Kaiser, C.M., Hartl, F.U., and Barral, J.M. (2005). De novo folding of GFP fusion proteins: high efficiency in eukaryotes but not in bacteria. *J Mol Biol* *353*, 397-409.

Chaudhuri, T.K., Farr, G.W., Fenton, W.A., Rospert, S., and Horwich, A.L. (2001). GroEL/GroES-mediated folding of a protein too large to be encapsulated. *Cell* *107*, 235-246.

Chen, D.H., Song, J.L., Chuang, D.T., Chiu, W., and Ludtke, S.J. (2006). An expanded conformation of single-ring GroEL-GroES complex encapsulates an 86 kDa substrate. *Structure* *14*, 1711-1722.

Chen, L., and Sigler, P.B. (1999). The crystal structure of a GroEL/peptide complex: plasticity as a basis for substrate diversity. *Cell* *99*, 757-768.

Chen, X., Sullivan, D.S., and Huffaker, T.C. (1994). Two yeast genes with similarity to TCP-1 are required for microtubule and actin function in vivo. *Proc Natl Acad Sci U S A* *91*, 9111-9115.

Clare, D.K., Stagg, S., Quispe, J., Farr, G.W., Horwich, A.L., and Saibil, H.R. (2008). Multiple states of a nucleotide-bound group 2 chaperonin. *Structure* *16*, 528-534.

Cong, Y., Baker, M.L., Jakana, J., Woolford, D., Miller, E.J., Reissmann, S., Kumar, R.N., Redding-Johanson, A.M., Batth, T.S., Mukhopadhyay, A., *et al.* (2010). 4.0-A resolution cryo-EM structure of the mammalian chaperonin TRiC/CCT reveals its unique subunit arrangement. *Proc Natl Acad Sci U S A* *107*, 4967-4972.

Cong, Y., Schroder, G.F., Meyer, A.S., Jakana, J., Ma, B., Dougherty, M.T., Schmid, M.F., Reissmann, S., Levitt, M., Ludtke, S.L., *et al.* (2011). Symmetry-free cryo-EM structures of the chaperonin TRiC along its ATPase-driven conformational cycle. *EMBO J*.

Craggs, T.D. (2009). Green fluorescent protein: structure, folding and chromophore maturation. *Chem Soc Rev* *38*, 2865-2875.

Cramer, A., Whitehorn, E.A., Tate, E., and Stemmer, W.P. (1996). Improved green fluorescent protein by molecular evolution using DNA shuffling. *Nat Biotechnol* *14*, 315-319.

Cuellar, J., Martin-Benito, J., Scheres, S.H., Sousa, R., Moro, F., Lopez-Vinas, E., Gomez-Puertas, P., Muga, A., Carrascosa, J.L., and Valpuesta, J.M. (2008). The structure of CCT-Hsc70 NBD suggests a mechanism for Hsp70 delivery of substrates to the chaperonin. *Nat Struct Mol Biol* *15*, 858-864.

Davis, B.J. (1964). Disc Electrophoresis. II. Method and Application to Human Serum Proteins. *Ann N Y Acad Sci* *121*, 404-427.

Dekker, C., Roe, S.M., McCormack, E.A., Beuron, F., Pearl, L.H., and Willison, K.R. (2011a). The crystal structure of yeast CCT reveals intrinsic asymmetry of eukaryotic cytosolic chaperonins. *EMBO J*.

Dekker, C., Stirling, P.C., McCormack, E.A., Filmore, H., Paul, A., Brost, R.L., Costanzo, M., Boone, C., Leroux, M.R., and Willison, K.R. (2008). The interaction network of the chaperonin CCT. *EMBO J* *27*, 1827-1839.

Dekker, C., Willison, K.R., and Taylor, W.R. (2011b). On the evolutionary origin of the chaperonins. *Proteins* *79*, 1172-1192.

Dill, K.A., and Chan, H.S. (1997). From Levinthal to pathways to funnels. *Nat Struct Biol* *4*, 10-19.

Dill, K.A., Ozkan, S.B., Shell, M.S., and Weikl, T.R. (2008). The protein folding problem. *Annu Rev Biophys* *37*, 289-316.

Ditzel, L., Lowe, J., Stock, D., Stetter, K.O., Huber, H., Huber, R., and Steinbacher, S. (1998). Crystal structure of the thermosome, the archaeal chaperonin and homolog of CCT. *Cell* 93, 125-138.

Dobson, C.M. (2003). Protein folding and misfolding. *Nature* 426, 884-890.

Doolittle, R.F. (1995). The origins and evolution of eukaryotic proteins. *Philos Trans R Soc Lond B Biol Sci* 349, 235-240.

Douglas, N.R., Reissmann, S., Zhang, J., Chen, B., Jakana, J., Kumar, R., Chiu, W., and Frydman, J. (2011). Dual action of ATP hydrolysis couples lid closure to substrate release into the group II chaperonin chamber. *Cell* 144, 240-252.

Doyle, T., and Botstein, D. (1996). Movement of yeast cortical actin cytoskeleton visualized in vivo. *Proc Natl Acad Sci U S A* 93, 3886-3891.

Duden, R. (2003). ER-to-Golgi transport: COP I and COP II function (Review). *Mol Membr Biol* 20, 197-207.

Duden, R., Hosobuchi, M., Hamamoto, S., Winey, M., Byers, B., and Schekman, R. (1994). Yeast beta- and beta'-coat proteins (COP). Two coatomer subunits essential for endoplasmic reticulum-to-Golgi protein traffic. *J Biol Chem* 269, 24486-24495.

Ebeling, W., Hennrich, N., Klockow, M., Metz, H., Orth, H.D., and Lang, H. (1974). Proteinase K from *Tritirachium album* Limber. *Eur J Biochem* 47, 91-97.

Ekman, D., Bjorklund, A.K., Frey-Skott, J., and Elofsson, A. (2005). Multi-domain proteins in the three kingdoms of life: orphan domains and other unassigned regions. *J Mol Biol* 348, 231-243.

Ellis, J. (1987). Proteins as molecular chaperones. *Nature* 328, 378-379.

Ellis, R.J. (2001). Macromolecular crowding: obvious but underappreciated. *Trends Biochem Sci* 26, 597-604.

Erickson, H.P. (2007). Evolution of the cytoskeleton. *Bioessays* 29, 668-677.

Etchells, S.A., Meyer, A.S., Yam, A.Y., Roobol, A., Miao, Y., Shao, Y., Carden, M.J., Skach, W.R., Frydman, J., and Johnson, A.E. (2005). The cotranslational contacts between ribosome-bound nascent polypeptides and the subunits of the hetero-oligomeric chaperonin TRiC probed by photocross-linking. *J Biol Chem* 280, 28118-28126.

Eugster, A., Frigerio, G., Dale, M., and Duden, R. (2004). The alpha- and beta'-COP WD40 domains mediate cargo-selective interactions with distinct di-lysine motifs. *Mol Biol Cell* 15, 1011-1023.

Fabrizio, P., Lagerbauer, B., Lauber, J., Lane, W.S., and Luhrmann, R. (1997). An evolutionarily conserved U5 snRNP-specific protein is a GTP-binding factor closely related to the ribosomal translocase EF-2. *EMBO J* 16, 4092-4106.

Fenton, W.A., Kashi, Y., Furtak, K., and Horwich, A.L. (1994). Residues in chaperonin GroEL required for polypeptide binding and release. *Nature* 371, 614-619.

Ferbitz, L., Maier, T., Patzelt, H., Bukau, B., Deuerling, E., and Ban, N. (2004). Trigger factor in complex with the ribosome forms a molecular cradle for nascent proteins. *Nature* 431, 590-596.

Fischer, M., Kaech, S., Knutti, D., and Matus, A. (1998). Rapid actin-based plasticity in dendritic spines. *Neuron* 20, 847-854.

Frazer, L.N., Nancollis, V., and O'Keefe, R.T. (2008). The role of Snu114p during pre-mRNA splicing. *Biochem Soc Trans* 36, 551-553.

Gao, Y., Melki, R., Walden, P.D., Lewis, S.A., Ampe, C., Rommelaere, H., Vandekerckhove, J., and Cowan, N.J. (1994). A novel cochaperonin that modulates the ATPase activity of cytoplasmic chaperonin. *J Cell Biol* 125, 989-996.

Gao, Y., Thomas, J.O., Chow, R.L., Lee, G.H., and Cowan, N.J. (1992). A cytoplasmic chaperonin that catalyzes beta-actin folding. *Cell* 69, 1043-1050.

Gautschi, M., Lilie, H., Funfschilling, U., Mun, A., Ross, S., Lithgow, T., Rucknagel, P., and Rospert, S. (2001). RAC, a stable ribosome-associated complex in yeast formed by the DnaK-DnaJ homologs Ssz1p and zuotin. *Proc Natl Acad Sci U S A* 98, 3762-3767.

Gautschi, M., Mun, A., Ross, S., and Rospert, S. (2002). A functional chaperone triad on the yeast ribosome. *Proc Natl Acad Sci U S A* 99, 4209-4214.

Gavin, A.C., Aloy, P., Grandi, P., Krause, R., Boesche, M., Marzioch, M., Rau, C., Jensen, L.J., Bastuck, S., Dumpelfeld, B., *et al.* (2006). Proteome survey reveals modularity of the yeast cell machinery. *Nature* 440, 631-636.

Graceffa, P., and Dominguez, R. (2003). Crystal structure of monomeric actin in the ATP state. Structural basis of nucleotide-dependent actin dynamics. *J Biol Chem* 278, 34172-34180.

Graumann, J., Dunipace, L.A., Seol, J.H., McDonald, W.H., Yates, J.R., 3rd, Wold, B.J., and Deshaies, R.J. (2004). Applicability of tandem affinity purification MudPIT to pathway proteomics in yeast. *Mol Cell Proteomics* 3, 226-237.

Gutsche, I., Essen, L.O., and Baumeister, W. (1999). Group II chaperonins: new TRiC(k)s and turns of a protein folding machine. *J Mol Biol* 293, 295-312.

Hageman, J., Vos, M.J., van Waarde, M.A., and Kampinga, H.H. (2007). Comparison of intra-organellar chaperone capacity for dealing with stress-induced protein unfolding. *J Biol Chem* 282, 34334-34345.

Han, J.H., Batey, S., Nickson, A.A., Teichmann, S.A., and Clarke, J. (2007). The folding and evolution of multidomain proteins. *Nat Rev Mol Cell Biol* 8, 319-330.

Hansen, W.J., Cowan, N.J., and Welch, W.J. (1999). Prefoldin-nascent chain complexes in the folding of cytoskeletal proteins. *J Cell Biol* 145, 265-277.

Harrison, C.J., Hayer-Hartl, M., Di Liberto, M., Hartl, F., and Kuriyan, J. (1997). Crystal structure of the nucleotide exchange factor GrpE bound to the ATPase domain of the molecular chaperone DnaK. *Science* 276, 431-435.

Hartl, F.U., Bracher, A., and Hayer-Hartl, M. (2011). Molecular chaperones in protein folding and proteostasis. *Nature* 475, 324-332.

Hartl, F.U., and Hayer-Hartl, M. (2002). Molecular chaperones in the cytosol: from nascent chain to folded protein. *Science* 295, 1852-1858.

Heidemann, S.R., Kaech, S., Buxbaum, R.E., and Matus, A. (1999). Direct observations of the mechanical behaviors of the cytoskeleton in living fibroblasts. *J Cell Biol* 145, 109-122.

Heim, R., Prasher, D.C., and Tsien, R.Y. (1994). Wavelength mutations and posttranslational autoxidation of green fluorescent protein. *Proc Natl Acad Sci U S A* 91, 12501-12504.

Hemmingsen, S.M., Woolford, C., van der Vies, S.M., Tilly, K., Dennis, D.T., Georgopoulos, C.P., Hendrix, R.W., and Ellis, R.J. (1988). Homologous plant and bacterial proteins chaperone oligomeric protein assembly. *Nature* 333, 330-334.

Higashi-Fujime, S., Suzuki, M., Titani, K., and Hozumi, T. (1992). Muscle actin cleaved by proteinase K: its polymerization and in vitro motility. *J Biochem* 112, 568-572.

Ho, Y., Gruhler, A., Heilbut, A., Bader, G.D., Moore, L., Adams, S.L., Millar, A., Taylor, P., Bennett, K., Boutilier, K., *et al.* (2002). Systematic identification of protein complexes in *Saccharomyces cerevisiae* by mass spectrometry. *Nature* 415, 180-183.

Hohfeld, J., and Jentsch, S. (1997). GrpE-like regulation of the hsc70 chaperone by the anti-apoptotic protein BAG-1. *EMBO J* 16, 6209-6216.

Hohfeld, J., Minami, Y., and Hartl, F.U. (1995). Hip, a novel cochaperone involved in the eukaryotic Hsc70/Hsp40 reaction cycle. *Cell* 83, 589-598.

Horwich, A.L., Apetri, A.C., and Fenton, W.A. (2009). The GroEL/GroES cis cavity as a passive anti-aggregation device. *FEBS Lett* 583, 2654-2662.

Horwitz, J. (2003). Alpha-crystallin. *Exp Eye Res* 76, 145-153.

Huang, P., Gautschi, M., Walter, W., Rospert, S., and Craig, E.A. (2005). The Hsp70 Ssz1 modulates the function of the ribosome-associated J-protein Zuo1. *Nat Struct Mol Biol* 12, 497-504.

Huo, Y., Hu, Z., Zhang, K., Wang, L., Zhai, Y., Zhou, Q., Lander, G., Zhu, J., He, Y., Pang, X., *et al.* (2010). Crystal structure of group II chaperonin in the open state. *Structure* 18, 1270-1279.

Ishii, N., Taguchi, H., Sumi, M., and Yoshida, M. (1992). Structure of holo-chaperonin studied with electron microscopy. Oligomeric cpn10 on top of two layers of cpn60 rings with two stripes each. *FEBS Lett* 299, 169-174.

Jacob, E., Horovitz, A., and Unger, R. (2007). Different mechanistic requirements for prokaryotic and eukaryotic chaperonins: a lattice study. *Bioinformatics* 23, i240-248.

Jacobson, G.R., and Rosenbusch, J.P. (1976). ATP binding to a protease-resistant core of actin. *Proc Natl Acad Sci U S A* 73, 2742-2746.

Jayasinghe, M., Tewmey, C., and Stan, G. (2009). Versatile substrate protein recognition mechanism of the eukaryotic chaperonin CCT. *Proteins* 78, 1254-1265.

Jorgensen, R., Merrill, A.R., and Andersen, G.R. (2006). The life and death of translation elongation factor 2. *Biochem Soc Trans* 34, 1-6.

Jorgensen, R., Merrill, A.R., Yates, S.P., Marquez, V.E., Schwan, A.L., Boesen, T., and Andersen, G.R. (2005). Exotoxin A-eEF2 complex structure indicates ADP ribosylation by ribosome mimicry. *Nature* 436, 979-984.

Jorgensen, R., Ortiz, P.A., Carr-Schmid, A., Nissen, P., Kinzy, T.G., and Andersen, G.R. (2003). Two crystal structures demonstrate large conformational changes in the eukaryotic ribosomal translocase. *Nat Struct Biol* 10, 379-385.

Jorgensen, R., Yates, S.P., Teal, D.J., Nilsson, J., Prentice, G.A., Merrill, A.R., and Andersen, G.R. (2004). Crystal structure of ADP-ribosylated ribosomal translocase from *Saccharomyces cerevisiae*. *J Biol Chem* 279, 45919-45925.

Kabani, M., McLellan, C., Raynes, D.A., Guerriero, V., and Brodsky, J.L. (2002). HspBP1, a homologue of the yeast Fes1 and Sls1 proteins, is an Hsc70 nucleotide exchange factor. *FEBS Lett* 531, 339-342.

Kabsch, W., and Holmes, K.C. (1995). The actin fold. *FASEB J* 9, 167-174.

Kabsch, W., Mannherz, H.G., Suck, D., Pai, E.F., and Holmes, K.C. (1990). Atomic structure of the actin:DNase I complex. *Nature* 347, 37-44.

Kafri, G., Willison, K.R., and Horovitz, A. (2001). Nested allosteric interactions in the cytoplasmic chaperonin containing TCP-1. *Protein Sci* 10, 445-449.

Kaiser, C.M., Chang, H.C., Agashe, V.R., Lakshminpathy, S.K., Etchells, S.A., Hayer-Hartl, M., Hartl, F.U., and Barral, J.M. (2006). Real-time observation of trigger factor function on translating ribosomes. *Nature* 444, 455-460.

Kalisman, N., Adams, C.M., and Levitt, M. (2012). Subunit order of eukaryotic TRiC/CCT chaperonin by cross-linking, mass spectrometry, and combinatorial homology modeling. *Proc Natl Acad Sci U S A*.

Kerner, M.J., Naylor, D.J., Ishihama, Y., Maier, T., Chang, H.C., Stines, A.P., Georgopoulos, C., Frishman, D., Hayer-Hartl, M., Mann, M., *et al.* (2005). Proteome-wide analysis of chaperonin-dependent protein folding in *Escherichia coli*. *Cell* 122, 209-220.

Kettern, N., Dreiseidler, M., Tawo, R., and Hohfeld, J. (2010). Chaperone-assisted degradation: multiple paths to destruction. *Biol Chem* 391, 481-489.

Kiefhaber, T. (1995). Kinetic traps in lysozyme folding. *Proc Natl Acad Sci U S A* 92, 9029-9033.

Kim, S., Willison, K.R., and Horwich, A.L. (1994). Cytosolic chaperonin subunits have a conserved ATPase domain but diverged polypeptide-binding domains. *Trends Biochem Sci* 19, 543-548.

Klumpp, M., Baumeister, W., and Essen, L.O. (1997). Structure of the substrate binding domain of the thermosome, an archaeal group II chaperonin. *Cell* 91, 263-270.

Komoszynski, M., and Wojtczak, A. (1996). Apyrases (ATP diphosphohydrolases, EC 3.6.1.5): function and relationship to ATPases. *Biochim Biophys Acta* 1310, 233-241.

Korn, E.D. (1982). Actin polymerization and its regulation by proteins from nonmuscle cells. *Physiol Rev* 62, 672-737.

Kozak, M. (1987). An analysis of 5'-noncoding sequences from 699 vertebrate messenger RNAs. *Nucleic Acids Res* 15, 8125-8148.

Kramer, G., Boehringer, D., Ban, N., and Bukau, B. (2009). The ribosome as a platform for co-translational processing, folding and targeting of newly synthesized proteins. *Nat Struct Mol Biol* 16, 589-597.

Krogan, N.J., Cagney, G., Yu, H., Zhong, G., Guo, X., Ignatchenko, A., Li, J., Pu, S., Datta, N., Tikuisis, A.P., *et al.* (2006). Global landscape of protein complexes in the yeast *Saccharomyces cerevisiae*. *Nature* 440, 637-643.

Krzycki, J.A. (2005). The direct genetic encoding of pyrrolysine. *Curr Opin Microbiol* 8, 706-712.

Kubota, H., Hynes, G., and Willison, K. (1995). The chaperonin containing t-complex polypeptide 1 (TCP-1). Multisubunit machinery assisting in protein folding and assembly in the eukaryotic cytosol. *Eur J Biochem* 230, 3-16.

Kubota, S., Kubota, H., and Nagata, K. (2006). Cytosolic chaperonin protects folding intermediates of Gbeta from aggregation by recognizing hydrophobic beta-strands. *Proc Natl Acad Sci U S A* 103, 8360-8365.

Kuznetsova, I.M., Biktashev, A.G., Khaitlina, S.Y., Vassilenko, K.S., Turoverov, K.K., and Uversky, V.N. (1999). Effect of self-association on the structural organization of partially folded proteins: inactivated actin. *Biophys J* 77, 2788-2800.

Laemmli, U.K. (1970). Cleavage of structural proteins during the assembly of the head of bacteriophage T4. *Nature* 227, 680-685.

Langer, T., Pfeifer, G., Martin, J., Baumeister, W., and Hartl, F.U. (1992). Chaperonin-mediated protein folding: GroES binds to one end of the GroEL cylinder, which accommodates the protein substrate within its central cavity. *EMBO J* 11, 4757-4765.

Lazarides, E., and Lindberg, U. (1974). Actin is the naturally occurring inhibitor of deoxyribonuclease I. *Proc Natl Acad Sci U S A* 71, 4742-4746.

Lee, C., and Goldberg, J. (2010). Structure of coatamer cage proteins and the relationship among COPI, COPII, and clathrin vesicle coats. *Cell* 142, 123-132.

Lee, J.Y., Duan, L., Iverson, T.M., and Dima, R.I. (2012). Exploring the role of topological frustration in actin refolding with molecular simulations. *J Phys Chem B* *116*, 1677-1686.

Leitner, A., Joachimiak, L.A., Bracher, A., Monkemeyer, L., Walzthoeni, T., Chen, B., Pechmann, S., Holmes, S., Cong, Y., Ma, B., *et al.* (2012). The Molecular Architecture of the Eukaryotic Chaperonin TRiC/CCT. Structure.

Lewis, S.A., Tian, G., and Cowan, N.J. (1997). The alpha- and beta-tubulin folding pathways. *Trends Cell Biol* *7*, 479-484.

Lin, P., and Sherman, F. (1997). The unique hetero-oligomeric nature of the subunits in the catalytic cooperativity of the yeast Cct chaperonin complex. *Proc Natl Acad Sci U S A* *94*, 10780-10785.

Lindquist, S., and Craig, E.A. (1988). The heat-shock proteins. *Annu Rev Genet* *22*, 631-677.

Liou, A.K., and Willison, K.R. (1997). Elucidation of the subunit orientation in CCT (chaperonin containing TCP1) from the subunit composition of CCT micro-complexes. *EMBO J* *16*, 4311-4316.

Llorca, O., Martin-Benito, J., Ritco-Vonsovici, M., Grantham, J., Hynes, G.M., Willison, K.R., Carrascosa, J.L., and Valpuesta, J.M. (2000). Eukaryotic chaperonin CCT stabilizes actin and tubulin folding intermediates in open quasi-native conformations. *EMBO J* *19*, 5971-5979.

Llorca, O., McCormack, E.A., Hynes, G., Grantham, J., Cordell, J., Carrascosa, J.L., Willison, K.R., Fernandez, J.J., and Valpuesta, J.M. (1999a). Eukaryotic type II chaperonin CCT interacts with actin through specific subunits. *Nature* *402*, 693-696.

Llorca, O., Smyth, M.G., Carrascosa, J.L., Willison, K.R., Rademacher, M., Steinbacher, S., and Valpuesta, J.M. (1999b). 3D reconstruction of the ATP-bound form of CCT reveals the asymmetric folding conformation of a type II chaperonin. *Nat Struct Biol* *6*, 639-642.

Lu, J., and Deutsch, C. (2005). Folding zones inside the ribosomal exit tunnel. *Nat Struct Mol Biol* *12*, 1123-1129.

Lukov, G.L., Baker, C.M., Ludtke, P.J., Hu, T., Carter, M.D., Hackett, R.A., Thulin, C.D., and Willardson, B.M. (2006). Mechanism of assembly of G protein betagamma subunits by protein kinase CK2-phosphorylated phosphatidylinositol-like protein and the cytosolic chaperonin complex. *J Biol Chem* *281*, 22261-22274.

Ma, J., Sigler, P.B., Xu, Z., and Karplus, M. (2000). A dynamic model for the allosteric mechanism of GroEL. *J Mol Biol* *302*, 303-313.

Maeder, C., Kutach, A.K., and Guthrie, C. (2009). ATP-dependent unwinding of U4/U6 snRNAs by the Brr2 helicase requires the C terminus of Prp8. *Nat Struct Mol Biol* 16, 42-48.

Maloney, A., and Workman, P. (2002). HSP90 as a new therapeutic target for cancer therapy: the story unfolds. *Expert Opin Biol Ther* 2, 3-24.

Mannherz, H.G., Goody, R.S., Konrad, M., and Nowak, E. (1980). The interaction of bovine pancreatic deoxyribonuclease I and skeletal muscle actin. *Eur J Biochem* 104, 367-379.

Mariotti, M., Ridge, P.G., Zhang, Y., Lobanov, A.V., Pringle, T.H., Guigo, R., Hatfield, D.L., and Gladyshev, V.N. (2012). Composition and evolution of the vertebrate and mammalian selenoproteomes. *PLoS One* 7, e33066.

Martin-Benito, J., Boskovic, J., Gomez-Puertas, P., Carrascosa, J.L., Simons, C.T., Lewis, S.A., Bartolini, F., Cowan, N.J., and Valpuesta, J.M. (2002). Structure of eukaryotic prefoldin and of its complexes with unfolded actin and the cytosolic chaperonin CCT. *EMBO J* 21, 6377-6386.

Martin-Benito, J., Grantham, J., Boskovic, J., Brackley, K.I., Carrascosa, J.L., Willison, K.R., and Valpuesta, J.M. (2007). The inter-ring arrangement of the cytosolic chaperonin CCT. *EMBO Rep* 8, 252-257.

Martin, R.B. (1988). Ternary hydroxide complexes in neutral solutions of Al<sup>3+</sup> and F. *Biochem Biophys Res Commun* 155, 1194-1200.

Mayer, M.P., and Bukau, B. (2005). Hsp70 chaperones: cellular functions and molecular mechanism. *Cell Mol Life Sci* 62, 670-684.

McCallum, C.D., Do, H., Johnson, A.E., and Frydman, J. (2000). The interaction of the chaperonin tailless complex polypeptide 1 (TCP1) ring complex (TRiC) with ribosome-bound nascent chains examined using photo-cross-linking. *J Cell Biol* 149, 591-602.

McCormack, E.A., Llorca, O., Carrascosa, J.L., Valpuesta, J.M., and Willison, K.R. (2001a). Point mutations in a hinge linking the small and large domains of beta-actin result in trapped folding intermediates bound to cytosolic chaperonin CCT. *J Struct Biol* 135, 198-204.

McCormack, E.A., Rohman, M.J., and Willison, K.R. (2001b). Mutational screen identifies critical amino acid residues of beta-actin mediating interaction between its folding intermediates and eukaryotic cytosolic chaperonin CCT. *J Struct Biol* 135, 185-197.

McKeehan, W., and Hardesty, B. (1969). The mechanism of cycloheximide inhibition of protein synthesis in rabbit reticulocytes. *Biochem Biophys Res Commun* 36, 625-630.

McLaughlin, J.N., Thulin, C.D., Hart, S.J., Resing, K.A., Ahn, N.G., and Willardson, B.M. (2002). Regulatory interaction of phosducin-like protein with the cytosolic chaperonin complex. *Proc Natl Acad Sci U S A* *99*, 7962-7967.

Melki, R., and Cowan, N.J. (1994). Facilitated folding of actins and tubulins occurs via a nucleotide-dependent interaction between cytoplasmic chaperonin and distinctive folding intermediates. *Mol Cell Biol* *14*, 2895-2904.

Meyer, A.S., Gillespie, J.R., Walther, D., Millet, I.S., Doniach, S., and Frydman, J. (2003). Closing the folding chamber of the eukaryotic chaperonin requires the transition state of ATP hydrolysis. *Cell* *113*, 369-381.

Mornet, D., and Ue, K. (1984). Proteolysis and structure of skeletal muscle actin. *Proc Natl Acad Sci U S A* *81*, 3680-3684.

Munoz, I.G., Yebenes, H., Zhou, M., Mesa, P., Serna, M., Park, A.Y., Bragado-Nilsson, E., Beloso, A., de Carcer, G., Malumbres, M., *et al.* (2011). Crystal structure of the open conformation of the mammalian chaperonin CCT in complex with tubulin. *Nat Struct Mol Biol* *18*, 14-19.

Nagai, K., and Thogersen, H.C. (1984). Generation of beta-globin by sequence-specific proteolysis of a hybrid protein produced in *Escherichia coli*. *Nature* *309*, 810-812.

Neiryck, K., Waterschoot, D., Vandekerckhove, J., Ampe, C., and Rommelaere, H. (2006). Actin interacts with CCT via discrete binding sites: a binding transition-release model for CCT-mediated actin folding. *J Mol Biol* *355*, 124-138.

Netzer, W.J., and Hartl, F.U. (1998). Protein folding in the cytosol: chaperonin-dependent and -independent mechanisms. *Trends Biochem Sci* *23*, 68-73.

Nissen, P., Kjeldgaard, M., Thirup, S., Polekhina, G., Reshetnikova, L., Clark, B.F., and Nyborg, J. (1995). Crystal structure of the ternary complex of Phe-tRNA<sup>Phe</sup>, EF-Tu, and a GTP analog. *Science* *270*, 1464-1472.

Oh, H.J., Chen, X., and Subject, J.R. (1997). Hsp110 protects heat-denatured proteins and confers cellular thermoresistance. *J Biol Chem* *272*, 31636-31640.

Ormo, M., Cubitt, A.B., Kallio, K., Gross, L.A., Tsien, R.Y., and Remington, S.J. (1996). Crystal structure of the *Aequorea victoria* green fluorescent protein. *Science* *273*, 1392-1395.

Ornstein, L. (1964). Disc Electrophoresis. I. Background and Theory. *Ann N Y Acad Sci* *121*, 321-349.

Packschies, L., Theyssen, H., Buchberger, A., Bukau, B., Goody, R.S., and Reinstein, J. (1997). GrpE accelerates nucleotide exchange of the molecular chaperone DnaK with an associative displacement mechanism. *Biochemistry* 36, 3417-3422.

Parks, T.D., Leuther, K.K., Howard, E.D., Johnston, S.A., and Dougherty, W.G. (1994). Release of proteins and peptides from fusion proteins using a recombinant plant virus proteinase. *Anal Biochem* 216, 413-417.

Pauling, L., Corey, R.B., and Branson, H.R. (1951). The structure of proteins; two hydrogen-bonded helical configurations of the polypeptide chain. *Proc Natl Acad Sci U S A* 37, 205-211.

Pereira, J.H., Ralston, C.Y., Douglas, N.R., Meyer, D., Knee, K.M., Goulet, D.R., King, J.A., Frydman, J., and Adams, P.D. (2010). Crystal structures of a group II chaperonin reveal the open and closed states associated with the protein folding cycle. *J Biol Chem* 285, 27958-27966.

Polier, S., Dragovic, Z., Hartl, F.U., and Bracher, A. (2008). Structural basis for the cooperation of Hsp70 and Hsp110 chaperones in protein folding. *Cell* 133, 1068-1079.

Ramachandran, G.N., Ramakrishnan, C., and Sasisekharan, V. (1963). Stereochemistry of polypeptide chain configurations. *J Mol Biol* 7, 95-99.

Reissmann, S., Parnot, C., Booth, C.R., Chiu, W., and Frydman, J. (2007). Essential function of the built-in lid in the allosteric regulation of eukaryotic and archaeal chaperonins. *Nat Struct Mol Biol* 14, 432-440.

Richards, F.M. (1992). Linderstrom-Lang and the Carlsberg Laboratory: the view of a postdoctoral fellow in 1954. *Protein Sci* 1, 1721-1730.

Richardson, J.S., and Richardson, D.C. (2002). Natural beta-sheet proteins use negative design to avoid edge-to-edge aggregation. *Proc Natl Acad Sci U S A* 99, 2754-2759.

Rivenzon-Segal, D., Wolf, S.G., Shimon, L., Willison, K.R., and Horovitz, A. (2005). Sequential ATP-induced allosteric transitions of the cytoplasmic chaperonin containing TCP-1 revealed by EM analysis. *Nat Struct Mol Biol* 12, 233-237.

Rospert, S., Dubaquie, Y., and Gautschi, M. (2002). Nascent-polypeptide-associated complex. *Cell Mol Life Sci* 59, 1632-1639.

Rouwental, G.J., Mendes, O., Wolbert, E.J., and Douwe de Boer, A. (1997). Enhanced expression in tobacco of the gene encoding green fluorescent protein by modification of its codon usage. *Plant Mol Biol* 33, 989-999.

Rye, H.S., Burston, S.G., Fenton, W.A., Beechem, J.M., Xu, Z., Sigler, P.B., and Horwich, A.L. (1997). Distinct actions of cis and trans ATP within the double ring of the chaperonin GroEL. *Nature* 388, 792-798.

Saibil, H. (1996). The lid that shapes the pot: structure and function of the chaperonin GroES. *Structure* 4, 1-4.

Saibil, H.R., Zheng, D., Roseman, A.M., Hunter, A.S., Watson, G.M., Chen, S., Auf Der Mauer, A., O'Hara, B.P., Wood, S.P., Mann, N.H., *et al.* (1993). ATP induces large quaternary rearrangements in a cage-like chaperonin structure. *Curr Biol* 3, 265-273.

Sakikawa, C., Taguchi, H., Makino, Y., and Yoshida, M. (1999). On the maximum size of proteins to stay and fold in the cavity of GroEL underneath GroES. *J Biol Chem* 274, 21251-21256.

Schagger, H., and von Jagow, G. (1991). Blue native electrophoresis for isolation of membrane protein complexes in enzymatically active form. *Anal Biochem* 199, 223-231.

Schedl, P., Artavanis-Tsakonas, S., Steward, R., Gehring, W.J., Mirault, M.E., Goldschmidt-Clermont, M., Moran, L., and Tissieres, A. (1978). Two hybrid plasmids with *D. melanogaster* DNA sequences complementary to mRNA coding for the major heat shock protein. *Cell* 14, 921-929.

Schoehn, G., Hayes, M., Cliff, M., Clarke, A.R., and Saibil, H.R. (2000). Domain rotations between open, closed and bullet-shaped forms of the thermosome, an archaeal chaperonin. *J Mol Biol* 301, 323-332.

Schuermann, J.P., Jiang, J., Cuellar, J., Llorca, O., Wang, L., Gimenez, L.E., Jin, S., Taylor, A.B., Demeler, B., Morano, K.A., *et al.* (2008). Structure of the Hsp110:Hsc70 nucleotide exchange machine. *Mol Cell* 31, 232-243.

Schwyster, D., Phillips, M., and Reisler, E. (1989). Subtilisin-cleaved actin: polymerization and interaction with myosin subfragment 1. *Biochemistry* 28, 5889-5895.

Shaner, L., and Morano, K.A. (2007). All in the family: atypical Hsp70 chaperones are conserved modulators of Hsp70 activity. *Cell Stress Chaperones* 12, 1-8.

Siegert R., Leroux M.R., Scheufler C., Hartl F.U., and Moarefi, I. (2000). Structure of the molecular chaperone prefoldin: unique interaction of multiple coiled coil tentacles with unfolded proteins. *Cell* 103, 621-632.

Sigler, P.B., Xu, Z., Rye, H.S., Burston, S.G., Fenton, W.A., and Horwich, A.L. (1998). Structure and function in GroEL-mediated protein folding. *Annu Rev Biochem* 67, 581-608.

Small, E.C., Leggett, S.R., Winans, A.A., and Staley, J.P. (2006). The EF-G-like GTPase Snu114p regulates spliceosome dynamics mediated by Brr2p, a DExD/H box ATPase. *Mol Cell* 23, 389-399.

Smith, T.F., Gaitatzes, C., Saxena, K., and Neer, E.J. (1999). The WD repeat: a common architecture for diverse functions. *Trends Biochem Sci* 24, 181-185.

Soe, R., Mosley, R.T., Justice, M., Nielsen-Kahn, J., Shastry, M., Merrill, A.R., and Andersen, G.R. (2007). Sordarin derivatives induce a novel conformation of the yeast ribosome translocation factor eEF2. *J Biol Chem* 282, 657-666.

Spieß, C., Meyer, A.S., Reissmann, S., and Frydman, J. (2004). Mechanism of the eukaryotic chaperonin: protein folding in the chamber of secrets. *Trends Cell Biol* 14, 598-604.

Spieß, C., Miller, E.J., McClellan, A.J., and Frydman, J. (2006). Identification of the TRiC/CCT substrate binding sites uncovers the function of subunit diversity in eukaryotic chaperonins. *Mol Cell* 24, 25-37.

Stemp, M.J., Guha, S., Hartl, F.U., and Barral, J.M. (2005). Efficient production of native actin upon translation in a bacterial lysate supplemented with the eukaryotic chaperonin TRiC. *Biol Chem* 386, 753-757.

Stirling, P.C., Cuellar, J., Alfaro, G.A., El Khadali, F., Beh, C.T., Valpuesta, J.M., Melki, R., and Leroux, M.R. (2006). PhLP3 modulates CCT-mediated actin and tubulin folding via ternary complexes with substrates. *J Biol Chem* 281, 7012-7021.

Sun, Y., and MacRae, T.H. (2005). The small heat shock proteins and their role in human disease. *FEBS J* 272, 2613-2627.

Swamy, M., Minguet, S., Siegers, G.M., Alarcon, B., and Schamel, W.W. (2007). A native antibody-based mobility-shift technique (NAMOS-assay) to determine the stoichiometry of multiprotein complexes. *J Immunol Methods* 324, 74-83.

Szpikowska, B.K., Swiderek, K.M., Sherman, M.A., and Mas, M.T. (1998). MgATP binding to the nucleotide-binding domains of the eukaryotic cytoplasmic chaperonin induces conformational changes in the putative substrate-binding domains. *Protein Sci* 7, 1524-1530.

Tang, Y.C., Chang, H.C., Roeben, A., Wischnewski, D., Wischnewski, N., Kerner, M.J., Hartl, F.U., and Hayer-Hartl, M. (2006). Structural features of the GroEL-GroES nano-cage required for rapid folding of encapsulated protein. *Cell* 125, 903-914.

Tian, G., Vainberg, I.E., Tap, W.D., Lewis, S.A., and Cowan, N.J. (1995). Specificity in chaperonin-mediated protein folding. *Nature* 375, 250-253.

Tong, A.H., Evangelista, M., Parsons, A.B., Xu, H., Bader, G.D., Page, N., Robinson, M., Raghibizadeh, S., Hogue, C.W., Bussey, H., *et al.* (2001). Systematic genetic analysis with ordered arrays of yeast deletion mutants. *Science* 294, 2364-2368.

Vainberg, I.E., Lewis, S.A., Rommelaere, H., Ampe, C., Vandekerckhove, J., Klein, H.L., and Cowan, N.J. (1998). Prefoldin, a chaperone that delivers unfolded proteins to cytosolic chaperonin. *Cell* 93, 863-873.

Valpuesta, J.M., Martin-Benito, J., Gomez-Puertas, P., Carrascosa, J.L., and Willison, K.R. (2002). Structure and function of a protein folding machine: the eukaryotic cytosolic chaperonin CCT. *FEBS Lett* 529, 11-16.

van den Ent, F., Amos, L.A., and Lowe, J. (2001). Prokaryotic origin of the actin cytoskeleton. *Nature* 413, 39-44.

Verkhusha, V.V., Tsukita, S., and Oda, H. (1999). Actin dynamics in lamellipodia of migrating border cells in the *Drosophila* ovary revealed by a GFP-actin fusion protein. *FEBS Lett* 445, 395-401.

Villebeck, L., Moparthi, S.B., Lindgren, M., Hammarstrom, P., and Jonsson, B.H. (2007a). Domain-specific chaperone-induced expansion is required for beta-actin folding: a comparison of beta-actin conformations upon interactions with GroEL and tail-less complex polypeptide 1 ring complex (TRiC). *Biochemistry* 46, 12639-12647.

Villebeck, L., Persson, M., Luan, S.L., Hammarstrom, P., Lindgren, M., and Jonsson, B.H. (2007b). Conformational rearrangements of tail-less complex polypeptide 1 (TCP-1) ring complex (TRiC)-bound actin. *Biochemistry* 46, 5083-5093.

Vinh, D.B., and Drubin, D.G. (1994). A yeast TCP-1-like protein is required for actin function in vivo. *Proc Natl Acad Sci U S A* 91, 9116-9120.

Wahl, M.C., Will, C.L., and Luhrmann, R. (2009). The spliceosome: design principles of a dynamic RNP machine. *Cell* 136, 701-718.

Walsh, P., Bursac, D., Law, Y.C., Cyr, D., and Lithgow, T. (2004). The J-protein family: modulating protein assembly, disassembly and translocation. *EMBO Rep* 5, 567-571.

Wandinger, S.K., Richter, K., and Buchner, J. (2008). The Hsp90 chaperone machinery. *J Biol Chem* 283, 18473-18477.

Wegele, H., Muller, L., and Buchner, J. (2004). Hsp70 and Hsp90--a relay team for protein folding. *Rev Physiol Biochem Pharmacol* 151, 1-44.

Weiss, M.S., Jabs, A., and Hilgenfeld, R. (1998). Peptide bonds revisited. *Nat Struct Biol* 5, 676.

Willardson, B.M., and Howlett, A.C. (2007). Function of phosphoinositide-like proteins in G protein signaling and chaperone-assisted protein folding. *Cell Signal* 19, 2417-2427.

Xu, Z., Horwich, A.L., and Sigler, P.B. (1997). The crystal structure of the asymmetric GroEL-GroES-(ADP)<sub>7</sub> chaperonin complex. *Nature* 388, 741-750.

Xu, Z., and Sigler, P.B. (1998). GroEL/GroES: structure and function of a two-stroke folding machine. *J Struct Biol* 124, 129-141.

Yam, A.Y., Xia, Y., Lin, H.T., Burlingame, A., Gerstein, M., and Frydman, J. (2008). Defining the TRiC/CCT interactome links chaperonin function to stabilization of newly made proteins with complex topologies. *Nat Struct Mol Biol* 15, 1255-1262.

Yebenes, H., Mesa, P., Munoz, I.G., Montoya, G., and Valpuesta, J.M. (2011). Chaperonins: two rings for folding. *Trends Biochem Sci* 36, 424-432.

Yifrach, O., and Horovitz, A. (1995). Nested cooperativity in the ATPase activity of the oligomeric chaperonin GroEL. *Biochemistry* 34, 5303-5308.

Yoon, Y., Pitts, K., and McNiven, M. (2002). Studying cytoskeletal dynamics in living cells using green fluorescent protein. *Mol Biotechnol* 21, 241-250.

Zhang, J. (2000). Protein-length distributions for the three domains of life. *Trends Genet* 16, 107-109.

Zhang, J., Baker, M.L., Schroder, G.F., Douglas, N.R., Reissmann, S., Jakana, J., Dougherty, M., Fu, C.J., Levitt, M., Ludtke, S.J., *et al.* (2010). Mechanism of folding chamber closure in a group II chaperonin. *Nature* 463, 379-383.

Zhang, J., Ma, B., DiMaio, F., Douglas, N.R., Joachimiak, L.A., Baker, D., Frydman, J., Levitt, M., and Chiu, W. (2011). Cryo-EM structure of a group II chaperonin in the prehydrolysis ATP-bound state leading to lid closure. *Structure* 19, 633-639.

Zolkiewski, M., Zhang, T., and Nagy, M. (2012). Aggregate reactivation mediated by the Hsp100 chaperones. *Arch Biochem Biophys* 520, 1-6.

## 7. Abbreviations

ADP	Adenosine 5'-diphosphate
AlFx	Aluminum fluoride
AMP-PNP	Adenosine 5'-( $\beta,\gamma$ -imido)triphosphate
APS	Ammonium persulfate
ATP	Adenosine 5'-triphosphate
ATP $\gamma$ S	Adenosine 5'-( $\gamma$ -thio)triphosphate
BFP	Blue Fluorescent Protein
BSA	Bovine Serum Albumin
CCT	Chaperonin Containing TCP-1
cDNA	complementary DNA
CHO	Chinese Hamster Ovary
DM-MBP	Double Mutant form of Maltose Binding Protein
DNA	Deoxyribonucleic Acid
DNase	Deoxyribonuclease
dNTP	Deoxyribonucleotide
DTT	Dithiothreitol
EDTA	Ethylenediaminetetraacetic acid
EGTA	Ethylene glycol-bis(2-aminoethylether)-N,N,N',N'-tetraacetic acid
EM	Electron Microscopy
FL	Full-Length
FRET	Förster Resonance Energy Transfer

GDP	Guanosine 5'-diphosphate
GFP	Green Fluorescent Protein
GTP	Guanosine 5'-triphosphate
HA	Hemagglutinin
HEPES	4-(2-Hydroxyethyl)piperazine-1-ethanesulfonic acid
Hsp	Heat Shock Protein
IgG	Immunoglobulin G
LB	Lysogeny Broth
Mm-cpn	<i>Methanococcus maripaludis</i> Chaperonin
MOPS	3-(N-Morpholino)propanesulfonic acid
MPIB	Max Planck Institute of Biochemistry
mRNA	messenger RNA
NAC	Nascent chain Associated Complex
NBD	Nucleotide Binding Domain
NEF	Nucleotide Exchange Factor
OD	Optical Density
PAGE	Polyacrylamide Gel Electrophoresis
PBS	Phosphate Buffered Saline
PCR	Polymerase Chain Reaction
PDB	Protein Data Bank
PFD	Prefoldin
PhLPs	Phosducin-Like Proteins

PK	Proteinase K
PMSF	Phenylmethanesulfonyl fluoride
PTC	Peptidyl Transferase Center
RAC	Ribosome Associated Complex
RNA	Ribonucleic Acid
rpm	Revolutions Per Minute
RRL	Rabbit Reticulocyte Lysate
SAXS	Small Angle X-ray Scattering
SDS	Sodium Dodecyl Sulfate
SGA	Synthetic Genetic Array
SHR	Steroid Hormone Receptor
snRNA	small nuclear RNA
TAE	Tris-Acetate-EDTA
TCP-1	T-Complex Polypeptide-1
TEMED	Tetramethylethylenediamine
TEV	Tobacco Etch Virus
TF	Trigger Factor
TRiC	TCP-1 Ring Complex
Tris	Tris(hydroxymethyl)aminomethane
tRNA	transfer RNA
VHL	von Hippel-Lindau